Phenomenology of Hidden Sector Physics

by

Yanou Cui

A dissertation submitted in partial fulfillment
of the requirements for the degree of
Doctor of Philosophy
(Physics)
in The University of Michigan
2008

Doctoral Committee:

Associate Professor James D. Wells, Chair
Professor Fred C. Adams
Professor Gordon L. Kane
Professor Jianming Qian
Assistant Professor Aaron T. Pierce

Copyright © Yanou Cui All Rights Reserved 2008

DEDICATION

To my parents

ACKNOWLEDGMENTS

I would like to express my deep gratitude to my advisor James Wells for his encouragement and guidance throughout my Ph.D. studies, and for the many illuminating and enjoyable discussions on physics with him over these years. I'm also grateful to other professors in the particle theory group, most notably, Gordon Kane and Aaron Pierce, for the helpful suggestions on my studies they offered me during our discussions. I have also benefitted a lot from interactions with fellow students and postdocs in the group. I would like to thank them for the useful conversations on various aspects of physics I had with them, particularly David Morrissey, who is also my research collaborator.

I would also like to offer my heartfelt thanks to my parents, for their unfailing support and care from across the Ocean throughout these years. I also thank those good friends of mine, far and near, who have brought enjoyable moments into my life.

CONTENTS

LIST OF FIGURES

Figure

LIST OF TABLES

Table

ABSTRACT

Phenomenology of Hidden Sector Physics

by

Yanou Cui

Chair: James D. Wells

The existence of a *hidden sector*, composed of Standard Model (SM) singlets and the interactions between them, is well-motivated by many beyond-the-SM theories, such as GUT theories, string-inspired models and supersymmetry-breaking models. In addition to sharing weak gravity-induced interactions with the visible sector, such SM singlets can couple to the SM fields in various other ways. One well motivated hidden sector scenario is that associated with a beyond-the-SM gauge symmetry which is broken via the Higgs mechanism. Although the collider phenomenology of such models is rich and well-documented, few obvious cosmological signatures for them are known. The physics of cosmic strings provides a promising cosmological probe of such hidden sectors, applicable for a general class of symmetry breaking patterns in the hidden sector. This thesis discusses the phenomenology of hidden sectors, including LHC signatures of a hidden sector Higgs boson, the physics of cosmic strings from supersymmetric flat-directions, and dark matter production from a general cosmic string network. We conclude that there are viable prospects for seeing signals of a *hidden* sector both at the LHC and in cosmological observations.

CHAPTER 1

Motivation for Hidden Sector

1.1 What is Hidden Sector? Why do we care about it?

The Standard Model (SM), as the benchmark theory for particle physics, has given a precise description for the interactions and matter content of the *visible* world, based on the gauge symmetry group $G_{\rm SM} = SU(3)_C \times SU(2)_L \times U(1)_Y$ and the breaking of the electro-weak subgroup through the Higgs mechanism. However, the SM has received challenges both from experimental observations (e.g. lack of prediction of tiny neutrino mass, dark matter, etc.), as well as the criteria for a self-consistent, 'ultimate' theory. In this introduction I am going to focus on the theoretical challenges for the SM, and demonstrate how the efforts to solve these problems motivate a *hidden* sector (in addition to the SM—-the *visible* sector). Before moving on, let us provide a concrete definition of *hidden sector* first. A hidden sector consists of singlets under $G_{\rm SM}$, i.e. fields that do not feel the strong and electro-weak forces that the fields of the SM do. Therefore, we cannot easily 'visualize' them, i.e. see their influence on visible sector via interactions mediated by the SM gauge bosons. This is why they are called 'hidden'.

In this sense, the hidden sector appears to be almost irrelevant to our *visible* world. However, this is a naive impression. The majority of this thesis will demonstrate how hidden sector can influence the phenomenology of the visible sector in nontrivial

ways, and how they can produce interesting signatures at collider experiments and for cosmology[1]. As a quick preview, here are three examples as to why a hidden sector can be nontrivial:

1. The hidden sector itself can have rich structure of physics, e.g. global or gauge symmetries $G_{\rm hid}$, as an extension of the symmetries we have seen in the SM.

2. The hidden sector can interact with the visible sector in more significant ways than the pessimistically weak gravitational effect. For example, it can interact with the SM through loop effects or non-renormalizable interactions mediated by some messenger sector field with charges under both $G_{\rm SM}$ and $G_{\rm hid}$. Most interestingly, there can be renormalizable tree-level coupling between the two sectors through $U(1)$ kinetic mixing if the hidden sector possesses a $U(1)'$ gauge symmetry, or through Higgs mixing terms like $|\Phi_{\rm SM}|^2|\Phi_{\rm hid}|^2$ if the hidden sector has a broken gauge symmetry (either Abelian or non-abelian). In Chapter 2 I will talk about my work on the effect of this quartic Higgs mixing.

3. One very interesting possibility is, although hidden sector fields are singlets under the $G_{\rm SM}$, SM fields may be charged under $G_{\rm hid}$. This means, there can be some 'fifth' force acting on the visible world which we are familiar with. We will see some examples of this in section 2.1, where we discuss the Z' gauge boson coupling to SM fields via neutral currents or covariant derivative interactions. The reason we have not seen the effects of this force can be: the force is very short-ranged, or equivalently the gauge boson mediating this force is

[1]Here it is worth clarifying that, in some earlier references, *hidden* sector can be referred to SM singlets that only talk with the SM fields through very weak gravitational effects. In this sense, the sector is almost irrelevant for low energy experiments and are truly 'hidden'. However, as will be demonstrated in this thesis, SM singlets are in fact very interesting as they can have various non-gravitational channels to influence the SM phenomenology.

rather heavy, so that we have not found such resonance at previous collider experiments—but we may expect to detect it in the LHC era.

Let us now return to the practical motivation for hidden sector from theoretical concerns. A big *dream* of theorists is to find a unified description for the four known fundamental interactions in nature: the weak and electromagnetic forces (already unified at the weak scale) and the strong (color) strong forces of the SM, and gravity which is well described by general relativity. Grand Unified Theories (GUTs) have been trying to embed the $G_{\rm SM}$ into a single, larger, simple Lie group, or to unify the the three non-gravitational forces. These theories typically introduce extended gauge structure, including SM singlets charged under some additional gauge group–this is a type of hidden sector. To be more ambitious, people have been searching for a framework to give a unified description for all the SM forces *and* gravity. One of the most promising frameworks at present is superstring theory. It has been found that many string models which successfully include the SM at low scale also bring in a set of particles which are singlets under $G_{\rm SM}$ but transform non-trivially under additional 'shadow' sector group[4]– this is again a good motivation for a hidden sector. A more detailed explanation for the generality of hidden sectors in GUT/string inspired models will be given in section 1.2.

Another significant barrier for a self-consistent understanding of both electroweak scale physics and gravity is the *gauge hierarchy problem*, i.e. why there is such a big hierarchy between the weak scale $\sim$ 100GeV and the reduced Planck scale $M_p = (8\pi G_{\rm Newton})^{-1/2} = 2.4 \times 10^{18}$GeV, where the quantum gravitational effects become non-negligible. The gauge hierarchy problem is always accompanied by another *technical hierarchy problem*, i.e. how to stabilize the hierarchy between the weak scale and Planck scale–this is especially relevant in theories involving a Higgs-like field or

fields, where in the absence of fine-tuning, quantum corrections will drive the Higgs mass up to Planck scale, even if a weak scale mass is generated at tree level. Various approaches in the spirit of dynamical symmetry breaking can solve the two related hierarchy problems simultaneously; these typically involve extended gauge structure and SM singlets–hidden sector, e.g. technicolor models, little Higgs models, etc. For alternative theories which involve a perturbative Higgs, like supersymmetry (SUSY) models, at first sight there seems to be no motivation for extended gauge structure. However, SUSY itself only solves the technical hierarchy problem by introducing SUSY partners of SM fields to cancel quadratic divergence to the Higgs mass. But in order to provide a natural explanation for why the electroweak (EW) or (related) SUSY breaking scale is much lower than M_p, or to solve the gauge hierarchy problem, a hidden sector which breaks SUSY dynamically and transfers the effect to the SM via certain messengers is necessary. Further explanation on this point will be given in section 1.2.1.

1.2 Examples for Hidden Sector Motivation

By now we have seen how generically the need for a hidden sector arises in various extensions of the SM. As outlined earlier, in this section, I will briefly review some more concrete examples of this general phenomenon.

1.2.1 The Need for a *hidden* Supersymmetry-Breaking Sector

Let's start with a general, renormalizable, supersymmetric, gauge invariant theory and motivate a hidden sector as needed for generating a SUSY-breaking mass spectrum which is consistent with experimental observations. We assume the matter fields are in the chiral superfield representation of supersymmetry algebra (i labels different species)

$$\Phi_i = \phi_i(x) + \sqrt{2}\theta\psi_i(x) + \theta\theta F_i(x) \tag{1.1}$$

and the gauge fields are in the vector superfield representation. In Wess-Zumino gauge:

$$V = \left[-\theta\sigma^{\mu}\bar{\theta}A^{a}_{\mu}(x) - i\bar{\theta}\bar{\theta}\theta\lambda^{a}(x) + i\theta\theta\bar{\theta}\bar{\lambda}^{a}(x) + \frac{1}{2}\theta\theta\bar{\theta}\bar{\theta}(D^{a}(x) + i\partial_{\mu}A^{a\mu}(x))\right]T^{a} \quad (1.2)$$

where the component fields ϕ, ψ, A_{μ} and λ are scalar, matter fermion, gauge boson and gaugino respectively. F and D fields are auxiliary fields necessary to ensure off-shell closure of supersymmetry transformations. T^{a} are the generators for the non-abelian gauge group (for the abelian case, T^{a} is replaced by the hypercharge $Y/2$).

We can thereby write down the supersymmetric gauge-invariant Lagrangian as:

$$\begin{aligned}
\mathcal{L} &= \frac{1}{16\kappa g^{2}}\mathrm{Tr}\left(\int d\theta^{2}\mathcal{W}^{\alpha}\mathcal{W}_{\alpha} + \mathrm{h.c.}\right) + \int d\theta^{4}\Phi_{i}^{+}e^{2gV}\Phi_{i} + \left(\int d\theta^{2}W(\Phi_{i}) + h.c.\right) \\
&= -\frac{1}{4}F^{a}_{\mu\nu}F^{a\mu\nu} - i\lambda^{\dagger a}\bar{\sigma}^{\mu}D_{\mu}\lambda^{a} - D^{\mu}\phi^{*i}D_{\mu}\phi_{i} - i\psi^{\dagger i}\bar{\sigma}^{\mu}D_{\mu}\psi_{i} - \sqrt{2}g(\phi_{i}^{*}T^{a}\psi_{i})\lambda^{a} \\
&\quad -\sqrt{2}g\lambda^{\dagger a}(\psi^{\dagger}T^{a}\phi) - \frac{1}{2}\left(W^{ij}\psi_{i}\psi_{j} + W^{*}_{ij}\psi^{\dagger i}\psi^{\dagger j}\right) - W_{i}^{*}W^{i} - \frac{1}{2}\sum_{a}g^{2}(\phi_{i}^{*}T^{a}\phi_{i})^{2}
\end{aligned}$$

where g is the gauge coupling. D_{μ} is gauge covariant derivative. $\mathrm{Tr}T^{a}T^{b} = \kappa\delta^{ab}$ defines the Dynkin index κ. $\mathcal{W}_{\alpha} = \bar{D}\bar{D}e^{-2gV}D_{\alpha}e^{2gV}$ is the SUSY generalization of the field strength, with $\bar{D}_{\alpha}, D_{\alpha}$ as the supersymmetric covariant derivative[2]. W is a general superpotential, $W^{i} = -F_{i}^{*}\frac{\delta W}{\delta\phi_{i}}$, $W^{ij} = \frac{\delta^{2}}{\delta\phi_{i}\delta\phi_{j}}W$. As we will see soon, from non-kinetic terms in eq.(1.3) we can extract the tree-level mass matrices for component fields after SUSY breaking .

In order to get close to the observed phenomenology, we need to move on and see how supersymmetry is broken spontaneously and what the resulting mass spectrum looks like. We first need to briefly review the standard lore about vacuum structure for global SUSY theory.

[2]For more details of the conventions used here, please refer to [1, 184]

Let $Q_\alpha, Q^\dagger_{\dot\alpha}$ be supersymmetry generators, and $|0\rangle$ indicates the vacuum state. When supersymmmetry is broken, $|0\rangle$ is not invariant under SUSY transformation, i.e. $Q_\alpha \neq 0$ and $Q^\dagger_{\dot\alpha} \neq 0$. For global SUSY, due to the SUSY algebra relation $\{Q_\alpha, Q^\dagger_{\dot\beta}\} = 2\sigma^\mu_{\alpha\dot\beta} P_\mu$, the Hamiltonian is directly related to the SUSY generators as:

$$H = P^0 = \frac{1}{4}(Q_1 Q_1^\dagger + Q_1^\dagger Q_1 + Q_2 Q_2^\dagger + Q_2^\dagger Q_2)$$

Based on the above relation, we find that the vacuum energy in SUSY breaking phase must be positive since

$$\langle 0|H|0\rangle = \frac{1}{4}\left(\|Q_1^\dagger|0\rangle\|^2 + \|Q_1|0\rangle\|^2 + \|Q_2^\dagger|0\rangle\|^2 + \|Q_2|0\rangle\|^2\right) > 0 \tag{1.3}$$

When spacetime-dependent effects and fermion condensates are neglected, $\langle 0|H|0\rangle = \langle 0|V|0\rangle$ where V is the scalar potential which can be easily extracted from eq.(1.3):

$$V(\phi, \phi^*) = F^{*i}F_i + \frac{1}{2}\sum_a D^a D^a = W_i^* W^i + \frac{1}{2}\sum_a g^2(\phi_i^* T^a \phi_i)^2 \tag{1.4}$$

We therefore see that in order to spontaneously break supersymmetry, F_i and/or D^a, or more explicitly, $\langle\phi\rangle, \langle W^i\rangle$ etc. should be non-vanishing in the ground state. Now based on eq.(1.3) we are ready to write down the squared mass matrices for scalar, fermion and vector component fields:

Scalar in the (ϕ^{*i}, ϕ_i) basis:

$$\mathbf{m}_S^2 = \begin{pmatrix} W^*_{ij}W^{ik} + g^2[(T^a\phi)_j(\phi^* T^a)^i + T^{ai}_j D^a] & W^*_{ijk}W^k + g^2(T^a\phi)_i(\phi^* T^a)_j \\ W^{ijk}W^*_k + g^2(T^a\phi)^i(\phi^* T^a)^j & W^*_{ik}W^{jk} + g^2[(T^a\phi)_i(\phi^* T^a)^j + T_i^{aj} D^a] \end{pmatrix} \tag{1.5}$$

Fermion in (λ^a, ψ_i) basis:

$$\mathbf{m}_F^\dagger \mathbf{m}_F = \begin{pmatrix} 2g^2(\phi^* T^a)_i(T^b\phi)^i & \sqrt{2}g(T^b\phi)_k W^{ik} \\ \sqrt{2}g(\phi^* T^a)_k W^*_{ik} & W^*_{jk}W^{ik} + 2g^2(T^a\phi)_i(\phi^* T^a)^i \end{pmatrix} \tag{1.6}$$

vector boson in (A^a, A^b) basis:

$$\mathbf{m}_V^2 = g^2(\phi_i^*\{T^a, T^b\}\phi_i) \tag{1.7}$$

From eqs. (1.5-1.7), we get the sum over the squared-mass eigenvalues respectively as:

$$\begin{aligned} \mathrm{Tr}(\mathbf{m}_S^2) &= 2W^*_{ik}W^{ik} + 2g^2[C(i)\phi^{*i}\phi_i + \mathrm{Tr}(T^a)D^a] && (1.8)\\ \mathrm{Tr}(\mathbf{m}_F^\dagger \mathbf{m}_F) &= W^*_{ik}W^{ik} + 4g^2C(i)\phi^{*i}\phi_i && (1.9)\\ \mathrm{Tr}(\mathbf{m}_V^2) &= 2g^2C(i)\phi^{*i}\phi_i && (1.10) \end{aligned}$$

where C_i are quadratic Casimir gauge group invariant of matter specie i. Now we come to an important relation. The supertrace of the tree-level squared-mass eigenvalues defined as a weighted sum over all particles with spin j

$$\mathrm{STr}(m^2) \equiv \sum_j (-1)^j (2j+1)\mathrm{Tr}(m_j^2) \tag{1.11}$$

satisfying the sum rule

$$\mathrm{STr}(m^2) = \mathrm{Tr}(\mathbf{m}_S^2) - 2\mathrm{Tr}(\mathbf{m}_F^\dagger \mathbf{m}_F) + 3\mathrm{Tr}(\mathbf{m}_V^2) = 2g^2\mathrm{Tr}(T^a)D^a = 0 \tag{1.12}$$

The last equality is valid for any non-anomalous gauge symmetry.

When applied to phenomenological models like minimal supersymmetric standard model (MSSM) (where three different gauge groups are involved), the tree-level sum rule eq.(1.12) has an important implication. Without flavor mixing[3], the sum rule for a certain superpartner pair decouples from others, and we have, for example

$$m_{\tilde{e}_1}^2 + m_{\tilde{e}_2}^2 = 2m_e^2 \tag{1.13}$$

This conflicts with the fact that the experimental bound has pushed the selectron masses to be much larger than electron mass. In fact, besides the lesson from the sum rules, another reason that vetoes generating MSSM soft masses at tree level is:

[3]The sum rules can be evaded by introducing flavor-violating mixings, but it is very difficult to make a viable model in this way, since it typically results in large flavor-changing effect above experimental bounds.

in general it is hard to give masses to gauginos. This is easy to see if we look at eq.(1.3)–there is no (scalar)-(gaugino)-(gaugino) couplings that can generate gaugino mass.

Based on the above reasons, we expect that the MSSM soft terms arise from non-renormalizable coupling or loop effects, rather than from tree-level renormalizable couplings to SUSY-breaking order parameters (F, D). Therefore a viable realistic model in general *requires* a *hidden sector* with no or very small direct couplings to the *visible sector* as in the MSSM. SUSY breaking evidently occurs in such a hidden sector, and then transfers the effects to visible sector mediated by the shared interaction between these two sectors (such shared interaction can be gravitational or a gauge interaction). By now it is clear how generically a *hidden sector* is motivated by realistic SUSY breaking models.

1.2.2 The Need for *hidden* sector from GUT/String-Inspired Models

Now let's start a brief look at how hidden sector, especially extended gauge structure is motivated by GUT/string models. The focus will be additional $U(1)'$ gauge symmetry since it is probably the best motivated one.

For GUT models, one general reason for getting additional $U(1)'$ after symmetry breaking is due to the fact that it is more difficult to reduce the rank of the GUT group (i.e. to break the abelian generators) than it is to break the non-abelian factors[3]. Take a gauge group $G = SU(N)$ as a toy example. It has rank $N-1$, i.e. $N-1$ diagonal generators, among the total N^2-1 generators. One way to break G is to give a non-zero vacuum expectation value (VEV) to a real adjoint Higgs representation Φ, which can be represented by a traceless Hermitian $N \times N$ matrix

$$\Phi = \sum_{i=1}^{N^2-1} \phi^i L_i \tag{1.14}$$

where ϕ^i are real components of Φ and L_i are the $N \times N$ fundamental representation matrices. When Φ acquires a VEV $\langle\Phi\rangle$, the $SU(N)$ is broken to a subgroup generated by those generators that commutes with Φ. Without loss of generality, $\langle\Phi\rangle$ can be diagonalized by an $SU(N)$ transformation, so that the $N-1$ diagonal generators remain unbroken, and therefore a $U(1)^N$ survives. In special cases when K ($K < N$) diagonal elements of $\langle\Phi\rangle$ are equal, some of the unbroken generators can be embedded in unbroken $SU(K)$ subgroups. But the subgroups always contains at least $U(1)^N$. In practice, in GUT theories larger than original $SU(5)$ model, such as $SO(10)$ or E_6 models, they could break to $G_{\rm SM} \times U(1)'^n, n \geq 1$ [3].

String models which attempt to reproduce the 4-dimensional SM after compactification also motivate extended gauge structures. For heterotic string models based on the $E_8 \times E_8$ or $SO(32)$ group at string scale, the story is similar to that of the GUT theories, since they need to break those larger groups to $G_{\rm SM}$ after compactification. $E_8 \times E_8$ is in particular interesting, since it is natural to embed $G_{\rm SM}$ into one of the E_8, while reserving the second E_8 as a 'hidden sector' which may serve as the SUSY breaking sector required by phenomenology (referred to the earlier discussion in section 1.2.1). In another recently developed class of string models based on intersecting D-branes, there are two reasons to introduce 'hidden' sector. First, a stack of N D-branes on top of each other initially realizes a $U(N)$ gauge symmetry, which needs to be reduced to $SU(N)$ to reproduce the gauge groups for the SM. This process results in an extra $U(1)$ in addition to the desired $SU(N)$. The second motivation for hidden sector in D-brane models is due to the necessity to cancel tadpole[4] divergence–*hidden* branes are needed in addition to the brane where the SM lives in[4].

[4]In string theory, tadpole corresponds to a closed string appearing from or disappearing into the vacuum. It typically results in IR divergence because of the zero-momentum massless propagator.

CHAPTER 2

Interplay Between Hidden Sector and Higgs Physics–Signatures at the LHC

2.1 A Brief Review of the $U(1)'$ sector and its coupling to the SM

As we have seen from the Introduction, an additional $U(1)'$ gauge symmetry is a well-motivated hidden sector scenario. The current chapter and the next are dedicated to certain aspects of $U(1)'$ phenomenology, at the LHC and in cosmology, respectively. There have been extensive studies of $U(1)'$ physics, especially the associated Z' gauge boson ([3, 5] and references therein). Here I will first give a brief review on these works as background.

Breaking? Breaking scale?

The first thing we are curious about is whether the $U(1)'$ sector is broken and what the breaking scale is if it is broken, since mass scales of the exotic particles are crucial for their detectability and influence on the SM/cosmology. If this $U(1)'$ is unbroken, then the associated Z' would be massless. This implies an unacceptable long range force unless its coupling to ordinary matter is incredibly small, e.g. communicated by higher-dimensional operators or through very small kinetic mixing to the photon (we will come to this soon). For these reasons, we are generally interested in a broken $U(1)'$. In a non-supersymmetric context, there is no particular expectation for this breaking scale. But in both string theories and SUSY GUT theories both $U(1)'$ and

the SM electroweak $SU(2)_L \times U(1)_Y$ breaking scales are generically related to the soft SUSY breaking scale. Therefore, if SUSY is observed at the LHC, we can be optimistic about the observation of a string or GUT induced $U(1)'$ also. An exception to this is: potentials in supersymmetric theories typically have flat-directions which can be slightly lifted only when SUSY is broken because of the SUSY non-renormalization theorem. When the $U(1)'$ is broken along the (almost) flat direction, the Z' boson can get an intermediate scale mass $\sim \sqrt{mM}$ where m is the soft SUSY breaking mass scale, which we expect to be at TeV scale, and M is the GUT or string scale. In chapter 3 of this thesis, I will discuss my work on the cosmological implication of flat-direction $U(1)'$ breaking. Another very interesting aspect of the broken $U(1)'$ scenario is that the symmetry breaking would require an extended Higgs sector, which can have significant consequences for phenomenology. In section 2 of this chapter, I will present my work on the phenomenology of such hidden sector Higgs at the LHC through its mixing with the SM Higgs.

Couplings to the SM

Both the Z' gauge boson and the associated Higgs can have tree-level renormalizable mixing with the SM fields. This in general can have significant influence on the SM phenomenology, even though they are called 'hidden'. The Higgs mixing and its consequences will be discussed in detail in the next section. Here, I will briefly review the story for the Z' gauge boson.

If some of the SM fermions have non-trivial charge under $U(1)'$ (we have mentioned this interesting 'fifth force' possibility in the introduction), Z' can have direct couplings to the SM fermions via neutral current. In the SM, the neutral current

interaction of the fermions are described by the Lagrangian in gauge basis[1]

$$-\mathcal{L}_{\rm NC}^{\rm SM} = gJ_3^\mu W_{3\mu} + g'J_Y^\mu B_\mu \tag{2.1}$$

where g, g' are $SU(2)$ and $U(1)_Y$ gauge couplings, $W_{3\mu}$ is gauge boson associated with diagonal generator of $SU(2)$, B_μ is the $U(1)_Y$ gauge boson. The currents in this gauge basis are given by

$$\begin{aligned} J_3^\mu &= \sum_i \bar{f}_i\gamma^\mu[t_{3iL}P_L + t_{3iR}P_R]f_i \\ J_Y^\mu &= \sum_i \bar{f}_i\gamma^\mu[y_{iL}P_L + y_{iR}P_R]f_i \end{aligned} \tag{2.2}$$

f_i is the i^{th} fermion, t_{3i}, y_i are their 3rd component of weak isospin and hypercharge. For the known fermions, $t_{3u_L} = t_{3\nu_L} = 1/2$, $t_{3d_L} = t_{3e_L} = -1/2$, $t_{3i_R} = 0$

Observations require the spontaneous breaking of $SU(2)\times U(1)_Y$ to the subgroup electroweak $U(1)_{\rm EM}$. We can rotate by $\theta_W = arctan(g'/g)$ from the gauge eigenstates to mass eigenstates of photon field A_μ and Z_μ. Currents coupling to A_μ must reproduce the non-chiral electroweak coupling with the correct electric charge assigned to fermions. The neutral current interaction now becomes

$$\mathcal{L}_{\rm NC}^{\rm SM} = eJ_{em}^\mu A_\mu + g_1 J_1^\mu Z_{1\mu}^0 \tag{2.3}$$

where $e = g\sin\theta_W, g_1^2 = g^2 + g'^2$. The currents in this new basis are

$$\begin{aligned} J_{em}^\mu &= \sum_i q_i\bar{f}_i\gamma^\mu f_i \\ J_1^\mu &= \sum_i \bar{f}_i[\epsilon_L^1(i)P_L + \epsilon_R^1(i)P_R]f_i \end{aligned} \tag{2.4}$$

with chiral couplings

$$\epsilon_L^1(i) = t_{3iL} - \sin^2\theta_W q_i, \qquad \epsilon_R^1(i) = t_{3iR} - \sin^2\theta_W q_i \tag{2.5}$$

[1] I basically follow the conventions in [3]

electric charges are given by $q_i = t_{3iL} + y_{iL} = t_{3iR} + y_{iR}$.

When the SM electroweak group is extended by adding $U(1)'^n, n \geq 1$, neutral current interaction eq.(2.3) is generalized as

$$-\mathcal{L}_{\rm NC} = J^\mu_{em} A_\mu + \sum_{\alpha=1}^{n+1} g_\alpha J^\mu_\alpha Z^0_{\alpha\mu} \tag{2.6}$$

where quantities labelled by 1 in the sum are the SM contribution. The currents are given by

$$J^\mu_\alpha = \sum_i \bar{f}_i [\epsilon^\alpha_L(i) P_L + \epsilon^\alpha_R(i) P_R] f_i \tag{2.7}$$

where the chiral couplings $\epsilon^\alpha_{L,R}$ are model-dependent.

If the SM Higgs is charged under $U(1)_\alpha$ with charge $Q_{\alpha i}$, Z' can couple to Higgs ϕ_i via covariant derivative:

$$D_\mu \phi_i = \left(\partial_\mu + ieq_i A_\mu + i \sum_{\alpha=1}^{n+1} g_\alpha Q_{\alpha i} Z^0_{\alpha\mu} \right) \phi_i \tag{2.8}$$

Eq.(2.8) has an important implication on the SM Z mass since it introduces mass mixings between different Zs:

$$\mathcal{L}^{mass}_Z = \frac{1}{2} M^2_{\alpha\beta} Z^0_{\alpha\mu} Z^{0\mu}_\beta \tag{2.9}$$

with

$$M^2_{\alpha\beta} = 2 g_\alpha g_\beta \sum_i Q_{\alpha i} Q_{\beta i} |\langle \phi_i \rangle|^2 \tag{2.10}$$

$M_{11} \equiv M^2_{Z^0} = \frac{1}{2} g_1^2 \sum_i |\langle \phi_i \rangle|^2 = \frac{1}{4} g_1^2 v^2$ is the tree-level Z mass in the SM limit when all the Z' are decoupled, where $v^2 = (\sqrt{2} G_F)^{-1} \sim (246\,\text{GeV})^2$. To get a concrete idea of what the mass mixing looks like, let us take $n = 1$, i.e. add one Z' only.The mass matrix would be:

$$M^2_{Z-Z'} = \begin{pmatrix} 2g_1^2 \sum_i t^2_{3i} |\langle \phi_i \rangle|^2 & 2 g_1 g_2 \sum_i t_{3i} Q_i |\langle \phi_i \rangle|^2 \\ 2 g_1 g_2 \sum_i t_{3i} Q_i |\langle \phi_i \rangle|^2 & 2 g_2^2 \sum_i Q_i^2 |\langle \phi_i \rangle|^2 \end{pmatrix} \equiv \begin{pmatrix} M^2_{Z^0} & \Delta^2 \\ \Delta^2 & M^2_{Z'} \end{pmatrix} \tag{2.11}$$

The mass eigenvalues can be obtained by diagonalizing the mass matrix:

$$M_{1,2}^2 = \frac{1}{2}\left[M_{Z^0}^2 + M_{Z'}^2 \mp \sqrt{(M_{Z^0}^2 - M_{Z'}^2)^2 + 4\Delta^4}\right] \tag{2.12}$$

Obviously the mixing with Z' can shift the SM prediction for Z boson mass at tree-level. Therefore the Z' sector parameters are constrained by precision electroweak measurements[5].

Even though the $U(1)'$ is unbroken or the SM fields are singlets under the $U(1)'$, there is still a way of mixing Z' with the SM Z gauge boson and therefore coupling it to other SM fields–through *kinetic mixing*. It is worth mentioning that such mixing is unique for abelian groups, where the field strength tensor $F_{\mu\nu}$ is gauge invariant and therefore allowed. Consider the most general kinetic energy term for two gauge bosons $Z_{\alpha\mu}^0$ and $Z_{\beta\mu}^0$ in the gauge basis:

$$\mathcal{L}_{kin} = -\frac{c_\alpha}{4}F_\alpha^{0\mu\nu}F_{\alpha\mu\nu}^0 - \frac{c_\beta}{4}F_\beta^{0\mu\nu}F_{\beta\mu\nu}^0 - \frac{c_{\alpha\beta}}{2}F_\alpha^{0\mu\nu}F_{\beta\mu\nu}^0 \tag{2.13}$$

By rescaling, one can always transform the coefficients in eq.(2.13) into the canonical form $c_\alpha = 1, c_\beta = 1, c_{\alpha\beta} = \sin\chi$. The canonical diagonal kinetic energy terms can be obtained with another non-unitary rotation V:

$$\begin{pmatrix} Z_{1\mu}^0 \\ Z_{2\mu}^0 \end{pmatrix} = \begin{pmatrix} 1 & -\tan\chi \\ 0 & 1/\cos\chi \end{pmatrix} \begin{pmatrix} \hat{Z}_{1\mu}^0 \\ \hat{Z}_{2\mu}^0 \end{pmatrix} \equiv V \begin{pmatrix} \hat{Z}_{1\mu}^0 \\ \hat{Z}_{2\mu}^0 \end{pmatrix} \tag{2.14}$$

With this additional kinetic mixing, the mass matrix derived from mass mixing (eq.(2.11)) becomes $V^T M_{Z-Z'}^2 V'$, which needs to be diagonalized by an orthogonal rotation. But in order to see the essential feature of kinetic mixing, we can turn off pure mass mixing, i.e. set $\Delta = 0$ in eq.(2.11). We have

$$V^T M_{Z-Z'}^2 V = \begin{pmatrix} M_{Z^0}^2 & -M_{Z^0}^2\tan\chi \\ -M_{Z^0}^2\tan\chi & M_{Z^0}^2\tan^2\chi + M_{Z'}^2/\cos\chi \end{pmatrix} \tag{2.15}$$

We can see that in the limit $M^2_{Z^0} = 0$ there is a zero mass eigenvalue even for large mixing χ, i.e. the shift in the lighter mass induced by kinetic mixing is proportional to the lighter mass and therefore small. To be more concrete, for $|M^2_{Z^0} \ll M^2_{Z'}|, \Delta = 0, \chi \ll 1$, one gets $M^2_1 \sim M^2_{Z^0} - M^4_{Z^0}\chi^2/M^2_{Z'}$, which is a negligible shift.

2.2 Phenomenology of Hidden Sector Higgs and its LHC Signals

The phenomenology of Z' gauge boson induced by the mass mixing and kinetic mixing as we discussed in the previous section has been well studied[5]. In our work presented in [6] we focused on the phenomenology of the other 'portal' coupling between the SM and a symmetry-breaking hidden sector which applies to more general hidden gauge structure (not just Abelian groups): the renormalizable interaction of the SM Higgs with the hidden sector Higgs boson. There are few ways that the SM fields can interact with the hidden sector or phantom sector fields, and the Higgs boson, which can form a gauge-invariant dimension-2 operator all on its own, is a prime candidate to pursue this connection [8, 9, 10, 11, 12].

Concretely, the analysis in this work is based on the model presented in [8], where the SM Higgs Φ_{SM} couples to a hidden scalar Φ_H through the renormalizable term $|\Phi_{SM}|^2|\Phi_H|^2$. We also assume that the hidden sector has a rich gauge theory structure which is at least partly broken by $\langle\Phi_H\rangle \neq 0$. A nontrivial vev of Φ_H is necessary for the mass mixing between the SM Higgs and Φ_H, which results in two mass eigenstates, h, H. It is this mixing that brings in the two possible distinct signatures at the LHC which are of primary interest in this work: a narrow width trans-TeV Higgs boson and the observable $H \to hh$ decay.

Here is the outline of what follows. In section 2.2.1, we give a brief review of the model we will analyze. In section 2.2.2, we study the bounds on Higgs masses for this model, based on the considerations of perturbative unitarity, triviality and precision

electroweak measurements. We find that the canonical constraints on the upper limit of the Higgs mass do not apply for the heavier Higgs boson H because of the mixing effect. Based on the results of the earlier sections, we propose two possible intriguing features to be probed at future colliders: narrow trans-TeV Higgs boson and $H \to hh$ decay width. In section 2.2.3, we study the LHC implications of those two signatures in detail and demonstrate that they can be distinguishable and therefore shed new light on beyond SM physics.

2.2.1 Model Review

To be self-contained, we first briefly review the model in [8], which sets the framework and notation for what we analyze here. We assume that there is a hidden $U(1)$ gauge symmetry which is broken by a vacuum expectation value (vev) of the Higgs boson Φ_H. We denote the $U(1)_{hid}$ gauge boson as V, which gets a mass m_V after the breaking of $U(1)_{hid}$. In this model, the hidden sector Higgs boson Φ_H mixes with the SM Higgs Φ_{SM} through a renormalizable interaction $|\Phi_{SM}|^2|\Phi_H|^2$. The Higgs boson Lagrangian[2] under consideration is

$$\mathcal{L}_{Higgs} = |\mathcal{D}_\mu \Phi_{SM}|^2 + |\mathcal{D}_\mu \Phi_H|^2 + m^2_{\Phi_{SM}}|\Phi_{SM}|^2 + m^2_{\Phi_H}|\Phi_H|^2 - \lambda|\Phi_{SM}|^4 - \rho|\Phi_H|^4 - \eta|\Phi_{SM}|^2|\Phi_H|^2 \tag{2.16}$$

The component fields are written as

$$\Phi_{SM} = \frac{1}{\sqrt{2}} \begin{pmatrix} \phi_{SM} + v + iG^0 \\ G^\pm \end{pmatrix}, \quad \Phi_H = \frac{1}{\sqrt{2}}(\phi_H + \xi + iG') \tag{2.17}$$

where $v(\simeq 246\,\mathrm{GeV})$ and ξ are vevs around which the Φ_{SM} and Φ_H are expanded. The G fields are Goldstone bosons, which can be removed from actual calculation by imposing the unitary gauge. After diagonalizing the mass matrix, we rotate from the

[2] Although we do not discuss it specifically in this work, there is an analogous supersymmetric construction where the two Higgs fields interact via a D-term from a shared $U(1)$ symmetry [8].

gauge eigenstates ϕ_{SM}, ϕ_H to mass eigenstates h, H.

$$\phi_{SM} = \cos\omega h + \sin\omega H \tag{2.18}$$

$$\phi_H = -\sin\omega h + \cos\omega H \tag{2.19}$$

the mixing angle ω and the mass eigenvalues are given by

$$\begin{aligned} \tan\omega &= \frac{\eta v\xi}{(-\lambda v^2+\rho\xi^2)+\sqrt{(\lambda v^2-\rho\xi^2)^2+\eta^2v^2\xi^2}} \\ m^2_{h,H} &= (\lambda v^2+\rho\xi^2)\pm\sqrt{(\lambda v^2-\rho\xi^2)^2+\eta^2v^2\xi^2} \end{aligned} \tag{2.20}$$

For simplicity in writing subsequent formula, we assume that $m_h < m_H$ and write $c_\omega \equiv \cos\omega$, $s_\omega \equiv \sin\omega$.

If $m_H > 2m_h$, the signature of interest, $H \to hh$ decay, is allowed kinematically. The partial width of this decay is

$$\Gamma(H\to hh) = \frac{|\mu|^2}{8\pi m_H}\sqrt{1-\frac{4m_h^2}{m_H^2}} \tag{2.21}$$

where μ is the coupling of the relevant mixing operator in the Lagrangian $\triangle\mathcal{L}_{mix} = \mu h^2 H$.

$$\mu = -\frac{\eta}{2}(\xi c_\omega^3 + v s_\omega^3) + (\eta-3\lambda)vc_\omega^2 s_\omega + (\eta-3\rho)\xi c_\omega s_\omega^2 \tag{2.22}$$

Before going to the discussion of the Higgs mass bounds, it is helpful to do a parameter space analysis for this model. There are a total of 7 input parameters relevant for most of our later discussion: $g, \lambda, v, \eta, \rho, \xi, g_V$, where g is the $SU(2)_L$ gauge coupling, g_V is defined to be the gauge coupling constant of $U(1)_{hid}$. g_V in general would appear in the scattering amplitude of the graphs involving the $U(1)_{hid}$ gauge boson V, and therefore play a role in the discussion of perturbative unitarity (however, in section 3.1, we will make a reasonable assumption that results in g_V effectively disappearing in all the relevant formulae). Other possible input parameters that describe the details of the matter content of the hidden sector itself are uncertain and we do not include them here (in our work, they are only relevant to the RGE of ρ, where

we just introduce two representative parameters E and E'). g, v are already fixed by collider experiments, with the values $v = 246\text{GeV}$, $g = 0.65$. In order to study the phenomenology of the model, we construct some output parameters from these input parameters which are of more physical interest: $m_W, G_F, m_h, s_\omega, m_V, G_F^{'}, m_H, \mu$, where we define $G_F^{'}$ as the Fermi coupling for the $U(1)_{hid}$ defined in the same way as G_F in the SM. We will see in section 3.1 that $G_F^{'}$ plays an important role in the unitarity bounds. The relevant transformations in addition to eqs. (2.20)-(2.22) are:

$$m_W = \frac{1}{2}gv, \quad m_V = \frac{1}{2}g_V\xi, \quad G_F = \frac{1}{\sqrt{2}v^2}, \quad G_F^{'} = \frac{1}{\sqrt{2}\xi^2}. \tag{2.23}$$

Now we have determined that the 4 most important unknown input parameters are $\{\lambda, \rho, \eta, \xi\}$. The inverse transformation from $\{m_h^2, m_H^2, s_\omega, \mu\}$ to $\{\lambda, \rho, \eta, \xi\}$ are

$$\lambda = \frac{M_{11}^2}{2v^2} \tag{2.24}$$

$$\rho = \frac{M_{22}^2}{2v^2 s_\omega^2}\left[\frac{c_\omega^3 M_{12}^2 + 3c_\omega^2 s_\omega M_{11}^2 - 2c_\omega s_\omega^2 M_{12}^2 + 2\mu v}{-2c_\omega^2 M_{12}^2 + 3c_\omega s_\omega M_{22}^2 + s_\omega^2 M_{12}^2}\right]^2 \tag{2.25}$$

$$\eta = -\frac{M_{12}^2}{s_\omega v^2}\left[\frac{c_\omega^3 M_{12}^2 + 3c_\omega^2 s_\omega M_{11}^2 - 2c_\omega s_\omega^2 M_{12}^2 + 2\mu v}{-2c_\omega^2 M_{12}^2 + 3c_\omega s_\omega M_{22}^2 + s_\omega^2 M_{12}^2}\right] \tag{2.26}$$

$$\xi = s_\omega v\left[\frac{-2c_\omega^2 M_{12}^2 + 3c_\omega s_\omega M_{22}^2 + s_\omega^2 M_{12}^2}{-cw^3 M_{12}^2 - 3c_\omega^2 s_\omega M_{11}^2 + 2c_\omega s_\omega^2 M_{12}^2 - 2\mu v}\right] \tag{2.27}$$

where

$$M_{11}^2 = c_\omega^2 m_h^2 + s_\omega^2 m_H^2 \tag{2.28}$$

$$M_{12}^2 = c_\omega s_\omega (m_H^2 - m_h^2) \tag{2.29}$$

$$M_{22}^2 = s_\omega^2 m_h^2 + c_\omega^2 m_H^2 \tag{2.30}$$

In Tables 2.1 and 2.2 we provide 6 benchmark points in the parameter space, some of which will be used in section 4 for collider physics analysis. They all can satisfy the theoretical bounds as we shall see in section 3. We list them in Table 2.1 and Table 2.2.

$\Gamma(H \to hh)$ for points 1, 2, 3 are obtained based on the assumption that the

	Point A	Point B	Point C
s^2_ω	0.40	0.31	0.1
m_h (GeV)	143	115	120
m_H (GeV)	1100	1140	1100
$\Gamma(H \to hh)$ (GeV)	14.6	4.9	10
$BR(H \to hh)$	0.036	0.015	0.095

Table 2.1. Points illustrating parameters of trans-TeV mass Higgs boson. Point C is studied in detail in section 4.

	Point 1	Point 2	Point 3
s^2_ω	0.5	0.5	0.5
m_h (GeV)	115	175	225
m_H (GeV)	300	500	500
$\Gamma(H \to hh)$ (GeV)	2.1	17	17
$BR(H \to hh)$	0.33	0.33	0.33

Table 2.2. Points illustrating parameters that allow large branching fractions of $H \to hh$. Each of these points are studied in detail in section 4.

branching ratio BR($H \to hh$) = 1/3 where BR= $\frac{\Gamma(H\to hh)}{\Gamma(H\to hh)+s^2_\omega \Gamma^{SM}(m_H)}$. $\Gamma^{SM}(m_H)$ is the well-known SM result, which can be obtained from the HDECAY program [13].

2.2.2 Theoretical Bounds on Higgs Masses of the Model

Perturbative Unitarity Constraints

The possibility of a strongly interacting WW sector or Higgs sector above the TeV scale is an interesting alternative to a perturbative, light Higgs boson. However, this possibility implies the unreliability of perturbation theory. Although this is not a fundamental concern, it would imply a challenge to the successful perturbative description of precision electroweak data and would have major implications to LHC results. In order for the perturbative description of all electroweak interactions to be valid up to a high scale, the perturbative unitarity constraint would need to be satisfied. This issue has been carefully studied for the SM Higgs sector[14]. They obtained an upper bound on the Higgs mass by imposing the partial-wave unitarity

condition on the tree-level amplitudes of all the relevant scattering processes in the limit $s \to \infty$, where s is the center of mass energy. The result is $m^2_{\phi_{SM}} \leq \frac{4\pi\sqrt{2}}{3G_F} \simeq (700\ \text{GeV})^2$. To get this result, we apply a more restrictive condition as in [15]: $|Rea_J| \leq \frac{1}{2}$, where a_J is the J^{th} partial wave amplitude. This is also the condition we will apply for our model.

We derive the unitarity constraints for our model by methods analogous to ref. [14]. The addition of one more Higgs and the mixing effects introduce more relevant processes and more complex expressions. We impose the unitarity constraints on both the SM sector and the $U(1)_{hid}$ sector. The analysis for the diagrams involving V is very similar to those involving the Z boson. For simplicity, we assume that in the hidden sector, $m_V \ll m_H$, as an analogy to the case in the SM, where $m_W \ll m_H$. With this approximation, g_V will not appear in the scattering amplitude, only G'_F is relevant. We list the set of 15 inequalities in the Appendix, and their corresponding processes. For simplicity, we did not transform them to purely input or output parameter basis, but kept them in a mixing form as they were derived for compact expressions. Unlike the situation in the SM, it would be hard to solve this complex set of inequalities analytically to get the Higgs mass bounds. Instead using the Monte Carlo method, we generated $60^4 \sim 10^7$ points in the input parameter space with basis $\{\lambda, \eta, \rho, \xi\}$. In order to be consistent with our discussion of perturbative TeV physics, we liberally set the allowed regions of these input parameters to be:

$$\lambda \in [0, 4\pi], \rho \in [0, 4\pi], \eta \in [-4\pi, 4\pi], \xi \in [0, 5\,\text{TeV}] \tag{2.31}$$

Then we pick out the points that satisfy all 15 inequalities, and make $m_H - m_h$ plots for certain narrow ranges of the mixing angle s^2_ω which is an important output parameter for collider physics study. The allowed region can be read from the shape of these plots (obviously, for this multi-dimension parameter space, the bounds on Higgs mass are dependent on the mixing angle).

Fig. 2.1 combines the plots for 3 typical mixing regions – small mixing, medium

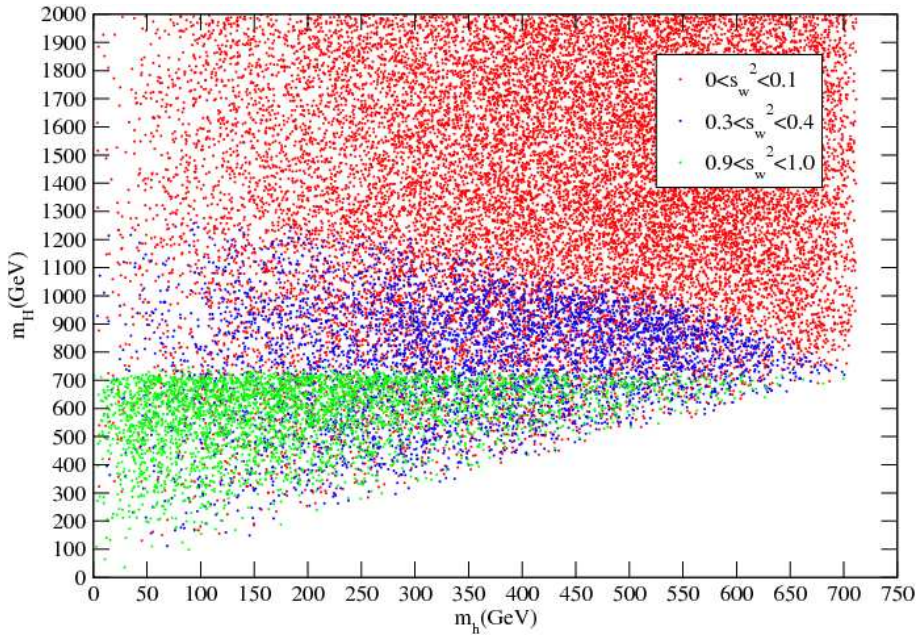

Figure 2.1. Scatter plot of solutions in the m_H vs. m_h plane that satisfies perturbative unitarity constraints. Separate colors are used depending on what range s_ω^2 falls within.

mixing and large mixing for comparison. We can tell that for the lighter physical Higgs boson mass, the upper bound always stays the same as the well-known SM case—around 700 GeV. However, for the heavier Higgs boson in the spectrum, the bound is loosened: for small mixing it can be as high as 15 TeV given our parameter ranges (in Fig. 2.1, we cut the upper limit at 2 TeV to reduce the size of the graph as well as improve the presentability of the graph), for medium mixing can be above 1 TeV — both are well above the canonical upper limit of the Higgs boson mass based on unitarity considerations. For large mixing limit, the canonical 700 GeV bound applies for both of the physical Higgs. These observations agree with our intuition. The intermediate mixing region is of significant phenomenological interest, since it can not only generate a heavy Higgs boson — especially a trans-TeV Higgs which is not well anticipated by the experiments, yet may be worth attention — but also can produce the heavy Higgs boson at a considerable production rate at colliders (we know that the coupling of H to SM particles is proportional to s_ω). That is why we amplify the plot for the medium mixing region in Fig. 2.2 to demonstrate the bound

shape more clearly. Meanwhile, the small mixing region can also be interesting, since as s_ω decreases, the decay width narrows down which is good for detection, although the production rate gets lower.

Based on the considerations described above, we choose 3 typical points from those that are allowed by all the perturbative unitarity bounds and that can generate a trans-TeV Higgs: points A, B and C, as we listed in Table 1 at the end of section 2. They are labelled by the output parameter basis $\{s^2_\omega, m_h, m_H, \Gamma(H \to hh)\}$. Point A and B are from medium mixing region ($s^2_\omega = 0.40$ for point A is actually the maximum mixing angle that can allow a m_H larger than 1.1 TeV among all the points that satisfy unitarity constraints), point C is from the small mixing region. We will make precision electroweak analysis for these 3 points in section 3.3 and study the collider physics of trans-TeV Higgs bosons in section 4.1.

Triviality bounds and Vacuum Stability Bounds

Besides perturbative unitarity, triviality and vacuum stability are two additional concerns which impose theoretical constraints on the Higgs mass. Now we want to see if they would put more stringent bounds on the Higgs mass than those given by unitarity. In the SM, both of them are actually relevant to the properties of the parameter λ at the high scale, which are analyzed using the RG equation of λ. The triviality bound is given based on the requirement that the Landau pole of λ from the low-scale theory perspective is above the scale of new physics. The vacuum stability bound is given based on the requirement that λ remains positive up to the scale of new physics. Now we already can see that the bounds derived from these two considerations are not definite, as they depend on the scale of new physics. In the SM, the bounds for the value of λ at the electroweak scale are equivalent to the upper and lower limits for the Higgs boson because of the simple proportion relation $m^2_{\Phi_{SM}} = 2\lambda v^2$, where $v \simeq 246\,\mathrm{GeV}$. As reviewed in [16], for a 1 TeV new physics scale, $160\,\mathrm{GeV} < m_H < 750\,\mathrm{GeV}$. (This is actually a rough estimation based on

1-loop RGE and without taking into threshold corrections. More accurate analysis would be subtle.) However, it is easy to tell that these constraints do not apply for our model where the physical Higgs spectra are determined by four input parameters λ, η, ρ, ξ, not just λ. Therefore, we need to first derive the RG equations for all these four parameters and see what we can say for the Higgs mass bounds based on them.

Here we give the 1-loop results. For convenience, we suppose that the RGEs run above the EWSB scale, so that all the masses are zero and we can safely work with gauge eigenstates. (Actually, as is well known, the RGEs of dimensionless couplings are independent of mass parameters, which supports the validity of our assumption.)

1-loop RGE for λ in the SM can be found in [15]. The addition of the hidden sector Higgs boson contributes another term to the RGE, which results from the mixing term in the Lagrangian $\frac{1}{4}\eta\phi_H^2\phi_{SM}^2$ (ϕ_H runs in the loop). The full result is:

$$\frac{d}{dt}\lambda = \frac{1}{16\pi^2}\left\{\frac{1}{2}\eta^2 + 12\lambda^2 + 6\lambda y_t^2 - 3y_t^4 - \frac{3}{2}\lambda(3g^2 + g_1^2) + \frac{3}{16}[2g^4 + (g^2 + g_1^2)^2]\right\} \tag{2.32}$$

where g_1 is the gauge coupling of $U(1)_Y$, y_t is the top Yukawa coupling. The first term comes from the interaction between ϕ_H and ϕ_{SM}.

For ρ, there is also a 1-loop contribution from the graph where ϕ_{SM} runs in the loop. The other terms in the RGE of ρ come from the self-interactions in the hidden sector, e.g. the coupling between ϕ_H and the hidden sector matter—we denote all these terms by E. The result is

$$\frac{d}{dt}\rho = \frac{1}{16\pi^2}(\eta^2 + 10\rho^2 + E) \tag{2.33}$$

The RGE of η involves only two graphs: with ϕ_{SM} or ϕ_H running in the loop. We eventually get:

$$\frac{d}{dt}\eta = \frac{1}{16\pi^2}\eta\left[6\lambda + 4\rho + 2\eta + 3y_t^2 - \frac{3}{4}(3g^2 + g_1^2) + E'\right] \tag{2.34}$$

We can see from eqs.(2.32)-(2.34) that the perturbative properties of λ, ρ and η can be nice although they are model dependent. However, we can hardly draw any

quantitative conclusions regarding, especially, the Higgs masses bounds – they depend on four unknown parameters, the detailed content of hidden sector matter represented by parameters E and E' (analogous to the definition for E, E' comes from the coupling between ϕ_h and other matter fields in the hidden sector), threshold corrections, etc. All of these uncertainties make the prediction for the triviality and stability bounds quite model dependent. Meanwhile, such large freedom allows us to reasonably expect that the points that satisfy the unitarity conditions are also allowed by triviality and stability constraints in a large region of full parameter space (with parameters for hidden sector itself included). A practical application of this observation is that now we can reasonably assume that the points from section 3.1 can also pass the test of triviality and vacuum stability.

Contraints from Precision Electroweak Measurements

Precision electroweak measurements also give indirect bounds on the Higgs boson mass based on the fact that the virtual excitations of the Higgs boson can contribute to physical observables, e.g. W boson mass, considered in precision tests of the SM. For the one doublet Higgs boson in the SM, precision EW analysis puts a 200 GeV upper limit at 95% C.L [17]. Here we do not plan to make a full analysis to derive the mass bounds in a general way. Alternatively, we focus on the point A, B and C, of which we have made an $S - T$ analysis to see if they can satisfy the constraints from experiments. This is actually a way to check for our model the 'existence' of the points allowed by precision EW measurements.

The relevant calculations are analogous to those for the SM Higgs boson. We just need to double the number of involved graphs, since there are two Higgs bosons now, and put s_ω or c_ω on some vertices. The resulting values for S and T for points A, B

and C are consistent with [17]:

$$\text{A} : (S,T) = (0.05, -0.10), \quad \text{B} : (S,T) = (0.02, -0.06), \quad \text{C} : (S,T) = (-0.01, -0.01) \tag{2.35}$$

and

$$1 : (S,T) = (0.01, -0.03), \quad 2 : (S,T) = (0.05, -0.07), \quad 3 : (S,T) = (0.06, -0.09) \tag{2.36}$$

where we have chosen $m_H = 150$ GeV as the SM reference point where $(S,T) = (0,0)$. We compare these results with the $S-T$ contour in [17] which gives the constraints on (S,T) from the most recent precision electroweak measurements. Point C is on the boundary of the allowed region, and therefore satisfies the precision EW constraints. Points 1-3, A and B seem to be mildly out of the 68% C.L. allowed region. According to the direction of their shifts relative to the center of the contour, they have the same effects as a heavy Higgs in the SM. However, contributions from the unspecified elements of the model – in particular the Z' contributions – can compensate the effect of a heavy Higgs by pulling the (S,T) back towards the center[18]. It is easy to tell that such a solution could also apply to our model by the Z' from its $U(1)_{hid}$ hidden sector gauge symmetry.

Therefore, now we can come to the conclusion that all the three interesting points can satisfy all the known theoretical bounds on Higgs mass under a few reasonable assumptions. The next step is to send them to the collider physics analysis so that we can tell whether we can discover such interesting phenomenology in future experiments.

2.2.3 Large Hadron Collider Studies

In this section, we consider phenomenological implications for new physics searches at the LHC. In our framework, we have two Higgs bosons that are in general mixtures of a SM Higgs boson and a Higgs boson that carries no charges under the SM gauge

groups. Thus, no state is precisely a SM Higgs boson and no state is precisely of a singlet nature. More importantly, by construction, neither H nor h have full SM Higgs couplings to any state in the SM. Production rates are therefore always reduced for h or H compared to the SM Higgs.

Reduced production cross-sections present a challenge for LHC discovery and study. Depending on the mass of the SM Higgs boson, there are already significant difficulties for discovery without the additional worry of reduced couplings. Nevertheless, opportunities present themselves as well. For one, the reduced production cross-section also correlates with a more narrow-width scalar state. The width of the SM Higgs boson grows so rapidly with its mass (by cubic power) that by the time its mass is above $\sim 800\,\text{GeV}$ the Higgs boson width is so large that it begins to lose meaning as a particle. Reduced couplings, and therefore a reduced width, of a heavy Higgs boson can bring it into the fold of familiar, narrow-width particles. We study this point below to demonstrate that even a Higgs boson with mass greater than 1 TeV (i.e., a trans-TeV Higgs boson) can be searched for and found at the LHC in this scenario.

Another attempt at turning a negative feature into a new angle for searching, is to accept that two heavily mixed Higgs states could exist, and search for the decay of the heavier one to the lighter. These $H \to hh$ decays could be copious enough that the first discovery of the Higgs boson would be through the simultaneous discovery of H and h via H production followed by $H \to hh$. We studied this possibility at the LHC and find that indeed this may be possible.

To begin the discussion, we first stated some of the choices we made to simulate LHC physics. We have used Madgraph [19] to generate all matrix elements. We then use MadEvent [20], with the CTEQ6 [21] PDF set, to generate both signal and background event samples for all the studies in this work. Renormalization and factorization scales are set to m_H for calculating signal cross-sections.

To partially simulate detector and showering effects, parton energies are smeared by a gaussian function of width $\sigma/E = 0.68/\sqrt{E} \oplus 0.044$ (E is in units of GeV), from Table 9-1 in [22]. Photon and lepton energies are not smeared. We assume a b-tagging efficiency of 50% and mistag rates for c,g, and uds partons of 10%, 1.5%, and 0.5%, respectively. All jets are required to have $p_T > 30$ GeV and $|\eta| < 4.5$, where η here refers to the pseudo-rapidity ($\eta = -\ln\tan(\theta/2)$ with θ being the polar angle with respect to the beam). Leptons and photons are required to be separated from jets by ΔR>0.4 and from one another by ΔR>0.2, where $\Delta R = \sqrt{(\Delta\eta)^2 + (\Delta\phi)^2}$ (ϕ is the azimuthal angle). Jets must be separated from each other by ΔR>0.7, or they are merged. We do not apply any triggering or reconstruction efficiencies.

Narrow Trans-TeV Higgs boson

Earlier we showed that a very heavy Higgs boson can be compatible with all known constraints. Its couplings will necessarily be less than those of the SM Higgs boson, but if it is mixed with the SM Higgs boson, the mass eigenstate H can be searched for and discovered even if its mass is above 1 TeV. We show here that a very narrow resonance, which is implied by the reduced couplings, may enable background normalizations to be determined using sideband techniques which are not possible with the very large widths for heavy SM Higgs bosons.

As we do not consider decays to new particles, the final state topologies are the same as the searches investigated for 1 TeV Higgs bosons (see [23]), though the cross-sections and width are both reduced by $\sin^2\omega$ compared to a SM Higgs of the same mass. We set $\sin^2\omega = 0.1$ and $M_H = 1.1$ TeV (see point C of Table 2.1). This leads to a width Γ_H=95 GeV and NLO cross-section σ_H= 7.1 fb for vector boson fusion. The comparison to SM values, which we augment to compute our decay widths and cross-section, are obtained from HDECAY [13] and [24].

We begin with a study of qqH production through vector boson fusion followed by $H \to WW \to \ell\nu jj$. The significant difference between previous SM studies [23]

and our study is that the reduced Higgs width allows for reducing systematic uncertainties in the measurement of background rates. We do not do a complete set of background calculations, but instead argue, based on the simulations we have done, that the normalizations for all backgrounds can be determined from mass reconstruction distributions.

We require one lepton (e,μ) with $p_T > 100$ GeV, $|\eta|$ <2.0 and missing energy transverse to the beam $\not{E}_T > 100$ GeV. We also require two "tagging" jets with $|\eta| >$ 2.0. Finally, we require the two highest p_T jets to have $p_T > 100$ GeV and reconstruct to within 20 GeV of the W mass. We relax the separation cut between these two jets to ΔR>0.3. (Reconstructing highly-boosted, hadronic W bosons has been studied [25].)

The $WWjj$ background is calculated with μ_F=μ_R=M_W. The W+4j background has not been simulated, but is not expected to have a kinematic shape which would complicate determining its normalization from data. The $t\bar{t}jj$ background is calculated with both scales set to M_{top}. We simulate $t\bar{t}jj$ such that the two jets from the production stage are explicitly the two tagging jets used in the analysis. While this is not a complete description of the $t\bar{t}$+n jet background, we wish only to make the point that there are no kinematic features that would complicate deriving its normalization from data. A more complete background analysis implies that full reconstruction and showering will not overwhelm the signal, as shown in ref. [23].

Fig. 2.3 shows the differential cross-section as a function of the invariant mass of the lepton, $\not{E}_T$ and two highest p_T jets. Below 900 GeV, the distribution is almost entirely background, allowing for an extraction of the W and $t\bar{t}$ normalizations. As the figure demonstrates, one can rather easily distinguish the trans-TeV Higgs boson from the background after all the cuts once there is enough data for the distribution to be filled. As expected, luminosity is critical. In this case, after all cuts, the integral of the signal from $1.0\,\mathrm{TeV} < M_{l\nu jj} < 1.3\,\mathrm{TeV}$ yields 12.8 events in $100\,\mathrm{fb}^{-1}$, while

the total background amounts to 7.7 events. For a more assured discovery and more accuracy on the Higgs boson mass, one would need more data. Nevertheless, this signal channel alone demonstrates the plausibility of discovering a Higgs boson in the trans-TeV mass region. Analysis of more decay channels, if these tantalizing results emerged, would further increase the significance and accuracy of discovery.

For example, a heavy Higgs boson that decays to WW with a sizeable branching fraction will also decay to ZZ, which can be used to increase the significance of the discovery and test the self-consistency of the theory. In this case we look at decays to two Z bosons which then decay to either $\ell\ell jj$ or $\ell\ell\nu\nu$. A mass reconstruction for the first case would yield a distribution similar in shape to Fig. 2.3, so we instead plot the transverse mass distribution for $\ell\ell\nu\nu$. This final state has the virtue of only one significant background ($ZZjj$) which is under better theoretical control than the Z+$\geq$4j background. Still, $ZZ \to \ell\ell jj$ has a larger rate, though a potentially large background from ZZ+$\geq$4j production, and should be considered as well.

We require same-flavor, opposite-sign leptons, each with $p_T > 100$ GeV and $|\eta| < 2.0$ which reconstruct to within 5 GeV of the Z mass. We also require two tagging jets with $|\eta| > 2.0$ and $\not{E}_T$ >100 GeV. The only significant SM background is from $ZZjj$ production. We calculate this background at LO using factorization and renormalization scales set to M_Z.

Fig. 2.4 shows the differential cross-section as a function of the transverse mass M_T, where $M_T^2 = 2\,|p_{T_{\ell\ell}}||\not{E}_T|\,(1-\cos\phi)$ and ϕ is the angle between the reconstructed leptonic Z and the $\not{E}_T$ in the transverse plane. The production cross-section and branching ratios are small enough in this model that this channel is not as important without large amounts of data, but the relatively small backgrounds and distinctive shape imply that it could be important for other models.

Fig. 2.4 demonstrates that the transverse mass variable is a good discriminator of signal to background as long as enough integrated luminosity is obtained at the

collider. The combination of this channel (and several others similar to it) with the $H \to WW$ results of the previous section increases the significance of discovery. In this particular example final state, there are 3.9 signal events compared to 1.4 background events in the transverse mass region $0.8\,\text{TeV} < M_T < 1.4\,\text{TeV}$ with $500\,\text{fb}^{-1}$. Discovering hidden sector Higgs theories with reasonable significance by adding up all possible channels[3] will come first at lower luminosity, but the results above indicate that careful checks of various final states and self-consistency are possible, albeit at a much higher luminosity stage of the collider. This would give us the opportunity to study the precise nature of the trans-TeV Higgs boson through its various branching fractions.

$H \to hh$ Signal

We now examine Higgs-to-Higgs decays, and consider whether these decays might be the first evidence for either the H or h boson [26] at the LHC. Although it might be possible to effectively search for both Higgs bosons when the heavier one is in the trans-TeV mass range, we focus on somewhat lighter Higgs boson masses in this section which clearly show the feasibility of this kind of search over much of parameter space.

We normalize $gg \to H$ production to the NNLO rates [27] of 10.3 pb and 5.7 pb for 300 GeV and 500 GeV SM Higgs bosons, respectively. VBF production is normalized to the NLO rates [28] of 1.3 pb and 0.54 pb for 300 GeV and 500 GeV SM Higgs bosons, respectively. Both cross-sections are then multiplied by $\sin^2\theta$=0.5 to obtain the production rates for H and h.

To begin with, let us suppose that the heavy and light Higgs mass eigenstates are $m_H = 300\,\text{GeV}$ and $m_h = 115\,\text{GeV}$, respectively (see point 1 of Table 2.2).

[3]There are many more channels to exploit, potentially including the ZZ channel arising from $gg \to H$ production. This could be a productive channel since tagging jets are not needed to reduce the $t\bar{t}X$ background.

Even if the 115 GeV mass eigenstate had full-strength SM couplings, its discovery is by no means easy. A SM Higgs with mass around 115 GeV relies principally on the $t\bar{t}h \to t\bar{t}b\bar{b}$ production channel as well as direct production $gg \to h \to \gamma\gamma$. If signal production is reduced by half (i.e., $\sin^2\omega = 1/2$) and/or background rates are greater than calculated, or systematic uncertainties prove larger than anticipated, the discovery of this lighter Higgs boson will require significantly more data. We consider the possibility that the lighter Higgs boson may be discovered instead through $H \to hh \to \gamma\gamma b\bar{b}$ decays. In our example point, as with all example points in this section, the branching ratio of $H \to hh$ is 1/3.

To determine the viability for discovery, we first calculate the background processes that could contribute to $\gamma\gamma b\bar{b}$ events in the SM. The factorization and renormalization scales (μ_F and μ_R) used for computing this background are set to the leading p_T jet in the event. The signal observable we define requires two photons and two jets, with at least one jet tagged as containing a b quark. We furthermore require $|m_h - m_{\gamma\gamma}| < 2$ GeV, $|m_h - m_{j_1 j_2}| < 20$ GeV, and $|m_H - m_{\gamma\gamma j_1 j_2}| < 20$ GeV. Fig. 2.5 shows the reconstructed invariant mass of the two photons and two jets with one b-tag.

The general strategy to extract the signal over SM background is the same as for the supersymmetric $H \to hh \to \gamma\gamma b\bar{b}$ search channel [29]. We argue here that this signature is important for a broad range of models. Although it is only considered important for supersymmetry scenarios with small $\tan\beta$, this decay channel looks to be important for a wide range of parameter space for Higgs-mixing scenarios because of its relatively high rate of triggering and narrow mass reconstruction.

As the numbers in Table 2.3 indicate, we find that signal-to-background ratios for both the single and double tag samples are sufficient for discovery. Even after detector triggering and reconstruction efficiencies are applied, there should still be enough events for a discovery in the first few years of data taking at the LHC. We thus

Channel	1 tag	2 tags
$H \to hh$	24	12
$\gamma\gamma bb$	0.4	0.2
$\gamma\gamma bc$	0.15	0.01
$\gamma\gamma bj$	1	0.009
$\gamma\gamma cc$	1.2	0.069
$\gamma\gamma cj$	3.6	0.042
$\gamma\gamma jj$	1.8	0.007
Total background	8.2	0.34

Table 2.3. Numbers of "$\gamma\gamma b\bar{b}$" (defined in the text) events for 30 fb^{-1} after applying all cuts with 1 or 2 b-tags required. Summation of charge conjugation is implied (e.g. b=b+$\bar{b}$) and j=u, d, s. The Higgs boson properties are those of point 1 in Table 2.

argue that, for this model, the light Higgs boson might be discovered through these $H \to hh \to \gamma\gamma b\bar{b}$ decays before appearing in the more conventional $t\bar{t}h$, $qq \to qqh$, or $gg \to h$ searches, especially if the systematics for those channels prove to be more challenging than expected.

If the lighter Higgs boson is above the $2m_W$ threshold, qualitatively new features of the signal develop that we explore now. For example, let us suppose that the lighter Higgs boson is 175 GeV and that the heavier Higgs boson mass is $m_H = 500\,\text{GeV}$, which allows $H \to hh$ decays with 1/3 branching fraction (see point 2 of Table 2.2). For this point we again have a reduction of 1/2 in the cross-section due to $s_\omega^2 = 1/2$.

In this case, the most common final state for $H \to hh$ decays will be four W bosons. This signature has been studied in the context of dihiggs production [30] but SM dihiggs production is on the order of 10-30fb [31]. In Higgs-mixing scenarios, $H \to hh$ production is generically an order of magnitude or two larger.

We divide the study up into two searches by the number of leptons in the final state. First, we require three leptons, where the opposite-sign pairs must have opposite flavor (OSOF). This follows the strategy in [30] for reducing the large $Z/\gamma W^\pm$ background. We also look at events with four leptons and demand that opposite-sign, same-flavor lepton pairs not reconstruct to within 5 GeV of M_Z. One could also use

Channel	σ (fb)	OSOF 3ℓ
$H \to hh \to WWWW$	920	56
$W^{\pm}W^{\pm}W^{\mp}$	109	5
$t\bar{t}Z$	580	1
$t\bar{t}W^{\pm}$	740	15

Table 2.4. Numbers of 3ℓ OSOF events for 30 fb^{-1}. The Higgs boson properties are those of point 2 in Table 2.

same-sign (SS) dilepton searches, but the backgrounds are significantly larger and more difficult to predict so we do not explore this here.

$W^{\pm}W^{\pm}W^{\mp}$ samples are all generated at $\mu_F = \mu_R = M_W$. The $t\bar{t}Z$ and $t\bar{t}W$ samples are generated with $\mu_F = \mu_R = M_{top} = 175$ GeV. All backgrounds are generated at LO and no K-factors are applied. A $\not{E}_T > 50$ GeV cut has been applied to all searches. Leptons that do not satisfy $p_T > 20$ GeV and $|\eta| < 2.0$, or are not isolated from other leptons or jets, are considered lost. $Z/\gamma W^{\pm}$ with $Z/\gamma \to \tau\bar{\tau}$ has been investigated for the OSOF 3ℓ and found to be small.

Table 2.4 shows the number of OSOF 3ℓ events expected for 30 fb^{-1}. The dominant $t\bar{t}W$ background may have large NLO corrections, but applying a b-jet veto would further reduce it by approximately 64%, while reducing the signal by only a few percent. Additionally, there are 8 four-lepton events which could be used.

For comparison, in this model we expect 9 $H \to ZZ \to 4\ell$ events for 30 fb^{-1} satisfying the lepton cuts described above, with each opposite-sign, same-flavor pair reconstructing to within 5 GeV of M_Z, and satisfying $|M_H - m_{4\ell}| < \Gamma_H$, where Γ_H=51 GeV. For the same cuts, the irreducible $pp \to ZZ$ background yields 8 events, using $\mu_F = \mu_R = M_Z$ and applying no K-factors.

Based on the numbers in Table 2.4, we argue that, for this model, the heavier Higgs boson can be discovered through the $H \to hh \to$ OSOF 3 ℓ channel in the first few years at the LHC. Furthermore, this channel may compete with more conventional searches, such as $H \to ZZ \to 4\ell$ for an early discovery.

Finally, we comment on the situation of point 3 in Table 2.2 where the lighter Higgs is heavier than $2M_Z$. In this case, the branching ratios to $WWZZ$ and $ZZZZ$ can be significant. For example, using the same parameters as above, if the mass of the lighter Higgs is raised to 225 GeV, the cross-sections for $H \to hh \to WWZZ$ and $H \to hh \to ZZZZ$ are 425 fb and 87 fb. The $WWWW$ final state is still the largest branching ratio, but other searches involving Z boson final states would aid discovery.

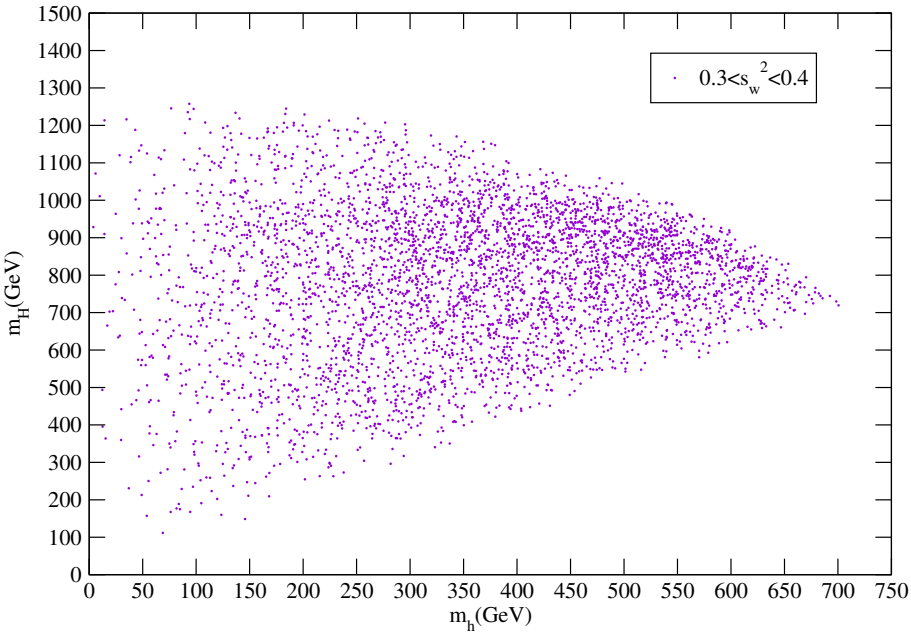

Figure 2.2. Scatter plot of solutions in the m_H vs. m_h plane that satisfies perturbative unitarity constraints. This plot is only for points that fall within $0.3 < s_\omega^2 < 0.4$.

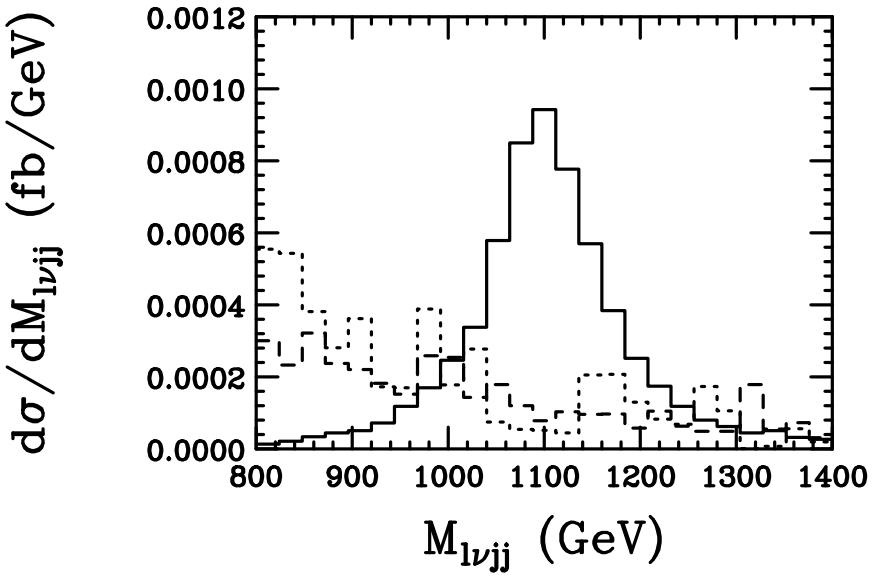

Figure 2.3. Differential cross-section as a function of the invariant mass of the ℓ, $\not{E}_T$ and two jets reconstructing to the W mass for $H \to WW \to \ell\nu jj$ (solid), $WWjj$ (dashed), and $t\bar{t}jj$ (dotted).

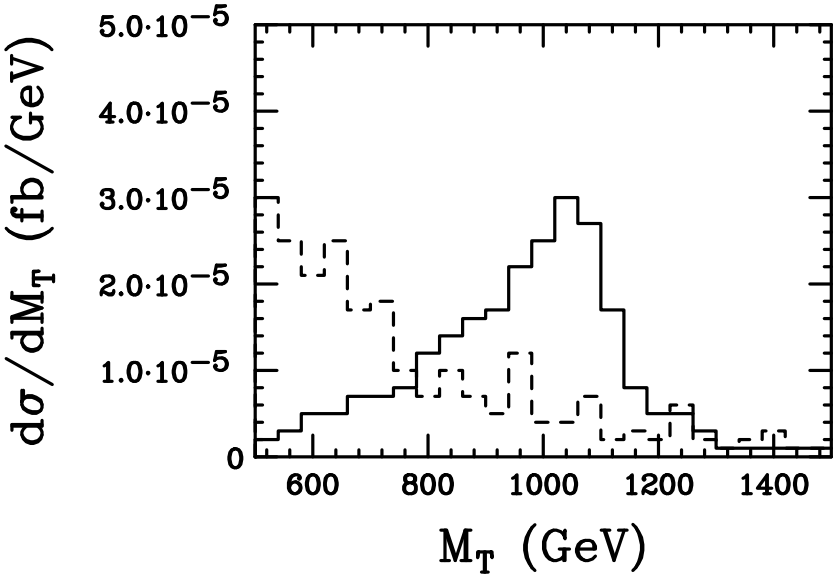

Figure 2.4. Differential cross-section as a function of transverse mass of the Z and $\not{E}_T$ for $H \to ZZ \to \ell\ell\nu\nu$ (solid) and the $ZZjj$ background (dashed).

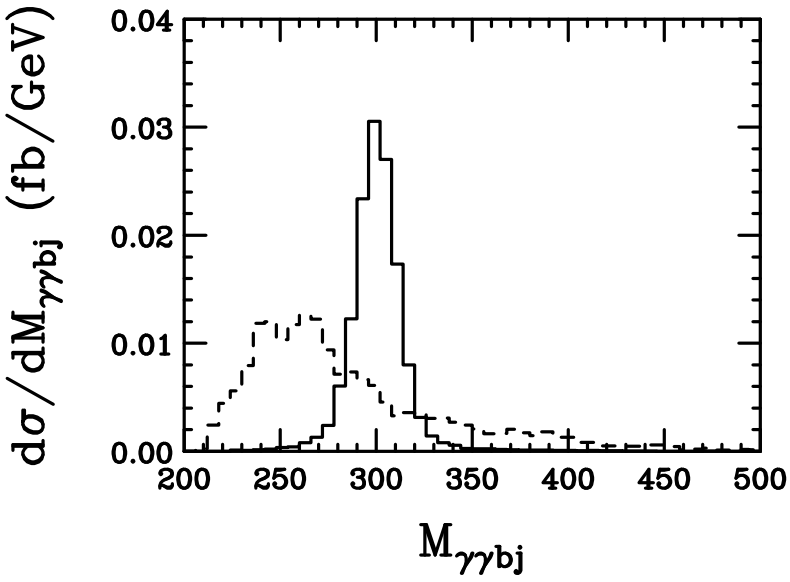

Figure 2.5. Differential cross-section as a function of invariant mass of $\gamma\gamma b\bar{b}$ for $H \to hh \to \gamma\gamma\bar{b}b$ (solid) and the sum of the backgrounds (dashed) requiring one b-tag.

CHAPTER 3

Hidden Sector with Supersymmetric Flat Directions–Signatures in Cosmology

3.1 Introduction: Cosmic String, SUSY Flat Directions

Besides the possibility to reveal itself in collider experiments as presented in chapter 2, the hidden sector can also leave fingerprints in cosmology, which provide both interesting signals for discovery and constraints on its existence. As we have seen by now, in well motivated scenarios, the hidden sector has a spontaneously broken gauge symmetry. Of particular interest in cosmology is the theoretical expectation that at high temperature or early universe, symmetries that are broken today were restored. Consequently, phase transitions are expected when the symmetries are broken as the universe cooled down. The vacuum structure in many spontaneously broken gauge theories is very rich: topologically stable configurations of gauge and Higgs fields exist as domain walls, cosmic strings, monopoles etc. These topological defects can form in early universe when the associated phase transition occurred. Among these, for the reasons we will see soon, cosmic strings are the most popular objects to study as probes for extended gauge group structure through cosmological observations.

Cosmic strings are one-dimensional topological defects that can be formed in the early universe [167, 168, 169] according to theoretical predictions. Although no confirmed observation has been made yet, due to their generic motivation and

potential interesting signals, they are still worthy of serious studies. Cosmic strings can be created if there is a phase transition in which the remaining vacuum manifold is not simply-connected, i.e. there is unshrinkable loop. In terms of topology, this means the first homotopy group of the vacuum manifold is nontrivial. One simple example is when a $U(1)$ group is completely broken. Cosmic strings are stable because they carry a conserved topological charge. This charge is integer-valued, corresponding to $\Pi_1(U(1)) = \mathbb{Z}$, and is related to the number of times the phase of the $U(1)$ breaking field winds at spatial infinity [170].

Unlike other types of topological defects, such as monopoles and domain walls, cosmic strings can be formed at a wide range of energy scales *after inflation* without severely contradicting the observed cosmology. The generic problem with topological defects is that, on account of their stability, they can easily come to dominate the energy density of the universe [169]. For cosmic strings there is an important loophole. Topological stability only applies to infinitely long strings. Cosmic string loops do not carry a net topological charge, and they can decay into particle or gravitational radiation. Such loops are formed when string segments intersect and exchange ends, or *reconnect* (or sometimes called *intercommute*). This allows a network of long cosmic strings to regulate its energy by chopping itself up into loops which radiate away. Indeed, for a wide range of initial string densities, analytic and numerical studies find that the competing processes of string stretching (from the cosmic expansion) and loop formation come to balance each other out. The network evolves towards a universal *scaling solution* whose properties are almost fully characterized by the cosmic string tension [177, 178, 179, 180, 181], independent of the initial conditions.

The vast majority of work on cosmic strings has focused on the abelian Higgs model, in which a $U(1)$ gauge symmetry is spontaneously broken by the condensation of a charged scalar field. In this model, the vacuum expectation value (VEV) of the complex scalar field determines the mass of the gauge field, m_V, and the physical

scalar Higgs field, m_S, through the relations

$$m_V \simeq g\,v, \qquad m_S \simeq \sqrt{\lambda}\,v, \tag{3.1}$$

where g is the gauge coupling, λ is the scalar quartic self-coupling, and v is the VEV of the scalar. The relative size of m_V and m_S determines how the strings interact. For $m_V < m_S$, parallel strings tend to repel at large distances while anti-parallel strings attract [169]. These strings are said to be Type-II, in analogy with superconductors. When $m_V > m_S$, the strings attract for any relative orientation, and they are said to be Type-I. The attractive force between parallel Type-I strings allows them to form stable higher-winding modes.

In most field theories, including the abelian Higgs model, the masses m_V and m_S are naturally of the same order. Much of the previous work on cosmic strings has therefore dealt with Type-II or weakly Type-I strings. In the present work, we will instead investigate the behavior of very strongly Type-I cosmic strings, corresponding to $m_V \gg m_S$. Our motivation to consider the extreme Type-I limit comes from supersymmetry [184]. As we will show below, there exist supersymmetric field theories in which $m_V \gg m_S$ arises in a natural way when a $U(1)$ gauge symmetry is broken along a flat-direction of the scalar potential. Supersymmetry is essential because it ensures that quantum corrections do not lift the flat direction.

The key ingredients in our construction, supersymmetry and a new $U(1)$ gauge symmetry, are each well-motivated in their own right independently of cosmic strings. Low-energy supersymmetry is one of the most elegant ways to explain the large hierarchy between the electroweak scale and the Planck scale [184]. It can also provide a candidate for the dark matter in the lightest superpartner particle (LSP), and in its minimal form, leads to an excellent unification of gauge couplings. Supersymmetry also plays an important role in superstring theories of gravity. Additional local $U(1)$ symmetries arise in many models of new physics such as grand unified models and D-brane constructions [42]. In supersymmetric models, such symmetries can also

help to solve the μ problem [172].

A common feature of supersymmetric theories is the existence of directions in the scalar potential that are almost flat. To be precise, an almost flat direction is one for which the curvature of the potential near the minimum is much smaller than the scale of the (symmetry-breaking) VEV at that minimum. Typically, these directions in field space are completely flat at tree-level, when only renormalizable operators are included in the potential, but they are lifted by higher-dimensional operators, quantum effects, and supersymmetry breaking. As long as the supersymmetry breaking effects are both soft and small, the residual approximate supersymmetry prevents quantum corrections from destroying the flatness of the potential. When a $U(1)$ gauge symmetry is broken along an almost-flat direction, the scalar excitation around the VEV along the flat direction is much lighter than the corresponding massive gauge boson. We will show that the cosmic strings associated with this pattern of gauge symmetry breaking are of the strongly Type-I sort [44, 45, 46, 47, 48, 50, 51].[1]

The interactions and cosmological consequences of strongly Type-I strings can be qualitatively different from those of Type-II and weakly Type-I strings [56, 57, 58]. When Type-I or Type-II cosmic strings intersect, they can reconnect or pass through each other. There is a third possible outcome when a pair of strongly Type-I strings intersect. Due to their mutual attraction, two strong Type-I strings with topological charges N_1 and N_2 can combine to form a single stable string with topological charge $N_{zip} = (N_1 + N_2)$ or $N_{zip} = |N_1 - N_2|$. At the point of intersection, the incident strings can coalesce into a single higher-winding string, which may then proceed to grow like a zipper [57]. If this growth continues indefinitely, the outcome will be a single higher-winding mode string of horizon length. For Type-II and weakly Type-I

[1] Let us also emphasize that the cosmic strings arising in general (approximately) supersymmetric theories need not be associated with a flat direction, and can also be of the Type-II variety. For examples, see Refs. [52, 53, 54, 55].

strings, previous calculations and simulations predict that the outcome of a string intersection is reconnection with a probability close to unity, $P_r \simeq 1$ [60, 61, 62, 63]. Since reconnection is essential to the formation of string loops, which in turn are essential for the strings to be cosmologically viable, deviations away from $P_r \simeq 1$ can significantly alter the picture of cosmic strings in the early universe. In particular, if string zippering is common, there can exist a stable population of higher winding mode strings as well [64, 65, 66, 67].

Many of the exotic properties exhibited by the strongly Type-I cosmic strings arising from supersymmetric flat directions are also found in the (p, q) cosmic strings emerging from superstring theory [68, 69, 70, 71, 72, 73, 74, 75], consisting of p fundamental F-strings and q D-strings. These cosmic superstrings can merge to form the equivalent of higher winding modes. In many cases they also have reconnection probabilities much less than unity, $P_r \lesssim 1$. However, flat-direction strings differ greatly from these (p, q) strings in their microscopic properties. This is borne out in the relationship between the (effective) topological charge and the string tension, as well as in the selection rules for string zippering. It may therefore be possible to distinguish (p, q) strings from flat-direction strings with the observation of several string lensing events, each with a different apparent relative value for the string tension.

In the present work [211] we study the properties and implications of cosmic strings derived from the breakdown of a $U(1)$ gauge symmetry along a supersymmetric flat direction. We begin in Section 3.2 by studying the internal structure of flat-direction strings. Here, we present a simple toy model for the flat direction breaking, and we investigate approximate solutions to the equations of motion and study the string tensions using variational methods. In Section 3.3 we discuss the interactions between cosmic strings. We apply these results in Section 3.4, where we study the formation and evolution of flat-direction string networks in the early universe. The observational

signatures produced by these networks will be the subject of Section 3.5.

Several earlier papers have investigated cosmic strings associated with flat-directions [44, 45, 46, 47, 48, 50, 51]. These studies have predominantly focused on the lowest ($N = 1$) winding mode. We expand on these studies by exhibiting an explicit and natural field theory model for the strings, and by discussing the new features that arise from the existence of stable higher ($N > 1$) winding modes. These modes significantly alter the cosmological picture of the strings.

3.2 String Profiles and Tensions

To begin, we introduce a simple class of models for a supersymmetric flat direction that could arise if there exists a $U(1)$ gauge group in addition to those contained in the MSSM. Within these models, we study the cosmic string solutions they support. In particular, we find approximate solutions to the classical equations of motion subject to the boundary conditions appropriate to a cosmic string, and we use these solutions to motivate a variational estimate of the string tension. Even though we focus on a particular class of models in the present section, we expect that many of the qualitative features that we find are also applicable to other cosmic string solutions associated with flat directions.

3.2.1 (a, b) Flat Directions

As a prototypical model for $U(1)$ symmetry breaking along a supersymmetric flat direction, we consider the (a, b) model discussed in Ref. [76]. The model consists of a supersymmetric $U(1)$ gauge theory containing chiral superfields Φ_a and Φ_{-b} with integer charges a and $-b$ respectively. Except for the special case $a = b = 1$ [77], we will assume that a and b are relatively prime with $a + b > 3$. Aside from the $(1, 1)$ model, other charged fields must be present in the theory for anomaly cancellation. However, these will decouple from the present discussion as long as they do not

develop VEVs.

When the charges a and b are relatively prime, the leading superpotential operator built from Φ_a and Φ_{-b} is

$$W \supset \frac{\lambda}{M_*^{a+b-3}} \Phi_a^b \Phi_{-b}^a, \tag{3.2}$$

where M_* is a large mass scale above which our effective theory breaks down. We also include the soft supersymmetry breaking operators

$$V_{soft} \supset -m_a^2 |\varphi_a|^2 - m_b^2 |\varphi_{-b}|^2 - \left(\frac{A}{M_*^{a+b-3}} \varphi_a^b \varphi_{-b}^a + h.c. \right), \tag{3.3}$$

where φ_a and φ_{-b} are the scalar component fields of Φ_a and Φ_{-b}, and A is a dimension-one coupling on the order of the soft supersymmetry breaking scale, $A \sim \sqrt{|m_a^2|} \sim \sqrt{|m_b^2|}$.[2] In writing this expression, we have implicitly redefined the scalar components of Φ_a and Φ_{-b} such that A is real and positive. We have also taken the soft masses for φ_a and φ_{-b} to be tachyonic.

The leading contributions to the scalar potential in the model are therefore

$$V_F = \frac{|\lambda|^2}{M_*^{2a+2b-6}} \left(|b\, \varphi_a^{b-1}\, \varphi_{-b}^a|^2 + |a\, \varphi_a^b\, \varphi_{-b}^{a-1}|^2 \right), \tag{3.4}$$

$$V_D = \frac{g^2}{2} \left(a|\varphi_a|^2 - b|\varphi_{-b}|^2 \right)^2, \tag{3.5}$$

$$V_{soft} = -m_a^2 |\varphi_a|^2 - m_b^2 |\varphi_{-b}|^2 - \left(\frac{A}{M_*^{a+b-3}} \varphi_a^b \varphi_{-b}^a + h.c. \right). \tag{3.6}$$

With A real and positive, there will be a global minimum of the potential with both φ_a and φ_{-b} real and positive. This minimum is unique up to gauge rotations.

If $a + b > 3$ the potential will be almost flat along the D-flat direction defined by

$$a|\varphi_a|^2 = b|\varphi_{-b}|^2. \tag{3.7}$$

Along this direction, the potential is destabilized at the origin by V_{soft}, and is only restabilized at large field values by the higher dimensional F term operators. Near the

[2] A simple spurion analysis indicates that other, non-holomorphic supersymmetry breaking terms from insertions in the Kähler potential are subleading [76].

minimum, the excitation along the flat direction is much lighter than the excitations orthogonal to it as well as the gauge bosons. This allows us to integrate out the heavy modes and obtain an effective potential for the light excitation.

Let us restrict ourselves to the flat direction by setting

$$\varphi_a = v\,\cos\alpha, \qquad \varphi_{-b} = v\,\sin\alpha, \tag{3.8}$$

where

$$\cos\alpha = \sqrt{\frac{b}{a+b}}, \qquad \sin\alpha = \sqrt{\frac{a}{a+b}}. \tag{3.9}$$

The scalar potential for v becomes

$$V(v) = -P\,v^2 - \left(\frac{2Q}{a+b}\right)\,(v^2)^{(a+b)/2} + \left(\frac{R}{a+b-1}\right)\,(v^2)^{a+b-1}, \tag{3.10}$$

with

$$\begin{aligned} P &= \frac{b\,m_a^2 + a\,m_b^2}{a+b}, \\ Q &= \frac{A}{M_*^{a+b-3}}\left[\frac{a^a b^b}{(a+b)^{a+b-2}}\right]^{1/2}, \\ R &= \frac{|\lambda|^2}{M_*^{2a+2b-6}}\left[\frac{a^a b^b}{(a+b)^{a+b-2}}\right](a+b-1). \end{aligned} \tag{3.11}$$

In terms of these variables, the minimum is given by

$$v = \left[\frac{1}{2\,R}\left(Q + \sqrt{Q^2 + 4\,P\,R}\right)\right]^{1/(a+b-2)}. \tag{3.12}$$

Parametrically, this is on the order of

$$v \sim \left(m M_*^{a+b-3}\right)^{1/(a+b-2)}, \tag{3.13}$$

where m is the generic soft mass. Thus, we expect $m \ll v \ll M_*$. The true minimum of the potential does not lie precisely along the flat direction if $m_a^2 \neq m_b^2$. However, the deviation is very small, and can be expanded in powers of $(m_a^2 - m_b^2)/g^2v^2 \ll 1$. We will discuss this further below.

For the special $(1,1)$ case with field charges ± 1, we disallow the bilinear term as in Ref. [77]e.g. by a string selection rule and *only* include the next-to-leading order term in the superpotential,

$$W_{(1,1)} = \frac{\lambda}{M_*}\Phi_1^2\Phi_{-1}^2. \tag{3.14}$$

The various terms in the potential are therefore

$$\begin{aligned} V_F &= \frac{4|\lambda|^2}{M_*^2}\left(|\varphi_1\varphi_{-1}^2|^2 + |\varphi_1^2\varphi_{-1}|^2\right), && (3.15)\\ V_D &= \frac{g^2}{2}\left(|\varphi_1|^2 - |\varphi_{-1}|^2\right)^2, && (3.16)\\ V_{soft} &= -m_1^2|\varphi_1|^2 - m_{-1}^2|\varphi_{-1}|^2 - \left(\frac{A}{M_*}\,\varphi_1^2\varphi_{-1}^2 + h.c.\right). && (3.17) \end{aligned}$$

In the following sections we will analyze in detail the equations of motion resulting from this scenario.

3.2.2 Equations of Motion and Approximate Solutions

The equations of motion for the system are

$$\begin{aligned} 0 &= D^\mu D_\mu\,\varphi_i + \frac{\partial V}{\partial \varphi_i^*}\,, && (3.18)\\ 0 &= \partial_\nu F^\nu{}_\mu + i\,g\sum_i Q_i\,(\varphi_i^*\overset{\leftrightarrow}{D}_\mu\,\varphi_i)\,, && (3.19) \end{aligned}$$

where $D_\mu = \partial_\mu + i\,g\,Q\,A_\mu$ is the gauge-covariant derivative.

To obtain an approximate solution to these equations that describes a cosmic string, it is convenient to introduce an Ansatz for the vector and scalar fields. Our Ansatz for a string with winding number N is

$$\begin{aligned} \varphi_a &= v\,(1+\epsilon)\,\cos\alpha\; e^{iNa\phi}\,f_a(r),\\ \varphi_{-b} &= v\,(1-\epsilon)\,\sin\alpha\; e^{-iNb\phi}\,f_b(r), && (3.20)\\ A_\phi &= \frac{N}{gr}\,\tilde{a}(r). \end{aligned}$$

In these expressions, r and ϕ are the radial and angular cylindrical coordinates relative to the string axis, v is the vacuum expectation value, and $\cos\alpha$ and $\sin\alpha$ are defined in

Eq. (3.9). The dimensionless parameter ϵ characterizes the deviation from D-flatness at the absolute minimum, and will be treated as a small number. The functions $f_a(r)$, $f_b(r)$, and $\tilde{a}(r)$ are undetermined string profiles. They are subject to the boundary conditions

$$f_a,\ f_b,\ \tilde{a} \to 0 \ \text{ as } \ r \to 0, \qquad\qquad f_a,\ f_b,\ \tilde{a} \to 1 \ \text{ as } \ r \to \infty. \tag{3.21}$$

The relative winding numbers of φ_a and φ_{-b} allow for both $D_\phi \varphi_a$ and $D_\phi \varphi_{-b}$ to fall off more quickly than $1/r$ as $r \to \infty$. This is a necessary condition for the string tension to be finite.

Inserting the profile functions into the equations of motion, we obtain

$$\begin{aligned}
0 &= f_a'' + \frac{1}{r} f_a' - \frac{N^2 a^2}{r^2}\,(1-\tilde{a})\, f_a - a\left(\frac{ab}{a+b}\right)\left[(1+\epsilon)^2 f_a^2 - (1-\epsilon)^2 f_b^2\right] f_a \\
&\quad - \frac{1}{v(1+\epsilon)\, c_\alpha}\,\frac{1}{g^2 v^2}\, e^{-iNa\phi}\frac{\partial \tilde{V}}{\partial \varphi_a^*}, \qquad (3.22) \\
0 &= f_b'' + \frac{1}{r} f_b' - \frac{N^2 b^2}{r^2}\,(1-\tilde{a})\, f_b + b\left(\frac{ab}{a+b}\right)\left[(1+\epsilon)^2 f_a^2 - (1-\epsilon)^2 f_b^2\right] f_b \\
&\quad - \frac{1}{v(1-\epsilon)\, s_\alpha}\,\frac{1}{g^2 v^2}\, e^{iNb\phi}\frac{\partial \tilde{V}}{\partial \varphi_{-b}^*}, \qquad (3.23) \\
0 &= \tilde{a}'' - \frac{1}{r}\tilde{a}' + \left(\frac{2ab}{a+b}\right)\left[a\,(1+\epsilon)^2\, f_a^2 + b\,(1-\epsilon)^2\, f_b^2\right]\,(1-\tilde{a}). \qquad (3.24)
\end{aligned}$$

In these expressions we have separated out the D-term part of the potential by defining $\tilde{V} = (V - V_D)$. We have also written the cylindrical radial coordinate r in units of $(gv)^{-1}$. Thus, when we discuss the value of r in absolute terms, it will always be relative to the scale $(gv)^{-1}$. The equations of motion are complicated and non-linear, but we can obtain approximate solutions in the three regions $r \ll 1$, $1 \ll r \ll gv/m$, and $r \gg gv/m$. We consider each of these regions in turn.

Region I: $r \ll 1$

For $r \ll 1$, we expect f_a, f_b, and $\tilde{a}$ to all be small. Expanding the equations of

motion to linear order in the profiles, we find

$$f_a \sim r^{|Na|}, \tag{3.25}$$

$$f_b \sim r^{|Nb|}, \qquad (r \ll 1) \tag{3.26}$$

$$\tilde{a} \sim r^2, \tag{3.27}$$

This behavior agrees with the expectation from Refs. [168, 169]

Region II: $1 \ll r \ll gv/m$

In the intermediate region $1 \ll r \ll gv/m$, we expect f_a, f_b, and $\tilde{a}$ to all be on the order of unity. As we will discuss below, in this region it is also self-consistent to neglect the contribution of $\tilde{V} = (V - V_D)$ to the equation of motion and to set $\epsilon = 0$. The equations of motion for f_a and f_b simplify if we rewrite them in terms of $f_+(r)$ and $f_-(r)$, defined by

$$\left\{ \begin{array}{rcl} f_+ &=& \frac{1}{2}(f_a + f_b) \\ f_- &=& (f_a - f_b) \end{array} \right. \Leftrightarrow \left\{ \begin{array}{rcl} f_a &=& f_+ + \frac{1}{2} f_- \\ f_b &=& f_+ - \frac{1}{2} f_- \end{array} \right. . \tag{3.28}$$

The equations of motion for f_a and f_b then imply

$$0 \simeq f_-'' + \frac{1}{r} f_-' - \left(\frac{2ab}{a+b} \right) \left[(a+b) f_+ + \frac{1}{2}(a-b) f_- \right] f_+ f_-, \tag{3.29}$$

$$0 \simeq f_+'' + \frac{1}{r} f_+' - \frac{1}{2} \left(\frac{2ab}{a+b} \right) \left[(a-b) f_+ + \frac{1}{2}(a+b) f_- \right] f_+ f_-, \tag{3.30}$$

As r grows larger than unity, the boundary conditions imply $f_+ \to 1$ and $f_- \to 0$. If f_+ is slowly varying in this region, the approximate solution for f_- is

$$f_- \sim K_0(\sqrt{2ab} f_+ r) \sim \sqrt{\frac{1}{r}}\, e^{-\sqrt{2ab}\, f_+ \, r}. \tag{3.31}$$

Thus, f_- falls off quickly, corresponding to the damping of the scalar excitation orthogonal to the flat direction. With f_- very small, the equation for f_+ reduces to

$$0 \simeq f_+'' + \frac{1}{r} f_+'. \tag{3.32}$$

The corresponding solution is

$$f_+ = f_0 \ln\left(\frac{r}{r_0}\right), \tag{3.33}$$

for some constants f_0 and r_0. Our approximate result is self-consistent because f_+ is indeed a slowly-varying function of r.

We can also use this expression for f_+ to check the range of r over which we can safely neglect the effects of the $\tilde{V}$ term in the equation of motion (eqs.3.22-3.24). For $f_- \ll 1$, $f_+ \sim 1$, this term is on the order of $(m^2/g^2v^2)\ f_+$, where m is the scale of the soft supersymmetry breaking terms. The necessary condition for ignoring the $\tilde{V}$ contribution to the equation of motion to the level of approximation we are working to is

$$f_+'',\ \frac{1}{r}f_+' \gg \left(\frac{m^2}{g^2v^2}\right) f_+ \qquad \Rightarrow \qquad r \ll \frac{g\,v}{m}. \tag{3.34}$$

To track the evolution of the gauge profile it helps to define $\delta\tilde{a} = 1 - \tilde{a}$. The corresponding equation of motion is

$$0 \simeq \delta\tilde{a}'' - \frac{1}{r}\delta\tilde{a}' - ab\, f_+^2 \delta\tilde{a}, \tag{3.35}$$

where we have made use of the fact that f_- is expected to damp out quickly and that $\epsilon \ll 1$. The solution is

$$\delta\tilde{a} \propto r\, K_1\left(\sqrt{2ab} f_+ r\right) \sim \sqrt{r}\, e^{-\sqrt{2ab} f_+ r}. \tag{3.36}$$

Therefore, $\delta\tilde{a}$ is damped out exponentially as well, and $\tilde{a}$ quickly approaches unity. Let us point out that the physical gauge boson mass is $\sqrt{2ab}\, g\, v$. Thus, this mass controls the width of the gauge field profile (remembering that r is expressed in units of $1/gv$ here), as well as the width of the profile of $f_-(r)$.

Region III: $r \gg gv/m$

In the very large field region, $r \gg gv/m$, the flat potential $\tilde{V}$ and the deviation of ϵ from zero become relevant to the evolution of f_+ and f_-. For these large values

of r, it is convenient to write

$$\delta f_+ = 1 - f_+, \tag{3.37}$$

since we expect $|\delta f_+| \ll 1$. Consider first the effect of $\tilde{V}$ and $\epsilon \neq 0$ on the evolution of f_-. The equation of motion to linear order in f_- and δf_+ becomes

$$0 = f_-'' + \frac{1}{r} f_-' - [2ab + \mathcal{O}(\epsilon)]\, f_- - 4\, ab\, \epsilon + \left(\frac{m_a^2 - m_b^2}{g^2 v^2} \right). \tag{3.38}$$

To be able to impose $f_- \to 0$, we must choose

$$\epsilon = \frac{1}{4\, ab} \left(\frac{m_a^2 - m_b^2}{g^2 v^2} \right). \tag{3.39}$$

This is consistent with our previous assumption that $\epsilon \ll 1$.

Inserting this value of ϵ into the linearized equation of motion for δf_+, we find

$$0 = \delta f_+'' + \frac{1}{r} \delta f_+' - m_S^2 \delta f_+, \tag{3.40}$$

where m_S^2 is a positive constant on the order of $m^2/g^2 v^2$. In the units we are using, this is of the same size as the mass of the light excitation about the almost-flat direction. A possible constant term in Eq. (3.40) vanishes through the minimization condition for v given in Eq. (3.12). The solution for δf_+ in the very large r region is therefore

$$\delta f_+ \propto K_0(m_S\, r) \simeq \sqrt{\frac{\pi}{2\, m_S\, r}}\, e^{-m_S\, r}. \tag{3.41}$$

Again, this is consistent with the results of Refs. [168, 169].

3.2.3 String Tensions

Having obtained approximate expressions for the string profiles, we estimate the tension of cosmic strings in the (a, b) model for various values of the winding number N. Using the Ansatz of Eq. (3.20), the contributions to the tension of a string in the

(a,b) model are

$$\begin{aligned}
\mu_{rad}/\pi\, v^2 &= 2\int_0^\infty dr\, r\left[\left(\frac{b}{a+b}\right)(f_a')^2+\left(\frac{a}{a+b}\right)(f_b')^2\right], \\
\mu_{ang}/\pi\, v^2 &= 2\,N^2\,ab\int_0^\infty dr\,\frac{1}{r}\left[\left(\frac{a}{a+b}\right)\,f_a^2+\left(\frac{b}{a+b}\right)\,f_b^2\right](1-\tilde{a})^2, \\
\mu_{mag}/\pi\, v^2 &= N^2\int_0^\infty dr\,\frac{1}{r}\,(\tilde{a}')^2, \\
\mu_{pot}/\pi\, v^2 &= \int_0^\infty dr\, r\,\frac{1}{g^2v^4}\,V(f_a,f_b).
\end{aligned} \tag{3.42}$$

Except near the origin, and certainly whenever the potential V given in eqs.(3.6) is relevant, it is a very good approximation to set $f_a = f_b = f_+$. In this limit, the potential can be written in the form

$$\frac{1}{g^2v^2}\,V(f) \simeq -\delta_1\,(f_+^2-1)-\left(\frac{2}{a+b}\right)\,\delta_2\,(f_+^{a+b}-1)+\left(\frac{\delta_2+\delta_1}{a+b-1}\right)\,(f_+^{2a+2b-2}-1). \tag{3.43}$$

Here, we have implicitly assumed that $a+b \geq 4$. The dimensionless constants δ_1 and δ_2 are given by

$$\begin{aligned}
\delta_1 &= \frac{1}{a+b}\left(\frac{b\,m_a^2+a\,m_b^2}{g^2v^2}\right), \\
\delta_2 &= \frac{1}{g^2v^2}\frac{A}{M_*^{a+b-3}}\left[\frac{a^ab^b}{(a+b)^{a+b-2}}\right]^{1/2}\,v^{a+b-2}.
\end{aligned} \tag{3.44}$$

Using the parametric value of the VEV given in Eq. (3.13), these constants are of size

$$\delta_{1,2} \sim \left(\frac{m}{M_*}\right)^{2(a+b-3)/(a+b-2)}. \tag{3.45}$$

For $M_* \sim M_{\rm Pl}$ and $m \sim$ TeV, we find $10^{-30} \lesssim \delta_{1,2} \lesssim 10^{-15}$. Although the expressions presented above were formulated for strings in the (a,b) theory, they can also be applied to $(1,1)$ theory cosmic strings. The correct formulae for the $(1,1)$ case are obtained by setting $a=b=1$ in the radial and angular components of the tension (μ_{rad} and μ_{ang} in Eq. (3.42)), but $a+b=4$ in the expression for the potential (Eq. (3.43)). This adjustment accounts for our inclusion of terms beyond the leading order for $(1,1)$ strings.

To estimate the string tensions, we have used variational methods as in Ref. [44]. Our trial profile functions are inspired by the approximate solutions found above. They are

$$
\begin{aligned}
f_a(r) &= \begin{cases} p_1 (r/r_1)^{|Na|} & r \le r_1 \\ p_5 + p_3 \, \ln\left(\frac{r}{r_1}\right) & r_1 < r < r_2 \\ 1 - p_4 \, e^{-(r-r_2)/r_3} & r \ge r_2 \end{cases} \\
f_b(r) &= \begin{cases} p_2 (r/r_1)^{|Nb|} & r \le r_1 \\ p_5 + p_3 \, \ln\left(\frac{r}{r_1}\right) & r_1 < r < r_2 \\ 1 - p_4 \, e^{-(r-r_2)/r_3} & r \ge r_2 \end{cases} \\
\tilde{a}(r) &= \begin{cases} a_0 \left[3 \left(\frac{r}{r_a}\right)^2 - 2 \left(\frac{r}{r_a}\right)^3 \right] & r \le r_a \\ 1 & r > r_a \end{cases} .
\end{aligned}
\tag{3.46}
$$

The undetermined parameters are $\{r_1, r_2, r_3, r_a, p_1, p_2, p_3, p_4, p_5\}$. We fix four of them, p_1, p_2, p_3, and p_4, by requiring continuity at $r = r_1$ and r_2, and differentiability at r_2 (where the solution is expected to be slowly varying) but not at r_1.

For a $(1,1)$ model string with winding number $N = 1$ and $\delta_1 = \delta_2 = 1 \times 10^{-20}$, our variational estimate of the tension is

$$
\begin{aligned}
\mu_{rad}/\pi v^2 &= 0.09093, \\
\mu_{ang}/\pi v^2 &= 0.00247, \\
\mu_{mag}/\pi v^2 &= 0.00228, \\
\mu_{pot}/\pi v^2 &= 0.00228, \\
\mu_{tot}/\pi v^2 &= 0.09796.
\end{aligned}
\tag{3.47}
$$

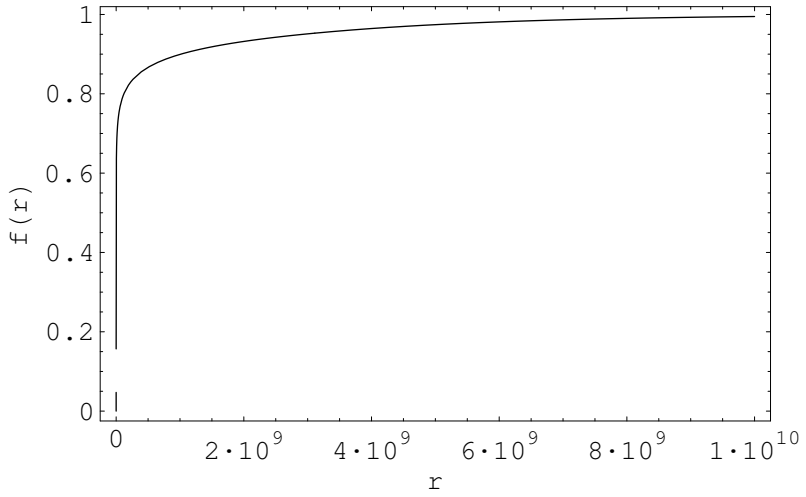

Figure 3.1. Profile function of the scalar field $f(r)$ for $N = 1$ strings in $(1, 1)$ model, where r is in unit of $1/gv$

The corresponding values of the variational parameters are

$$\begin{aligned} r_1 &= 14.01, \\ r_2 &\simeq r_3 = 3.112 \times 10^9, \\ r_a &= 36.26, \\ p_5 &= 0.04713. \end{aligned} \tag{3.48}$$

Recall that we express all dimensionful quantities in units of $1/gv$. We plot the profile functions for $(1, 1)$ model with $N = 1$ in Fig.3.1,3.2.

As expected, the gauge profile is much narrower than the scalar profiles (*i.e.*, $r_a \ll r_2$), which have substantial support out to $r \sim 1/\sqrt{\delta_{1,2}}$. The small r power-law form of the scalar profiles extends out about as far as the gauge profile (*i.e.*, $r_1 \simeq r_a$), after which it continues to grow logarithmically slowly until the profile reaches unity. We also find that the total string tension is dominated by the radial contribution.

To a very good approximation, the shape of the profiles and the value of the string

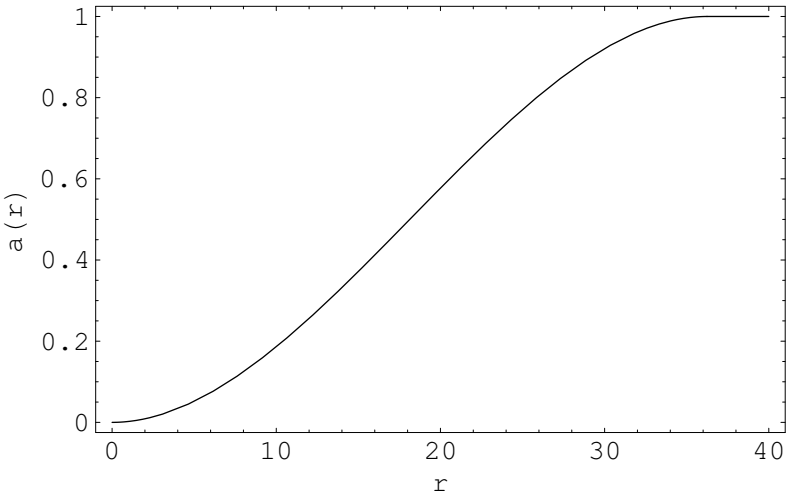

Figure 3.2. Profile function of the gauge field $a(r)$for $N = 1$ strings in $(1, 1)$ model,where r is in unit of $1/gv$

tension do not depend on δ_1 and δ_2 independently, but rather on the combination

$$\Delta = \delta_1 + \delta_2/2. \tag{3.49}$$

This can be seen explicitly by evaluating μ_{pot} using the Ansatz profiles of Eq. (3.46) and keeping only the leading terms in the expansion in $1/\ln(\delta_{1,2}) \ll 1$.

We have investigated a number of other sets of profile functions as well. As long as the trial scalar profile increases sufficiently (logarithmically) slowly in the region $1 \ll r \ll 1/\sqrt{\delta}$ and drops rapidly for larger r, we find that the resulting estimates for the string tension are very similar. This gives us confidence that our estimates are close to the exact values. [3]

[3]Exact solutions to the equations of motions for profile functions are unknown, since they are coupled to each other and non-linear. This is even true for the simpler Abelian-Higgs model (except for the 'critical coupling' case where $m_A = m_\phi$[169]). The approach we employed here is a generation of the one well applied for the Abelian Higgs model[44]–one solves the equations explicitly at asymptotic regions and then makes proper smooth connections in between–which is a good analytical parametrization.

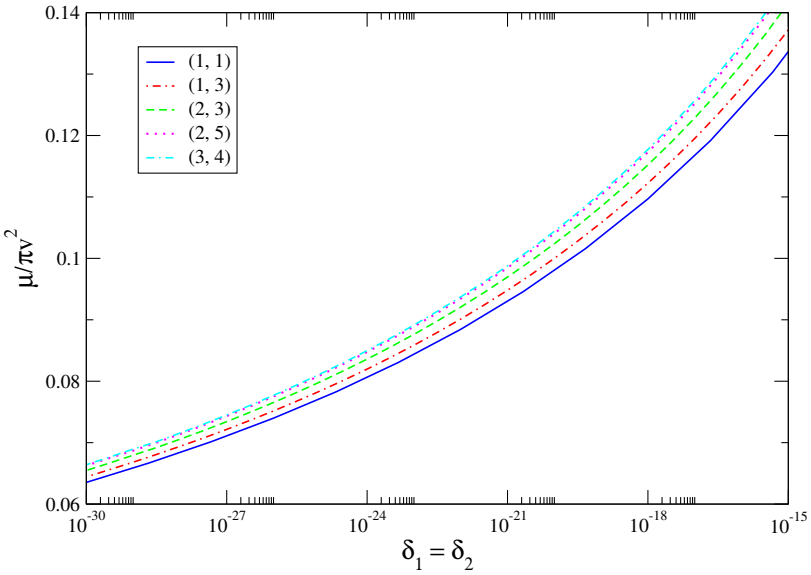

Figure 3.3. Tensions of $N = 1$ strings as a function of the potential parameters $\delta_1 = \delta_2$ for various (a, b) theories.

Fig. 3.3 shows the dependence of the string tension in the $(1, 1)$, $(1, 3)$, $(2, 3)$, $(2, 5)$, and $(3, 4)$ models on the value of $\delta_1 = \delta_2 = 2\Delta/3$ for a winding number $N = 1$. Even for very small values of $\delta_{1,2}$, corresponding to extremely flat potentials, the string tension is within about an order of magnitude of v^2. Thus, while the string is very wide in units of $1/g\,v$, the VEV still sets the size of the tension. The tensions are also very similar for different values of (a, b). This is not very surprising given that the radial portion of the string tension appears to be the dominant one. In the $r \gg 1$ region, we expect $f_a \simeq f_b$ so that the expression for the radial contribution to the tension in Eq. (3.42) does not depend explicitly on (a, b). The dependence on (a, b) only then comes about through the size of the terms in the potential. In generating Fig. 3.3, we neglected this dependence by specifying the value of $\delta_1 = \delta_2$ explicitly. Our results also suggest that the detailed form of the (non-D) potential does not play a significant role in determining the string tension or the string profiles other than to set the scale at which the scalar profiles are cut off.

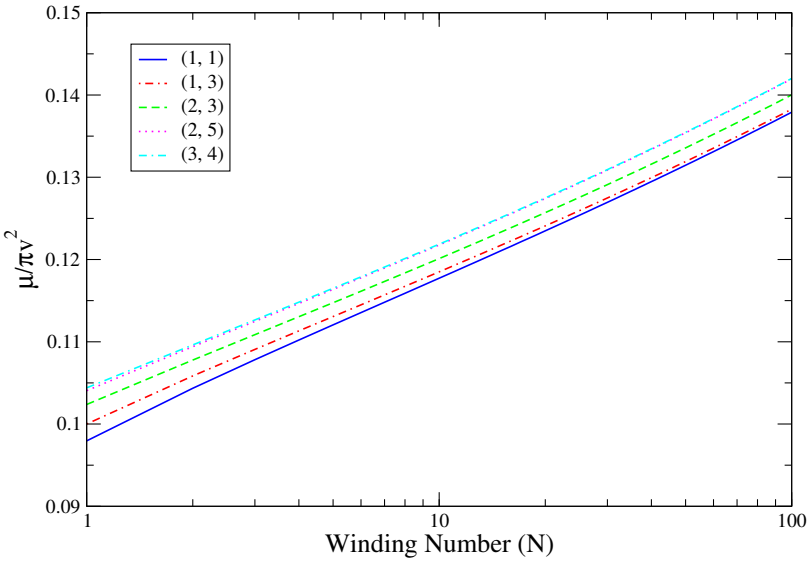

Figure 3.4. String tensions as a function of the winding number N for the potential parameters $\delta_1 = \delta_2 = 1 \times 10^{-20}$ in various (a, b) theories. Note that the tension of the $N = 2$ string is much smaller than twice the tension of the $N = 1$ string, thereby allowing stable $N = 2$ strings.

In Fig. 3.4 we illustrate the variation of the tension for strings in the $(1, 1)$, $(1, 3)$, $(2, 3)$, $(2, 5)$, and $(3, 4)$ models with the winding number N for $\delta_1 = \delta_2 = 1 \times 10^{-20}$. These tensions increase very slowly with N, approximately logarithmically. As the winding number increases, the widths of the vector field profile and the inner portion of the scalar profile do too. This allows the angular and magnetic contributions to the string tension to increase much more slowly than N^2. The increase of the profile radii r_1 and r_a with the winding number N is shown in Fig. 3.5 for a $(1, 1)$ model string with $\delta_1 = \delta_2 = 1 \times 10^{-20}$. For both r_1 and r_a, the increase with N is very close to linear. The corresponding plots for the other values of (a, b) discussed above are nearly identical. Unlike r_1 and r_a, varying N has very little effect on r_2.

We can combine the results presented above into a simple approximate parametrization of the string tensions. The string tension increases close to logarithmically with the winding number N, but has a more complicated dependence on δ_1 and δ_2, primarily through the combination $\Delta = \delta_1 + \delta_2/2$. In the range $1 < N < 100$,

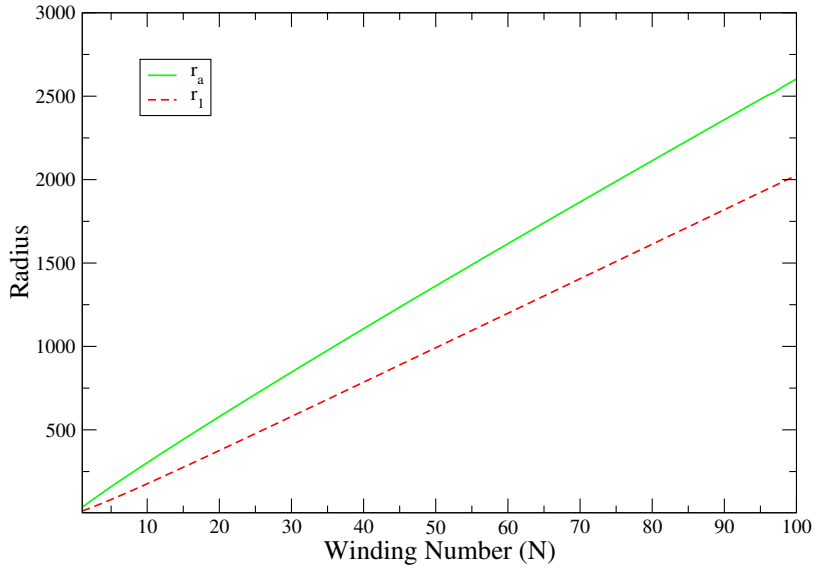

Figure 3.5. Dependence of the inner scalar profile width (r_1) and vector profile width (r_a) on the winding number number N for a $(1,1)$ model string with $\delta_1 = \delta_2 = 1 \times 10^{-20}$.

$10^{-30} < \Delta < 10^{-15}$, and δ_1 and δ_2 within an order of magnitude from each other, the tension of a $(1,1)$ string is reproduced to an accuracy of a few percent by the empirical formula

$$\mu/\pi\, v^2 \simeq \left[\frac{4.2}{\ln(1/\Delta)} + \frac{14}{\ln^2(1/\Delta)}\right] \left(1 + \left[\frac{2.6}{\ln(1/\Delta)} + \frac{57}{\ln^2(1/\Delta)}\right] \ln N\right). \qquad (3.50)$$

Since the tension of an (a,b) theory string is very similar to that of a $(1,1)$ theory string for a given set of values of δ_1 and δ_2, this formula also provides a reasonable approximation to the tension of strings in these more general theories.

In summary, we find that the cosmic strings that arise from breaking a $U(1)$ gauge symmetry along an almost flat direction within the (a,b) models are very strongly of the Type-I variety. The qualitative features of these strings can be characterized by two scales: the VEV v; and the scale of the curvature near the minimum m, which in the present case is set by the soft supersymmetry breaking scale $m \sim \sqrt{|m_a|^2} \sim \sqrt{|m_b|^2} \sim A$. It is the hierarchy $m \ll v$ that makes the potential flat. The tension of flat-direction strings is about $\mu \sim 0.1\pi v^2$, while their total thickness is $w \sim m^{-1}$.

The internal structure of the strings consists of a thin vector field core, of width close to v^{-1}, surrounded by a much broader scalar profile of radius m^{-1}. Flat-direction cosmic strings also have stable higher modes. The tension of these modes grows very slowly with the winding number N, increasing as $\ln N$ with a small coefficient.

These features are much different from those of ordinary cosmic strings derived from the abelian Higgs model, for which the relevant scales are all on the order of the VEV v. On the other hand, the qualitative structure and the tensions of strings derived from the (a, b) model presented above are in agreement with other studies of flat-direction cosmic strings [44, 45, 46, 48]. Within the (a, b) models, we find that the form of the string profile away from the central core and the tension can be described well from a knowledge of m and v alone, without reference to the precise form of the potential (or a and b). This suggests that many of the results of the following sections, where we investigate the phenomenological features of (a, b)-theory flat-direction cosmic strings, will apply to flat-direction strings derived from other theories as well.

3.3 String Interactions

When a pair of Type-II or weakly Type-I abelian strings with the same winding number intersect, there are effectively two possible outcomes. They can simply pass through each other, or they can exchange partners and reconnect (intercommute). When a pair of strongly Type-I $N = 1$ strings collide, there is a third possibility [57]. Studies of Type-I strings in the abelian Higgs model suggest that the force between string segments is attractive. Thus, the segments can pull together near the intersection point to form a length of $N = 2$ string, which is stable and lower in energy than a pair of $N = 1$ segments. Under favorable conditions this segment will grow, effectively *zippering* the pair of $N = 1$ strings into a single $N = 2$ string. When even higher-winding modes of strongly Type-I strings are stable as well, we can also

consider the outcome of the intersection of two strings with general winding numbers N_1 and N_2. Besides passing through each other, the topology of the configuration permits the formation of zippers with winding numbers $|N_1 + N_2|$ and $|N_1 - N_2|$.

Reconnection plays an essential role in the cosmological evolution of a cosmic string network. It allows the network to modulate its energy by forming string loops, which can decay away. Without reconnection and loop formation, the energy density in the string network could come to dominant the universe [168, 169]. Analytic estimates and numerical simulations of Type-II and weakly Type-I strings in the abelian Higgs model suggest that the probability that a pair of strings will reconnect after they intersect is close to one, $P_r \simeq 1$ [61, 62, 63]. However, this result need not apply to very strongly Type-I strings. These strings can form zippers, and therefore the probability of reconnection in a string collision may differ from unity. This can have important consequences for the evolution of a string network in the early universe.

In this section we investigate how flat-direction cosmic strings interact with each other. We begin by discussing the forces between a pair of string segments. Next, we study the reconnection and zippering of strings when they intersect. Zippering can reduce the probability of reconnection, and it can also lead to qualitatively new string structures that cannot be formed by Type-II strings. We investigate how these features alter the formation of string loops. The results of this section are applied in the sections to follow.

3.3.1 Inter-String Forces

We found in Section 3.2 above that the tension of an $N = 2$ flat-direction cosmic string is considerably lower than twice the tension of an $N = 1$ string. Therefore bringing a pair of $N = 1$ strings together (adiabatically) from infinity to form an $N = 2$ segment will lower the total energy of the system. As a result, we expect the (non-gravitational) force between a pair of parallel flat-direction cosmic strings to be

attractive. More generally, we expect the interstring force to be attractive for any other relative orientation as well.

Our expectation is supported by both analytic estimates of the interstring forces in the abelian Higgs model [78, 79, 80],[4] as well as in numerical investigations [81, 82, 83]. It is argued in these works that the contributions to the interstring force from the vector profile are attractive only for anti-parallel strings and repulsive otherwise, while the scalar profile contributions are always attractive. For Type-I strings, the scalar profile is wider than the vector profile and its contribution to the force has a longer range and is always dominant. The vector profile has a larger range for Type-II strings explaining why the force between parallel strings is repulsive. The scalar profile in flat-direction strings is much wider than the vector profile, so the results obtained in the abelian Higgs model suggest that the force between these strongly Type-I strings is attractive as well.

An alternative possibility, consistent with the energetics, is that the interstring force between flat-direction strings is repulsive at distances larger than the string width, and only becomes attractive when the strings overlap significantly. Even if this were true, it would likely not have a large effect on how these strings interact in the early universe. Since the strings we are studying are local (gauged), the interstring force has a very short range, falling off exponentially outside the string core. When a pair of strings approaches an intersection, the interstring forces will be non-trivial only in the small region near the intersection point, and hence the interaction energy will be finite. We expect the energy required to overcome this barrier, if it is present, to be much smaller than the initial kinetic energy carried by the incident string segments.

[4]However, when attempting to reproduce the argument of [79] we found an opposite sign in the scalar term at large string separations. Thus, we are not sure that argument is definitive.

3.3.2 String Reconnection and Zippering

A pair of strings with the same winding number is said to reconnect (or intercommute) if they exchange ends upon intersection. The result of this process is illustrated in Fig. 3.6, following Ref. [57]. The initial state consists of two infinite straight strings, each with speed ν and a relative angle α, approaching each other along the z-axis. After exchanging ends, causality implies that the segments of the strings very far (spacelike-separated) from the intersection point continue along their original trajectories. Connecting these asymptotic segments are new segments moving in the $\pm y$ directions. The labels 1 and 2 in the figure indicate which incident string the corresponding asymptotic string segment came from. The total length of string in the final configuration is clearly less than in the initial. Energy is conserved because the newly-formed segments carry a velocity ν' in the $\pm y$-directions.

Over distances that are large compared to the string width but small compared to the horizon size, the motion of cosmic strings should be well-described by treating them as ideal Nambu-Goto (NG) strings propagating in a flat spacetime background. Therefore a necessary condition for string reconnection is that the initial and final configurations be kinematically allowed in the NG approximation. It is not hard to check that for any initial relative velocity ν and for any relative angle α (as defined in Fig. 3.6), this is the case [57].

The existence of a classical string solution for reconnection does not imply that it actually occurs whenever a pair of strings intersect. The precise outcome depends on the internal structure of the strings, which is highly non-linear and very difficult to treat analytically. Much of the work on this topic has therefore consisted of lattice simulations of the corresponding classical field configurations in the abelian Higgs model for Type-II or weakly Type-I strings. These simulations generally find that the probability of reconnection in a string intersection is close to unity except for very large initial velocities, $\nu \gtrsim 0.9$ [61, 62, 63]. Early attempts to study this question

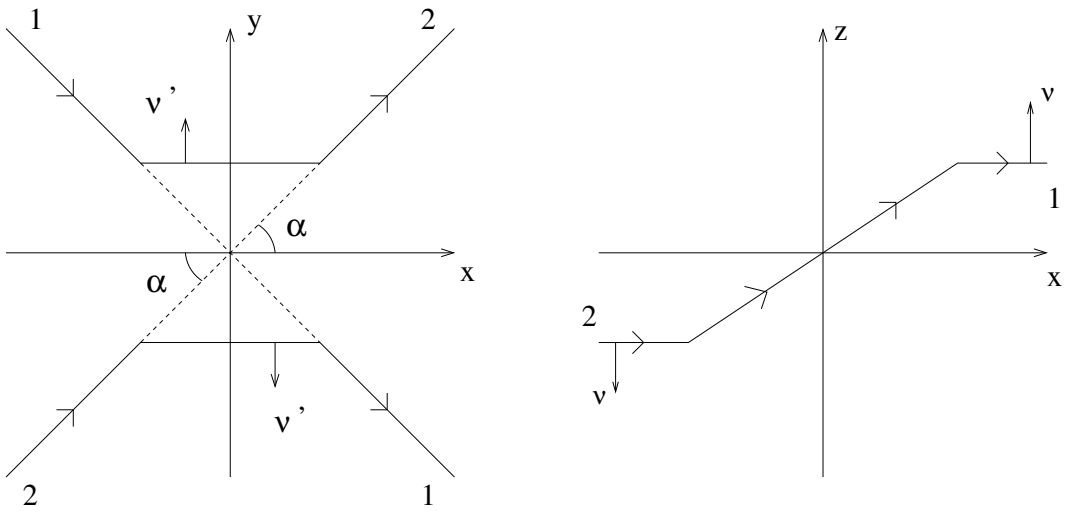

Figure 3.6. Pictorial representation of string reconnection in the xy and xz planes following Ref. [57]. The initial state consists of string 1 and string 2 approaching each other along the z-axis, each with speed ν. In the xz plane, we show only the lower string portion. The labels 1 and 2 indicate which of the incident strings the corresponding segment was derived from.

analytically, by comparing the interaction time of the fields in the string core to the time it takes for the pair of strings to pass through each other, find much the same result [60].

In addition to reconnecting or simply passing through each other, when a pair of strongly Type-I strings intersect they can also zipper into a segment with a higher (or lower) winding number [56, 57, 58]. This is illustrated in Fig. 3.7, following Ref. [57], where the initial state consists of two strings with the same winding number $N_1 = N_2 = N$ approaching each other along the z-axis, each with initial speed ν. When the strings intersect, a new segment of winding number $N_{zip} = 2N$ is formed along the x-axis. This is the *zipper*. When kinematically allowed (we will discuss this in detail later in this subsection (3.3.2)) it can proceed to grow along the x-axis at the speed ν_{zip}. The string segments far from the intersection point (labelled by 1 and 2 in Fig. 3.7) continue along their initial trajectories on account of causality.

Zippering has received much less attention than reconnection, and we know of only a handful of simulations that have studied it [56, 58, 84]. If string zippering

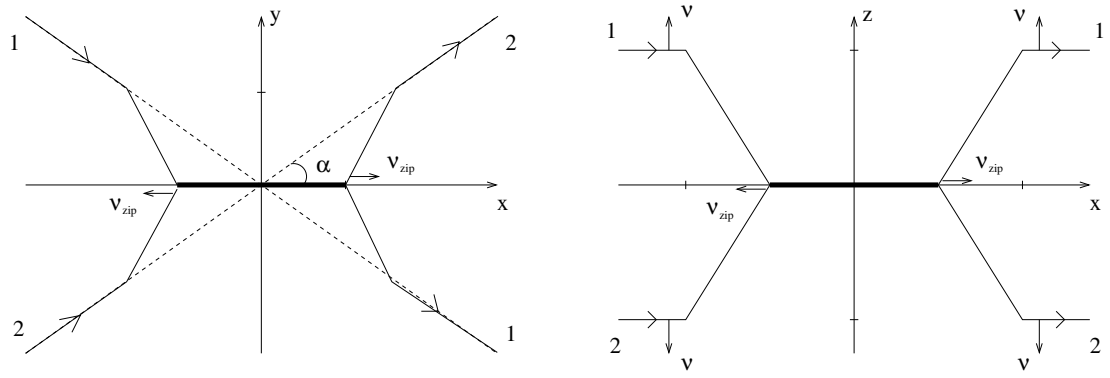

Figure 3.7. Pictorial representation of string zippering in the xy and xz planes following Ref. [57]. The initial state consists of string 1 and string 2 approaching each other along the z-axis, each with speed ν. In the xz plane, we show only the lower string portion. The labels 1 and 2 indicate which of the incident strings the corresponding segment was derived from.

is efficient, it will reduce the probability of reconnection. Given the importance of reconnection for the evolution of cosmic strings in the early universe, this is a crucial issue to be resolved.

As for reconnection, a necessary condition for string zippering is that it be classically allowed in the NG approximation. Again, this condition is only a necessary one, and the existence of a classical zippering solution does not imply that it actually takes place. Classical zippering solutions have been constructed in Refs. [57, 85]. Unlike for reconnection, there exist significant kinematic constraints on zippering due to energy conservation. For a pair of strings with identical winding numbers N, initial speeds ν, and a relative angle α, the kinematic constraint on forming a zipper with $N_{zip} = 2\,N$ is found to be [57]

$$\sqrt{1-\nu^2}\,\cos\alpha > \frac{\mu_{2N}}{2\,\mu_N}, \tag{3.51}$$

where μ_N is the tension of the incident segments and μ_{2N} is the tension of the zipper. The total length of the zippered configuration is greater than the initial state. Thus, a zipper can form only if it tends to lower the energy of the configuration due to the string tension, which requires $\mu_{2N} < 2\mu_N$.[5] On the other hand, zippering does

[5]The total energy of the configuration is conserved because parts of the interacting string seg-

not occur if the incident strings collide with too great a velocity ν, or if the relative opening angle between strings with the same winding orientation is too large.

In Fig. 3.8 we show the kinematic constraints on the zippering of a pair of $N = 1$ strings, in terms of the incident relative velocity ν and the relative angle α, defined in Fig. 3.7. The region where zippering is kinematically allowed lies below the curves. The dashed line for weakly Type-I strings was obtained assuming $\mu_2/\mu_1 = 1.9$. The solid line corresponding to the kinematic constraint on a strongly Type-I flat-direction string was obtained using the tensions from Eq. (3.50), and found to be $\mu_2/\mu_1 \simeq 1.06$. As we will discuss below, the typical relative velocity of a pair of strings in the early universe is expected to be less than about $\nu \lesssim 0.7$. Thus, zippering of flat-direction strings in the early universe is kinematically allowed for a wide range of relative angles. In the weakly Type-I case, zippering is only possible for small relative velocities and angles making it much less likely to occur. This is why flat-direction strings can have a qualitatively different behavior in the early universe from the strings in the abelian Higgs model. Recall that there are no kinematic constraints on reconnection.

More generally, zippering can occur between Type-I strings with different tensions. Incident strings with winding numbers N_1 and N_2 can zipper into segments with $N_{zip} = (N_1 + N_2)$ or $N_{zip} = |N_1 - N_2|$ [56]. The corresponding kinematic constraint for the zippering of strings with unequal tensions was deduced in Ref. [85]. Zippering is only possible when the tension of the zippered segment is less than the sum of the tensions of the incident segments. Even when this condition is met, zippering is only allowed for a limited range of relative incident velocities ν and relative angles α (as defined in Fig. 3.7). We illustrate these kinematic constraints in Fig. 3.9 for the incident string pairs $N_1 = 1$ and $N_2 = 2$, $N_1 = 1$ and $N_2 = 100$, and $N_1 = 100$ and $N_2 = 101$. The tensions of these strings were computed using Eq. (3.50) with $\Delta = 10^{-20}$, which applies to flat-direction strings in the (a, b) theory described in

ments gain kinetic energy.

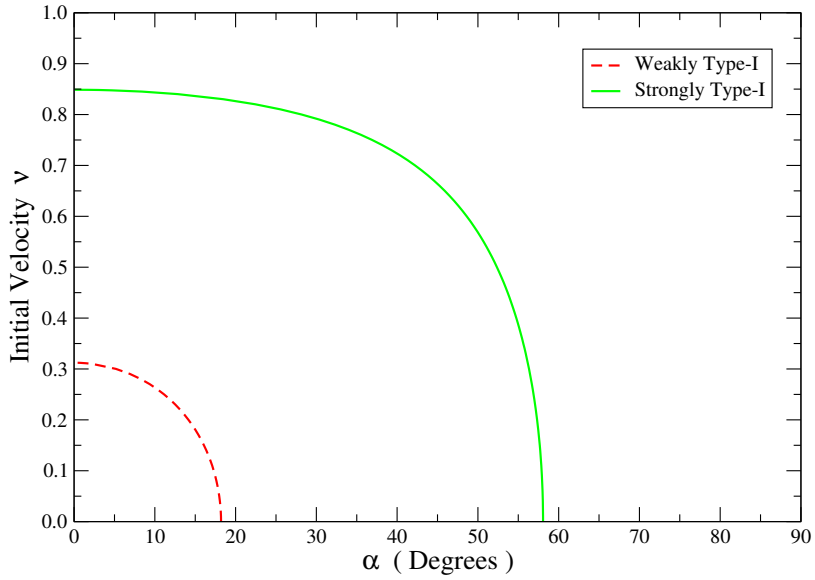

Figure 3.8. Kinematic constraints on zippering of two $N = 1$ strings to form an $N = 2$ string, in terms of the angle α indicated in Fig. 3.7 and the relative velocity ν. The allowed regions lie below the curves. The dashed line corresponds to weakly Type-I strings, with $\mu_2/\mu_1 = 1.9$. The solid line corresponds to strongly Type-I strings associated with a flat direction potential, with $\Delta = 10^{-20}$, and tensions computed according to Eq. (3.50), which gives $\mu_2/\mu_1 \simeq 1.06$.

Section 3.2. As before, the regions in which zippering is kinematically allowed lie below the curves. The kinematic constraints on flat-direction strings are not overly restrictive, and zippering of various sorts is possible over a wide range of relative velocities ν and relative angles α (as defined in Fig. 3.7).

When a pair of strings with winding numbers N_1 and N_2 intersect, they can pass through each other, or they can form a zipper with $N_{zip} = (N_1 + N_2)$ or $|N_1 - N_2|$. If $N_1 = N_2$, these strings can also reconnect.[6] There is no kinematic restriction on reconnection, and the kinematic constraints on zippering (into one of $|N_1 \pm N_2|$) are fairly mild. Having determined the possible outcomes, it is a much more difficult task to determine which of them actually occurs. The answer depends on complicated

[6]In fact, string reconnection can be treated as the formation of a *zipper* with $N_{zip} = 0$. The classical NG zippering solution reduces to the reconnection solution in this limit. The absence of a kinematic constraint on reconnection can be seen by setting $\mu_{zip} = 0$ in Eq. (3.51).

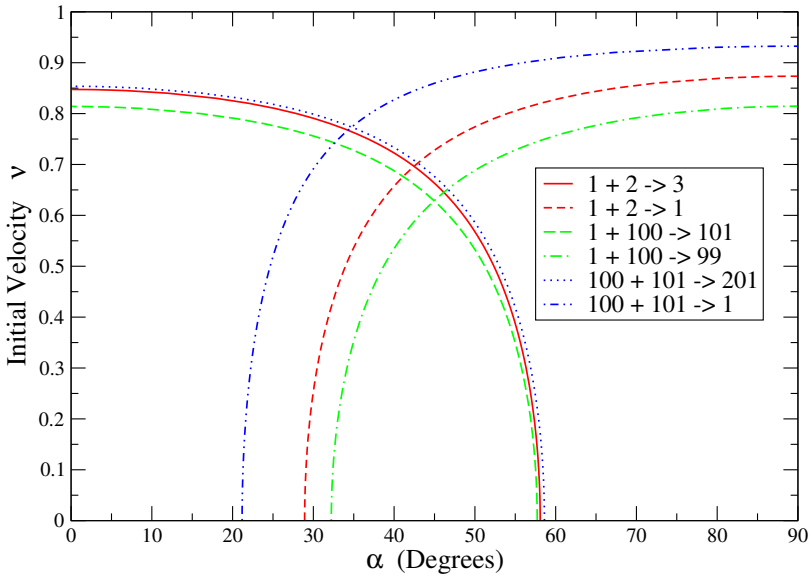

Figure 3.9. Kinematic constraints on zippering of strongly Type-I strings, for some examples involving higher winding numbers. The allowed regions lie below the curves. We have taken $\Delta = 10^{-20}$, and tensions computed according to Eq. (3.50).

non-linear field dynamics within the string cores, and would appear to be tractable only through numerical simulation. Unfortunately, even this approach is further complicated by the large disparity in scales between the sizes of the vector and scalar profiles within the strings. Such a simulation is beyond the scope of this work. However, our assumption that zippering is realized when kinematically allowed is compatible with several simulations we know of that treat the zippering of Type-I (abelian Higgs) strings [56, 58] and cosmic superstrings[59]. In these analyses, zippering appears to be a generic outcome of a low-speed string intersection. In Ref. [58], the strings are found to grow until they reach the size of the box used for the simulation, after which they pull apart. This appears to be the result of the boundary conditions applied to the box. We expect that in the applications of our assumptions about string zippering and reconnection, our qualitative results will still hold true provided the zippering and reconnection probabilities are of order unity.

To proceed, we will assume that zippering or reconnection are likely to occur when

they are kinematically allowed. Given the high probability of reconnection of abelian Higgs strings, this assumption does not seem overly optimistic. When both zippering and reconnection are possible, or when more than one kind of zippering is allowed, we will make use of the fact that the net force between a pair of strings is expected to be attractive. This suggests that, near the intersection point, the strings will pull together in whichever way is easiest. Thus, for a pair of strings with winding numbers N_1 and N_2, we will assume that a zipper with $N_{zip} = N_1 + N_2$ forms when $\alpha < 45^o$ (provided it is kinematically allowed), and that $N_{zip} = |N_1 - N_2|$ results for $\alpha > 45^o$. We identify the case $N_1 - N_2 = 0$ with reconnection.

We end this section with a brief comment of comparison regarding (p, q) cosmic strings arising from superstring theory. Like the flat-direction gauge-theory cosmic strings under consideration, (p, q) strings are also able to reconnect and form zippers [68]. Even so, there are several important differences between the inter-string interactions within these two classes of cosmic strings. The reconnection of (p, q) strings is a quantum mechanical process that can be related to amplitudes in superstring theory [69, 70, 71, 72, 73, 74, 75]. In this sense, it is more tractable than the non-linear classical calculation required for field theory strings. It is found that the reconnection probability for (p, q) strings can be much smaller than unity, $P_r \sim 10^{-3}$–1, depending on the underlying microscopic details. The rules for zippering are also different for (p, q) strings. An initial state consisting of the modes (p, q) and (p', q') can form a zippered state with $(|p \pm p'|, q \pm q')$, which is similar to the topological rule for Type-I field theoretic strings presented above. However, a (p, q) cosmic string is stable only if p and q are relatively prime integers, and thus the resulting zipper may sometimes decay into lower string modes. A recent numerical simulation of a toy-model for (p, q) cosmic superstrings has found that long-lived zippered states are formed provided the forces between the strings are short-ranged [84].

3.3.3 Loop Formation

Reconnection plays a crucial role in the evolution of a cosmic string network because it is the means by which string loops form. String loops are not topologically stable, and their decays transfer energy out of the string network. When cosmic strings are also able to form zippers there are new ways for string loops to form and interact. In the present section we enumerate some of these additional possibilities. We will discuss the resulting effects on the cosmological evolution of a string network in Sections 3.4 and 3.5.

In Fig. 3.10 we illustrate the two ways in which a loop can form when a string intersects itself. The first possibility produces a free loop through the reconnection of the intersecting segments. This can occur for both Type-I and Type-II strings, and is the standard mechanism for loop formation. The loop produced is free from the parent string. The second possibility for loop formation through self-intersection involves zippering of the connecting segments. The loop formed in this way remains bound to the parent string by a zippered segment of winding number $N_{zip} = 2\,N_1$, where N_1 is the winding number of the parent. We expect the zippered segment formed in this way to grow until the opening angle at the junction approaches the kinematic bound given in Eq. (3.51). Subsequently, provided there are no disturbances on the string large enough to rip the zipper apart, the bound string loop will remain attached to the parent string as it radiates and shrinks to naught.

String loops can also be formed by the double intersection of a pair of curved strings. Suppose the incident strings have winding numbers N_1 and N_2. The topologically-allowed loops that can form in this way are illustrated in Fig. 3.11. At each intersection, there are two ways for the strings to interact with each other by zippering; they can form segments of winding number $N_{zip} = N_1 + N_2$ or $N_{zip} = N_1 - N_2$. (Here and only here, the sign of N_i should be understood as specifying the relative orientation of the string segment.) Possibility 1, in which both intersections pro-

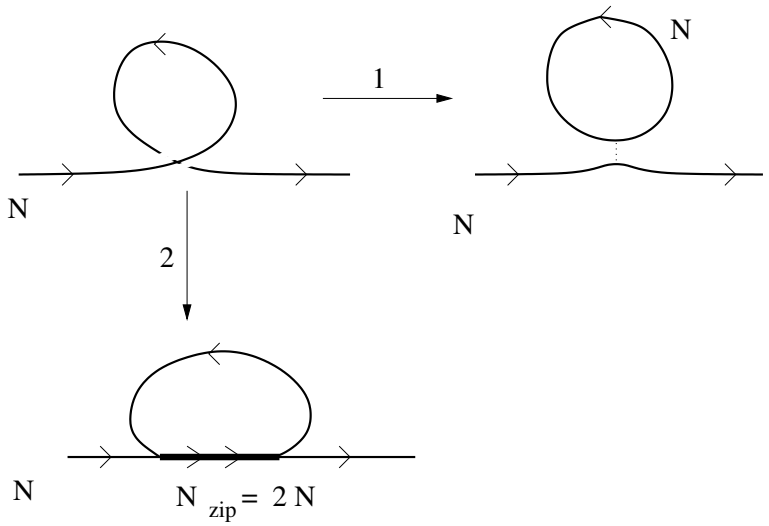

Figure 3.10. Two possible ways to form a loop from the self-intersection of a string segment. Possibility 1, in which a free loop is formed by string reconnection, can occur for both Type-I and Type-II strings. Possibility 2, in which the loop remains connected to the parent string by a zippered segment of a higher winding mode string, is only possible for Type-I strings.

duce segments of winding $N_{zip} = N_{1+2} = N_1 + N_2$ corresponds to the usual Type-II outcome when $N_1 = -N_2$. Possibility 2 has both zippered segments with windings $N_{zip} = N_{1-2} = N_1 - N_2$. It reduces to the standard Type-II case for $N_1 = N_2$. Possibility 3 has zippered segments with winding $N_1 + N_2$ and $N_1 - N_2$. It is not immediately obvious how these configurations will evolve, but we speculate that the loops will shrink, either through zipper growth or loop radiation, until only a single zippered segment remains. The multiple outcomes shown in Fig. 3.11 also illustrate some of the many new qualitative features of a string network consisting of strongly Type-I strings.

3.4 Cosmic String Formation and Evolution

Cosmic strings are much less strongly constrained by cosmology than most other types of topological defects [168, 169]. The reason for this is that a network of cosmic strings is able to regulate its energy density by forming loops, which radiate away. Without loop formation, the energy density in a cosmic string network would scale

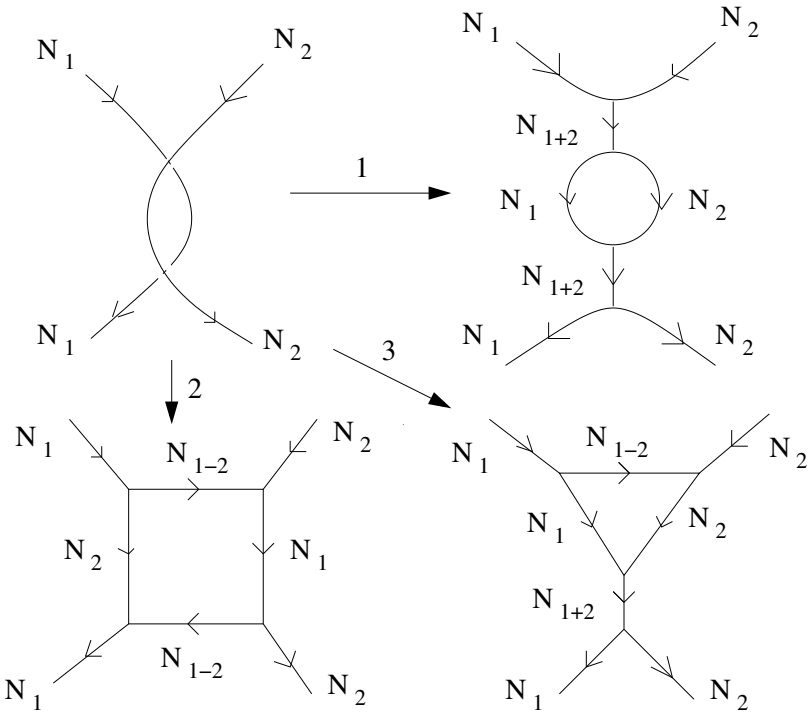

Figure 3.11. Three ways to form a loop from the overlapping intersection of a pair of Type-I cosmic strings with winding numbers N_1 and N_2. In the figure, we have labelled the net winding number of each string segment.

as a^{-2}, redshifting more slowly than both matter (a^{-3}) or radiation (a^{-4}), and could come to dominate the universe. Instead, when strings are able to form unstable loops, numerical and analytic simulations suggest that the energy density of a string network tracks the dominant background matter or radiation density [177, 178, 179, 180, 181]. This behavior is called *scaling*. In the scaling regime, the energy density of the string network makes up a fixed proportion of about $G\mu$ of the total energy density, and this proportion is nearly independent of the initial string density. As long as $G\mu$ is not too large, $G\mu \lesssim 3 \times 10^{-7}$ [95, 96, 97, 98, 99, 100], cosmic strings are generally consistent with existing cosmological bounds.

The behavior described above was deduced from the study of Type-II abelian Higgs string networks containing only a single string species [168, 169]. Strongly Type-I strings associated with supersymmetric flat directions can modify this picture in a couple of important ways. First, flat-direction strings have stable higher winding

modes. Even if modes with $N > 1$ are not formed initially, they can be produced as the network evolves by the zippering of lower string modes. This opens the possibility that flat-direction strings form a multi-tension string network consisting of many different species. The second reason why the evolution of flat-direction strings in the early universe is likely to be different than for ordinary strings is the flatness of the scalar potential. If the $U(1)$ gauge symmetry corresponding to the strings is restored after (or near the end of) primordial inflation, it is likely that there will be a second, later period of *thermal inflation* [86, 88]. Flat-direction strings would be formed at the end of thermal inflation, and hence their initial evolution is expected to be significantly different from that of abelian Higgs strings.

3.4.1 Thermal Inflation and String Formation

Thermal inflation occurs due to the sensitivity of flat potentials to thermal corrections [86, 87, 88]. This flatness can be quantified by the large disparity between the size of the curvature scale $m \sim 10^{2\text{–}3}$ GeV and the size of the VEV, $v \geq 10^{11}$ GeV. At the symmetry-preserving origin of the field space, there are additional light degrees of freedom. These induce significant corrections to the effective potential near the origin, making it stably concave at high temperatures, with a curvature scale on the order of the temperature T. For $m \ll T \ll v$, a second lower minimum can develop far from the origin, close to the $T = 0$ vacuum. If the system begins in the symmetry preserving phase, thermal corrections will trap it at the origin until the temperature falls down to $T \sim m$ [89, 46]. While the system is trapped at the origin, it has an excess vacuum energy on the order of m^2v^2. Once the temperature of the universe falls below $\sqrt{m\,v}$, the false vacuum energy can become dominant and drive a period of inflation.

Thermal inflation lasts only until T falls down to m. The number of e-foldings of

expansion is therefore less than [88]

$$N_i \simeq \frac{1}{2}\,\ln\left(v/m\right) \simeq 10 + \frac{1}{2}\ln\left[\left(\frac{v}{10^{14}\,\mathrm{GeV}}\right)\left(\frac{10^3\,\mathrm{GeV}}{m}\right)\right]. \tag{3.52}$$

This is not enough expansion to replace primordial inflation. At the end of thermal inflation the system evolves to the true minimum of the potential. In this regime the constituent fields Φ_a and Φ_{-b} both condense, and the theory can be described in terms of a light chiral supermultiplet corresponding to the flat direction along with a heavy massive vector supermultiplet [76]. The scalar component of the light chiral multiplet rolls down the potential to the true minimum and begins to oscillate. The false vacuum energy is transferred to the energy of the oscillations, which redshifts like matter, and dominates until the scalar field decays into radiation and reheats the universe.

The reheating process can be described by the system of Boltzmann equations

$$\dot{\rho}_\phi = -3\,H\,\rho_\phi - \Gamma_\phi\,\rho_\phi, \tag{3.53}$$

$$\dot{\rho}_r = -4\,H\,\rho_r + \Gamma_\phi\,\rho_\phi, \tag{3.54}$$

where ρ_ϕ is the energy density of the scalar field oscillations, ρ_r is the energy density in radiation, Γ_ϕ is the scalar field decay rate, and the Hubble constant H is given by

$$H = \frac{\dot{a}}{a} = \sqrt{\frac{8\pi G}{3}\rho_{tot}}. \tag{3.55}$$

Here, ρ_{tot} is the total energy density in the universe. During reheating, ρ_{tot} is dominated by ρ_r and ρ_ϕ. The initial values for these evolution equations are $\rho_r \simeq m^4$, $\rho_\phi \simeq m^2 v^2$, and $t_i \sim 10\,H_i^{-1} \sim 10\,M_{\rm Pl}/m\,v$. The generic value of the flat-direction decay rate is [88]

$$\Gamma_\phi = \gamma\,\frac{m^3}{v^2}, \tag{3.56}$$

with γ a constant less than or of order unity. Once the scalars decay at about the time $t_{RH} = \Gamma_\phi^{-1}$, the universe becomes radiation dominated with a reheating temperature

of

$$\begin{aligned} T_{RH} &\simeq g_*{}^{-1/4}(M_{\rm Pl}\Gamma)^{1/2} \\ &\simeq 100\ {\rm MeV}\ \left(\frac{g_*}{10}\right)^{-1/4}\left(\frac{\gamma}{0.1}\right)^{1/2}\left(\frac{10^{14}\ {\rm GeV}}{v}\right)\left(\frac{m}{10^3\ {\rm GeV}}\right)^{3/2}, \end{aligned} \tag{3.57}$$

where g_* is the number of relativistic degrees of freedom at temperature T_{RH} and $M_{\rm Pl} = 1/\sqrt{8\pi\, G} \simeq 2.4\times 10^{18}$ GeV is the reduced Planck mass. The reheating temperature must exceed about 5 MeV to preserve the predictions of nucleosynthesis [90, 91]. With $m = 10^3$ GeV and $\gamma = 1$, this puts an upper bound on $v \lesssim 10^{16}\,$GeV, while for $m = 200$ GeV and $\gamma = 0.1$, the upper bound is strengthened to $v \lesssim 10^{14}$ GeV. We will mostly focus on values of the VEV less than $v \leq 10^{14}$ GeV for the rest of the work.

If flat-direction strings are to form, the corresponding $U(1)$ gauge symmetry must be restored at or near the end of primordial inflation. Thus, if flat-direction strings are present in the universe today, they were most likely formed after a period of thermal inflation. The initial densities and properties of the strings depend on the details of the phase transition ending thermal inflation, when the flat-direction field overcomes the thermal barrier and starts to roll down to the true minimum. The nature of this transition has been studied in Refs. [89, 46]. These authors find the tunnelling rate through the thermal barrier to be negligibly small until $T \sim m$. Below this temperature the tunnelling suppression is not parametrically large, and bubbles nucleate rapidly. Of particular importance to string formation is the radius of the bubbles of true vacuum when they coalesce, ξ. The initial size and separation between string segments are approximately equal to ξ. Since the phase transition proceeds quickly once the temperature falls below m, we expect ξ to be within a few orders of magnitude of m^{-1}.

The mechanism for string formation in the (a, b) model of flat-direction strings can be most easily understood in terms of *flux-trapping*. The winding number of a

cosmic string is directly proportional to the net magnetic flux it carries in its core. In the broken phase, the magnetic flux is shielded. As a result, random fluctuations of the gauge field in the unbroken phase can be trapped between bubbles of broken phase. The scalar fields surrounding tubes of trapped flux then orient themselves to form a cosmic string with the appropriate flux quantum number. If ξ is the typical bubble size at coalescence, the mean winding number of the strings formed in this way is [92, 93]

$$N \sim \frac{g}{2\pi}\sqrt{\xi\, T_f}, \tag{3.58}$$

where T_f is the temperature at formation. Since the phase transition proceeds quickly once T falls below m, we expect that ξ will not be too much larger than $T_f^{-1} \sim m^{-1}$ [46]. Therefore only the lowest winding modes will be significantly populated at the beginning. Let us also point out that the net magnetic flux of the configuration of Eq. (3.20) is N, independent of a and b.

3.4.2 String Network Evolution

Once cosmic strings are formed, their density evolves under the influence of the spacetime expansion, as well as the processes of reconnection and zippering. String reconnection is particularly important because it allows the string network to form loops and thereby transfer its energy into radiation. In the case of ordinary (abelian Higgs model) cosmic strings, the processes of string growth and loop production are found to balance each other, leading to a scaling solution. Flat-direction strings can also interact by zippering. This permits the formation of higher winding modes starting from an initial population consisting only of the lowest few modes.

Cosmic string evolution has been studied extensively through numerical simulations [168, 169, 177, 178]. However, there has been no attempt that we know of to simulate a multi-tension string network including string zippering. In the absence of such simulations, we turn to analytic models of string evolution for guidance. A

number of simple models have been constructed, and they give a good reproduction of the behavior of the long (horizon-length) string structure seen in simulations of the abelian Higgs model. To investigate the evolution of long flat-direction strings, we will make use of the model of Tye, Wyman, and Wasserman (TWW) [64], which generalizes the formulation of Ref. [179]. The TWW model was constructed to study the behavior of long superstring cosmic strings, which also exhibit stable higher-winding modes and zippering, but with different rules for the outcome of string zippering.

In the TWW model, long cosmic strings are characterized by a mean velocity ν, a typical correlation length along the strings L, and a mean string number density n_a, where a labels the winding number of the string (*i.e.* $N = a$). The number density of the string species a is defined through its relation to the energy density according to

$$\rho_a = \frac{\mu_a \, n_a}{\sqrt{1-\nu^2}}, \tag{3.59}$$

where μ_a is the tension of the species. All string species are assumed to be described by the same ν and L. This is a reasonable simplification for two reasons. First, the tension of different strings is a slowly varying function of the winding number, so in the absence of interactions with other string species, each string type should evolve in much the same way. Second, higher winding modes are mainly formed by the zippering of lower winding modes. Thus it is feasible that the speed and the fluctuation size of different string varieties should be roughly similar.

The evolution equations for ν and L in the TWW model are taken to be

$$\frac{dL}{dt} = HL(1+\nu^2) + c_1\nu, \tag{3.60}$$

$$\frac{d\nu}{dt} = (1-\nu^2)\left[\frac{c_2}{L} - \nu\,(2H)\right]. \tag{3.61}$$

These equations are based on the model of Ref. [179], where they are derived from the averaged equations of motion for a string evolving in an expanding Friedmann-

Robertson-Walker background spacetime.[7]

The TWW model generalizes Ref. [179] by adding an independent density variable n_a for each species. The value of n_a is taken to evolve according to a Boltzmann-like equation

$$\begin{aligned} \dot{n}_a &= -2\,H\,n_a - \frac{c_2\,n_a\,\nu}{L} - P_a\,n_a^2\,\nu\,L \\ &\quad + F\,\nu\,L\sum_{b,c}\left[\frac{1}{2}P_{abc}\,n_b n_c\,(1+\delta_{bc}) - P_{bca}\,n_c n_a\,(1+\delta_{ac})\right]. \end{aligned} \tag{3.62}$$

Here, P_a is proportional to the probability of self-reconnection for a string of variety a, P_{abc} is the interaction probability for the process $b + c \to a$, and F is an overall non-self-interaction factor. Once the time dependence of H is specified, Eqs. (3.60, 3.61, 3.62) form a closed system describing the evolution of the long string component of a multi-tension string network.

The values of the constants appearing in Eqs. (3.60, 3.61, 3.62) can be fixed by comparing the scaling solution for a single (non-interacting) string to values obtained in string simulations. Ref. [64] reports that such an agreement is obtained with $c_1 = 0.21$, $c_2 = 0.18$, and $P_1 = 0.28$. We use the same values for c_1 and c_2, which are related to the efficiency of loop formation and the amount of small-scale structure on the strings, respectively. For P_a and F, we set them to $P_a = F = 0.28/2 = 0.14$. Since P_a is proportional to the probability of reconnection, this accounts for our assumption that a pair of strings is just as likely to zipper as to reconnect when both outcomes are kinematically allowed. We also set the coefficients P_{abc} to

$$P_{abc} = \begin{cases} 1; & a = |b \pm c|, \quad \nu < \nu_{\rm thresh}, \\ 0; & \text{otherwise.} \end{cases} \tag{3.63}$$

These values are in accord with our assumptions about zippering. Motivated by the

[7] Ref. [179] also considers frictional forces acting on cosmic strings. As in the TWW model, we do not include frictional effects in our analysis. We have checked that they are negligible for $v > \sqrt{m\,M_{\rm Pl}}$, which is expected for the flat-directions strings under consideration.

results of Section 3.3, we set the velocity threshold for zippering to $\nu_{\rm thresh} = 0.85$ in our numerical analysis.

To evaluate Eqs. (3.60, 3.61, 3.62) describing the evolution of the string network, we must also specify the evolution of the Hubble parameter H appearing in these equations. We do this by solving for the scale factor $a(t)$ using Eq. (3.55). After thermal inflation, the two dominant sources of energy density are ρ_ϕ, from the oscillations of the light scalar field, and ρ_r for radiation. We begin the evolution at the time $t_i = 10\, M_{\rm Pl}/mv$, as would be expected after thermal inflation. The initial radiation density is taken to be $\rho_r(t_i) = m^4$, while the initial scalar field energy density is set to $\rho_\phi(t_i) = m^2\, v^2$. After time t_i, ρ_ϕ and ρ_r evolve according to Eq. (3.53). Since we are interested in running the string evolution equations all the way to the present time, we also add a very small matter density at the end of thermal inflation, at $t_{RH} = \Gamma_\phi^{-1}$. The initial matter density is chosen such that it becomes the dominant form of energy at the approximate equality time $t_{eq} = 3 \times 10^{36}$ GeV^{-1}. For reference, the present time is about $t_0 \simeq 6.6 \times 10^{41}$ GeV^{-1}. With $m = 10^3$ GeV, $v = 10^{13}$ GeV, and $\gamma = 0.1$, the initial matter density is $\rho_m(t_{RH}) = (8.0 \times 10^{-3}\ {\rm GeV})^4$. At later times, this dilutes according to $d\rho_m/dt = -3\, H\, \rho_m$. Throughout the evolution of H, we self-consistently assume that the energy density due to the string network plays a negligible role[8].

We appeal to our expectations from thermal inflation to set the initial values of the variables ν, L, and n_a. The symmetry breaking phase transition after thermal inflation occurs quickly once the temperature falls below $T = m$. The mean bubble radius ξ when they coalesce should be therefore not much larger than the nucleation radius, which is close to m^{-1} [46]. Thus, we set $L(t_i) = 5m^{-1}$ and $n_1(t_i) = 1/(5m^{-1})^2$ as reasonable starting values. The initial densities of the higher winding modes, $a > 1$, are set to zero. We also choose $\nu(t_i) = 0.9$. While there is considerable arbitrariness

[8]This is because in general $\Omega_{string} \sim G\mu$ and observations constrain $G\mu \lesssim 10^{-6}$.

in these choices of initial conditions, we find that our results at late times are largely independent of them.

In Figs. 3.12 and 3.13 we show the numerical solutions of the string network equations for the model parameter values $m = 10^3$ GeV, $v = 10^{13}$ GeV, and $\gamma = 0.1$. For comparison with Section 3.2, this choice corresponds to a value of $\Delta = g^2 m^2/v^2 \simeq 10^{-20}$. Fig. 3.12 depicts the evolution of the densities of the five lowest winding modes in terms of the quantities

$$\tilde{\Omega}_a = \frac{\mu_1}{\mu_a}\Omega_a = \frac{\mu_1\, n_a}{\rho_c\sqrt{1-\nu^2}}, \tag{3.64}$$

where Ω_a is the ratio of the energy density of string species a relative to the critical density $\rho_c = 3\,H^2/8\pi\,G$, and μ_a is the tension of string species a. Normalizing by the tension makes $\tilde{\Omega}_a$ proportional to n_a times a quantity that is independent of the winding number. In Fig. 3.13 we show the evolution of the universal length scale L and universal string velocity ν.

Figs. 3.12 and 3.13 show that (within the TWW model) the string energy densities approach a *scaling* solution at late times as evidenced by HL, ν, and $\tilde{\Omega}_a$ all flowing to constant values. The scaling length, velocity, and densities are largely independent of the initial state of the string network. At late times, the string densities make up a nearly fixed fraction of the total energy density of the universe. We also find that the early era of oscillation dominance during reheating does not alter the final string densities in an appreciable way. These features are very similar to what is found in simulations of ordinary (abelian Higgs) string networks with only a single string species [177, 178].

The interesting new feature in the evolution of flat-direction cosmic strings is that nearly all string species flow towards very similar scaling values. This is the result of string zippering, which allows the formation of higher winding modes from lower ones. Note that the formation of these higher modes does not begin immediately. With the initial values specified above, the initial string length scale L is much smaller than its

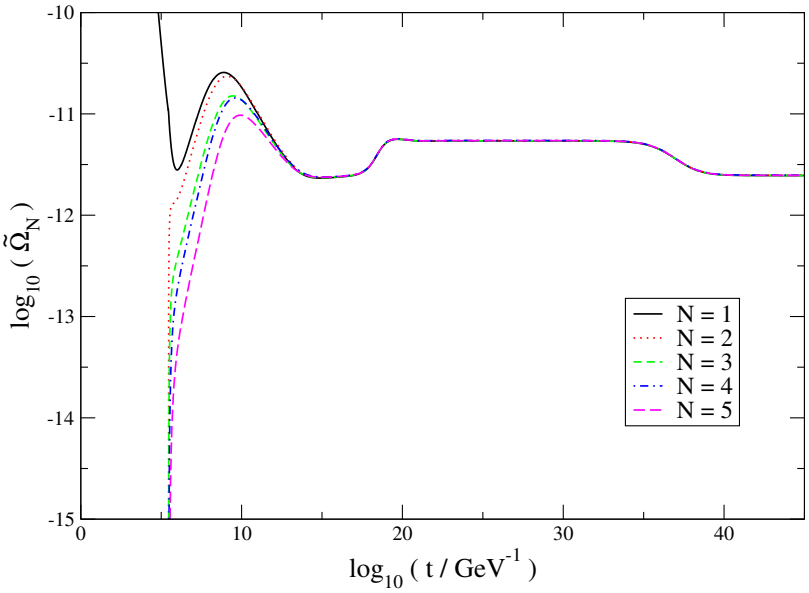

Figure 3.12. Evolution of cosmic string densities after thermal inflation with $v = 10^{13}$ GeV, $m = 10^3$ GeV, and $\gamma = 0.1$. We have also set $N_{max} = 50$ in generating this plot.

scaling value, which is close to the horizon scale. This has the effect of rapidly driving the string speed to its maximal value, $\nu \to 1$, at the outset, as can be seen in Fig. 3.13, which effectively shuts off string zippering. Once L and ν settle down to near their scaling values, zippering begins and the higher winding-mode densities quickly flow towards their scaling values. This scaling behavior is quite robust. Changing the values of F and $\nu_{\rm thresh}$ does not alter the qualitative string densities provided $\nu_{\rm thresh}$ is larger than the mean string velocity in the scaling regime.

The fact that many string species flow towards equal scaling values complicates the numerical analysis, since numerical limitations allow us to include only a finite number of winding modes up to an unphysical maximal value N_{max}. In making Figs. 3.12 and 3.13 we have set $N_{max} = 50$. We also find that the final, nearly universal scaling density of the strings depends on the artificial value of N_{max}. This feature is illustrated in Fig. 3.14. To a good approximation, the near-universal string

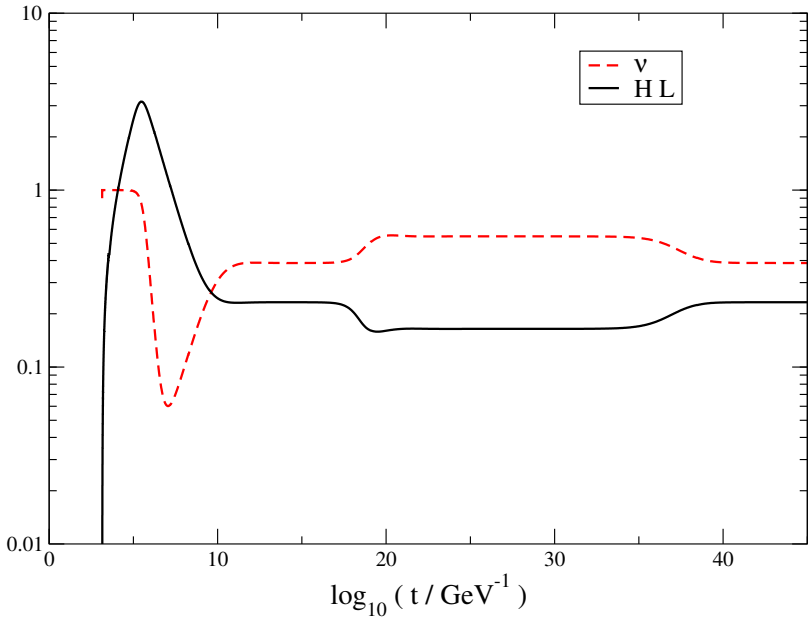

Figure 3.13. Evolution of cosmic string speed and length scales after thermal inflation with $v = 10^{13}$ GeV, $m = 10^3$ GeV, and $\gamma = 0.1$. We have also set $N_{max} = 50$ in generating this plot.

scaling density goes like

$$\tilde{\Omega}_a \propto \frac{1}{N_{max}}, \tag{3.65}$$

as illustrated by the dotted line in Fig. 3.14. (For each specie a, approximately there is another $\ln a$ factor to characterize the mild dependence on winding number.)There is a mild specie a dependence. Evidently, the string energy density gets spread out among the many string types. There is also the question of how to handle the zippering of strings whose winding numbers sum to greater than N_{max}. In principle, these strings can zipper into modes with $N > N_{max}$ which are not included in the simulation. In Figs. 3.12 and 3.13 and in the analyses to follow, we simply disallow all such zippering processes. This leads to slight increase in the scaling density of modes with $N \gtrsim N_{max}/2$. However, we have also studied other prescriptions for handling these zippering events, and for the examples we looked at, we find qualitatively similar results for the modes with $N \ll N_{max}$.

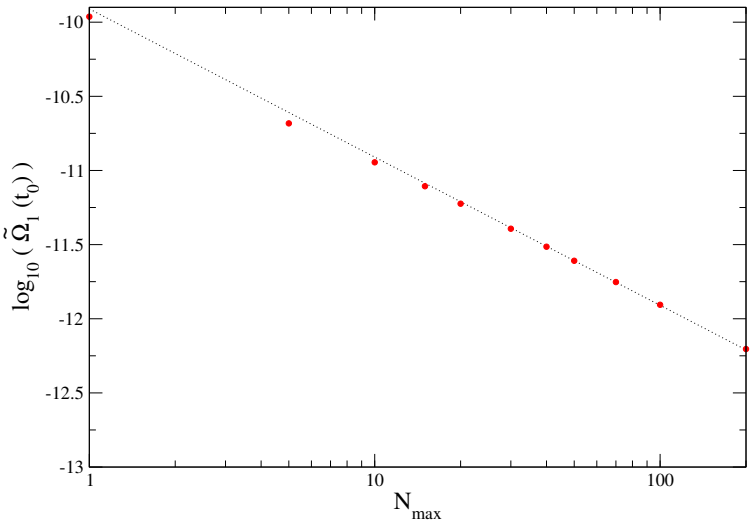

Figure 3.14. Dependence of the scaling-regime string density on the total number of string species included in the simulation, N_{max}. The dotted line shows a fit to $\tilde{\Omega}_1 \propto 1/N_{max}$.

The dependence of the scaling densities on N_{max} is clearly unphysical. We would like to take $N_{max} \to \infty$, but this has its own problems. Since the energy density at large N goes like $\ln a$ (from the logarithmic dependence of the tension on the winding number), if all string species flow towards a universal scaling density proportional to N_{max} the total network energy density goes like

$$\rho_{tot} \propto \frac{1}{N_{max}} \sum_{a=1}^{N_{max}} \ln a \simeq \ln N_{max}. \tag{3.66}$$

This diverges logarithmically as $N_{max} \to \infty$. In practice, however, this divergence is not realized. The initial string spectrum consists almost entirely of the lowest modes, the density of higher modes is built up from the lower modes by zippering, and these higher modes take longer to reach their scaling values. At any given time, only a finite number of strings have developed their scaling density.[9] Let us define $N_{eq}(t)$ as

[9]In this sense, our use of the term *scaling* for flat strings is somewhat more general than its meaning for ordinary cosmic strings because the string densities are not completely static, but very slowly varying.

the highest mode that has reached scaling by time t. Modes with $N > N_{eq}(t)$ all have densities well below their equilibrium scaling values. Thus, at time t, we effectively have $N_{max} = N_{eq}(t)$, and the total energy contained in the string network goes like $\ln N_{eq}(t)$.

In Fig. 3.15 we show the time evolution of $N_{eq}(t)$ for several values of N_{max}. All other parameters are the same as in Figs. 3.12. The curves for different values of N_{max} match up for $N \lesssim N_{max}/3$, but start to deviate from each other as the winding number N approaches N_{max}. Focusing on the apparently universal portion of these curves, the rate of increase of $N_{eq}(t)$ with time goes like $t^{0.22}$. If we can extrapolate this dependence to much larger winding numbers, the value of N_{eq} at the present time t_0 will be

$$N_{eq}(t_0) < \left(\frac{t_0}{t_i}\right)^{0.22} \simeq 10^8, \tag{3.67}$$

where we have used $t_i \simeq 10\, M_{\rm Pl}/m\, v \simeq 2.4 \times 10^3\, {\rm GeV}^{-1}$ and $t_0 \simeq 6.6 \times 10^{41}\ {\rm GeV}^{-1}$. This is a very large number, but it is not so large so as to be problematic. Recall that the string tension, given in Eq. (3.50), increases logarithmically with the winding number. The tension of a string with $N = 10^8$ is merely

$$\mu_N < 3\, \mu_1, \tag{3.68}$$

for $m = 10^3$ GeV and $v = 10^{13}$ GeV, corresponding to $\Delta \simeq 10^{-20}$ in Eq. (3.50). Moreover, the total string energy density in the network is less than about $\ln N_{eq}(t_0) \lesssim 20$ times the energy density of a network containing a single type of string with the same tension as the lowest mode. These values for the maximal tension and the total string density are not much larger than for an ordinary cosmic string, and they present no obvious cosmological difficulties.

In our analysis of flat-direction string network evolution described above we have used a very simple analytic model of string network evolution; we have made specific assumptions about the details of the string interactions; and, we have made

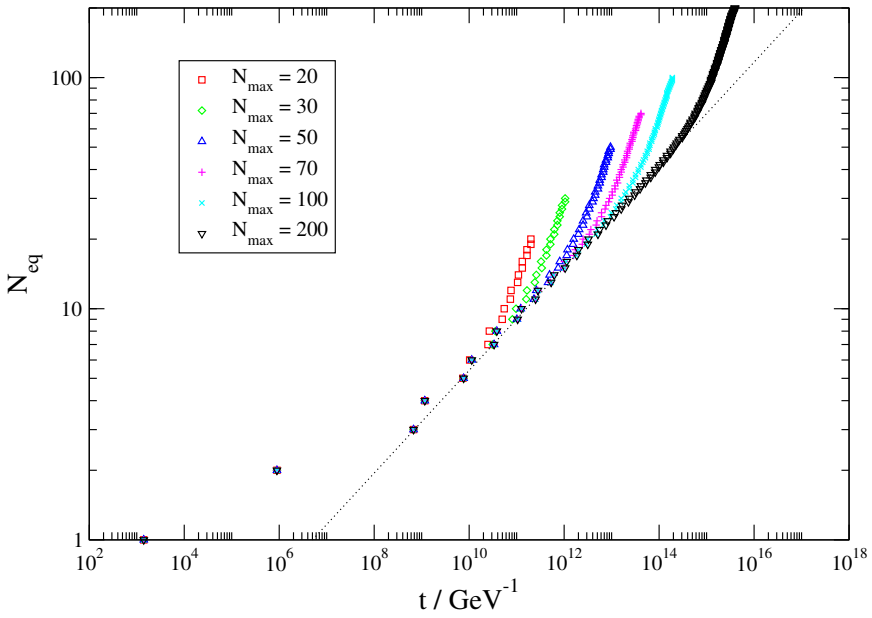

Figure 3.15. The number of string species that have reached scaling, N_{eq}, as a function of time in the aftermath of thermal inflation for different values of N_{max}, with the parameter values $v = 10^{13}$ GeV and $m = 10^3$ GeV. The dotted line indicates an approximate fit to $N_{eq}(t) \propto t^{0.22}$ in the region where the curves appear to be universal.

extrapolations into regions well beyond what we are able to probe analytically and numerically. Nevertheless, a simple picture for the evolution of a flat-direction string network emerges from our results, and is likely to be genuine, even if some of the underlying assumptions are not necessarily rigorous and the model used to study the network evolution is overly simple. In this picture, a very large number of string species reach similar scaling densities by the present time. The total energy of the network is within an order of magnitude or two of the energy density that a single abelian Higgs string species would have for the same value of the string tension. However, instead of being concentrated within a single species, the string energy density is nearly uniformly distributed among all the string species that have attained scaling. Thus, the flat-direction string network consists of a near *continuum* of string species, but with global properties that closely resemble those of a single species network.

Our argument for this picture is based on the very slow dependence of the flat-direction string tensions on the winding number. On account of this slow variation, the macroscopic properties of the many species that have attained scaling are very similar to each other. For example, Fig. 3.4 shows that the tension of a mode with $N = 100$ is only about 1.4 times that of the $N = 1$ mode for $\Delta \simeq 10^{-20}$. From this feature, as long as the zippering is reasonably efficient and the lowest mode is able to attain a scaling value for its density, we expect the densities of the string modes to be very similar to one another up to large values of the winding number $N \gg 1$.

One curious aspect of this picture from TWW model is that the total energy density in the network corresponds to less than a few hundred individual strings of horizon length. It is therefore curious that the TWW model applied to flat-direction strings predicts that there are many more string species than this in the scaling regime at the present time, each with a characteristic length scale of horizon size. We suggest that the scaling densities predicted by the TWW model for flat-direction strings should be interpreted as time-averaged values. At any given epoch in the scaling regime, there exist many fewer long strings than $N_{eq}(t)$. However, these strings are continually zippering into other string species, and averaged over time, many more string species are populated (with a lower density per string) than are present at any one time. It is also possible that this issue of discreteness leads to a value of $N_{eq}(t)$ that is smaller than what is predicted by the TWW model.

A definite confirmation of this picture of flat-direction string evolution would appear to require a full numerical simulation of the network (as well as lattice simulations to determine the zippering probabilities). This task is complicated by the need to include many different string species in the simulation and by the fact that with only, ~ 100 strings stochastic effects could be important. Such full simulation is beyond the scope of this work. We have, however, examined the effect of changing some of our assumptions about string zippering encoded in the coefficients P_{abc}, de-

fined in Eq. (3.63). For example, we find that reducing the probability for zippering into $a = (b + c)$ relative to $a = |b - c|$ does not significantly alter the final scaling densities. We have also looked into modifying the interaction terms in Eq. (3.62), as suggested in Ref. [67], and we again find the same qualitative picture of string network evolution. These results suggest that the picture of flat string evolution presented here is robust.

Before moving on, let us briefly compare our near-*continuum* picture of flat-direction cosmic strings to the cosmological picture of (p, q) superstring cosmic strings derived in Ref. [64]. These quasi-fundamental strings can be labelled by pairs of integers (p, q) with $p \geq 0$. A string state is stable only if p and q are relatively prime. States with (p, q) not relatively prime can be formed but are only marginally stable. They are expected to decay into lower, stable modes after they are created. In the analysis of Ref. [64], this additional dissipative channel led to a rapid decrease in the relative population of higher-tension modes. That superstring cosmic strings do not form a near-continuum scaling network is also not surprising given that the tensions of these strings increase fairly rapidly with the mode numbers [64],

$$\mu_{(p,q)} \propto \sqrt{g_s^2\, p^2 + q^2}, \tag{3.69}$$

where g_s is the superstring coupling.[10] Hence, even though flat-direction cosmic strings and (p, q) strings can both form stable winding modes through zippering, these two varieties of cosmic strings interact and evolve in significantly different ways.

3.5 String Signatures

If cosmic strings are present in the early universe they can give rise to a number of observable signatures. No evidence for cosmic strings has been found in the temperature power spectrum of the cosmic microwave background or in large-scale sky

[10] This formula applies in ten-dimensional flat space. It may receive corrections in other backgrounds [94].

surveys. This implies the constraint $G\mu \lesssim 3 \times 10^{-7}$, fairly independently of the underlying string model [95, 96, 97, 98, 99]. Beyond these limits, the most promising signatures for ordinary (abelian Higgs) cosmic strings are gravitational lensing and gravitational radiation [168, 169]. We find that these signals can be modified for flat-direction cosmic strings. Flat-direction cosmic strings are also more likely to radiate into their constituent particles than ordinary cosmic strings, leading to new classes of potential signatures. By combining observations of several different phenomena, it may be possible to distinguish flat-direction cosmic strings from ordinary cosmic strings as well as (p, q) cosmic superstrings.

3.5.1 Gravitational and Particle Radiation from Loops

Cosmic strings emit gravitational radiation primarily through the oscillations of string loops. For both ordinary and flat-direction cosmic strings, a single loop is expected to emit gravitational radiation with power

$$P_{gw} = \Gamma\, G\mu^2, \tag{3.70}$$

where $\Gamma = 10 - 100$ is a dimensionless constant whose precise value depends on how the loop is oscillating [189, 192, 195, 194, 196]. This rate is independent of the length of the loop, ℓ. The radiation frequencies do depend on ℓ and are

$$f_n = \frac{2\,n}{\ell}, \qquad n = 1, 2, 3, \ldots \tag{3.71}$$

with the relative power going into mode n decreasing at least as quickly as $n^{-4/3}$ for simple string loop solutions [192, 195, 194, 196].

To compute the gravitational wave background from a cosmic string network, one must convolute the power emitted by individual loops with the loop density distribution. Unfortunately, even for ordinary cosmic strings, the loop density distribution is not fully understood. The main uncertainty is the size of loops when they are formed.

It is standard to parametrize the typical initial loop length according to

$$\ell_i = \alpha\, t, \tag{3.72}$$

where t is the time of loop formation, and estimates for α range between the string width [180], to $(\Gamma\, G\mu)^\chi$ with $\chi \geq 1$ [201, 202, 203], all the way up to $\alpha = 0.1$ [198]. We will consider different values of α below.

Cosmic string loops can also radiate directly into particles [187, 111, 112]. This can arise both through the direct emission of particles from smooth strings [187, 111, 112], as well as from *cusp annihilation* [190]. For the string loops present in the early universe, cusp annihilation is usually the more important source of particle emission [190].[11] A *cusp* is a point on a string that reaches the speed of light at some instant during its (Nambu-Goto) evolution. Cusps are a generic feature of many simple solutions for the motion of a string loop, where they are found to occur about once per oscillation period [192, 169]. In the region near the cusp, the string segments fold back upon themselves such that the separation between the adjacent segments becomes smaller than the string width. This allows these string segments to annihilate each other. Cusps should not be confused with string *kinks*, which are points on a string where the tangent vector changes substantially over a very short distance, on the order of the string width [196]. Unlike at a cusp, there need not be any significant annihilation of the string segments in the vicinity of a kink, and kinks can persist for many loop oscillations [197]. Kinks can be created from string reconnection and zippering.

The effective length of the overlap region between the adjacent string segments

[11] This conclusion can change if there exist light (superstring) moduli fields with masses much smaller than w^{-1}, where w is the width of the string [111, 112]. For flat direction strings, both the string width and the typical moduli mass are set by the scale of supersymmetry breaking m. As a result, the rate of moduli emission by flat-direction strings is suppressed, and the corresponding bounds [114] are not relevant.

near a string cusp on a loop of length ℓ is about

$$\ell_c = \sqrt{w\,\ell}, \tag{3.73}$$

where w is the string width [193]. The overlapping string segments near the cusp are expected to annihilate, transferring most of the string energy within the overlap region to the constituent particles making up the string. The total average power released into particles through this process by a single string loop is [193]

$$P_{cusp} \simeq \mu\,\ell_c \left(\frac{c}{\ell}\right). \tag{3.74}$$

Here, c/ℓ is the cusp rate, where $1/\ell$ corresponds to the period of a loop oscillation, and c is the probability per period for a cusp to occur. We expect $c \sim 1$, although it has been argued that the presence of *kinks* on strings could push it to smaller values [196]. This is yet another uncertainty associated with the structure of cosmic strings on small scales.

For a given tension, flat-direction strings are much wider than ordinary cosmic strings; $w \sim m^{-1} \gg v^{-1}$ compared to $w \sim v^{-1} \sim \mu^{-1/2}$. The amount of string annihilated in a cusp is therefore greatly enhanced. The total particle radiation power from cusp annihilation by a flat-direction string loop is

$$P_{cusp} \simeq \frac{c\,\mu}{\sqrt{m\,\ell}}. \tag{3.75}$$

Relative to the gravitational radiation power, Eq. (3.70), we see that cusp annihilation dominates for sufficiently small loop sizes. The loop size at which the two powers become equal is

$$\ell_= \simeq m^{-1} \left(\frac{c}{\Gamma G\mu}\right)^2. \tag{3.76}$$

Recall that the loop size at formation is $\ell_i = \alpha\,t$. For $\ell_i \lesssim \ell_=$ the loops will decay primarily through particle emission, and not gravitational radiation. On the other hand, when $\ell_i \gg \ell_=$, most of the loop energy will go into gravity waves, except for a small burst of particles towards the end of the loop's existence.

Thus, the emission of particles by flat-direction cosmic strings through cusp annihilation is greatly enhanced relative to ordinary cosmic strings. If cusp annihilation dominates over gravitational radiation, many of the gravitational radiation signals will be suppressed compared to ordinary cosmic strings. In order to compare the relative signals from gravitational radiation and particle emission, it is helpful to concentrate on three particular epochs in the early universe: the reheating time t_{RH}; the time at which $\ell_i = \ell_= = \alpha\, t_=$; and the earliest time t_f at which a given gravitational wave frequency mode f can form.

We found in Section 3.4 that reheating after thermal inflation occurs when $t \simeq t_{RH} := \Gamma_\phi^{-1}$, where $\Gamma_\phi = \gamma\, m^3/v^2$ is the decay rate of the light flat-direction scalar field. This yields

$$t_{RH} \simeq \left(\frac{0.1}{\gamma}\right)\left(\frac{v}{10^{14}\ \mathrm{GeV}}\right)^2\left(\frac{10^3\ \mathrm{GeV}}{m}\right)^3 (10^{-4}\mathrm{sec}) \tag{3.77}$$

Recall that if the process of reheating after thermal inflation is to avoid disturbing the predictions of nucleosynthesis, we must have $v \lesssim 10^{16}$ GeV for $m = 1000$ GeV and $\gamma = 1$, and $v \lesssim 10^{14}$ GeV for $m = 200$ GeV and $\gamma = 0.1$.

The second moment of interest, the time after which newly-formed loops lose most of their energy in the form of gravity waves, occurs when $\ell_i = \ell_= = \alpha\, t_=$. This corresponds to the time

$$\begin{aligned} t_= &= \alpha^{-1}\left(\frac{c}{\Gamma G\mu}\right)^2 m^{-1} \\ &\simeq \alpha^{-1}\, c^2\left(\frac{50}{\Gamma}\right)^2\left(\frac{2\times 10^{-11}}{G\mu}\right)^2\left(\frac{10^3\ \mathrm{GeV}}{m}\right)(10^{-9}\mathrm{sec}). \end{aligned} \tag{3.78}$$

We have expressed $t_=$ in terms of $G\mu$ rather than the VEV v because it is this dimensionless combination that appears frequently in the estimates below. An approximate conversion between $G\mu$ and v is (see Fig. 3.3)

$$G\mu \simeq \left(\frac{v}{10^{14}\ \mathrm{GeV}}\right)^2 (2\times 10^{-11}). \tag{3.79}$$

Given the upper bound on v from reheating after thermal inflation, we will mostly focus on $v \lesssim 10^{14}$ GeV.

The third time of interest is t_f, the earliest moment at which a given gravitational wave frequency as low as f can be emitted. Recall that loops formed at time t_i have the initial size $\ell(t_i) = \alpha\, t_i$, and subsequently shrink and radiate into frequencies $f \geq 2/\ell$. For a mode observed at the present time with frequency $f = f(t_0)$ emitted at time $\tilde{t}$, the initial frequency was

$$f(\tilde{t}) = \frac{a(t_0)}{a(\tilde{t})}\, f. \tag{3.80}$$

Combining these facts, the earliest time t_f at which a mode with present frequency f could have been emitted is

$$\begin{aligned} t_f &= \frac{2}{\alpha\, f}\frac{a(t_f)}{a(t_0)} \qquad (3.81)\\ &\simeq \begin{cases} \alpha^{-3}\left(\frac{10^{-7}Hz}{f}\right)^3 (6.5\times 10^{10}\ \mathrm{GeV}^{-1}) & t_f > t_{eq} \\ \alpha^{-2}\left(\frac{10^{-7}Hz}{f}\right)^2 (2.5\times 10^{19}\ \mathrm{GeV}^{-1}) & t_{RH} < t_f < t_{eq} \\ \alpha^{-3}\left(\frac{10^{-7}Hz}{f}\right)^3 \left(\frac{10^{14}\ \mathrm{GeV}^{-1}}{t_{RH}}\right)^{1/2} (1.2\times 10^{22}\ \mathrm{GeV}^{-1}) & t_f < t_{RH} \end{cases} . \end{aligned}$$

Both $t_=$ and t_f depend on the parameter α that characterizes the typical size of a string loop when it is formed, $\ell_i = \alpha t_i$. The dynamics of loop formation are not completely understood, and as a result, estimates for α vary widely. Some recent simulations find that a significant portion of the loops formed are quite large, with $\alpha \simeq 0.001$ [199, 200] or $\alpha \simeq 0.1$ [198]. Other simulations find that the typical initial loop size approaches their resolution limits [180]. In this case, it is thought that gravitational radiation will smooth out very small fluctuations, and impose a lower limit on α [169]. The scale over which this smoothing occurs is also under ongoing investigation. Early estimates suggested $\alpha = \Gamma\, G\mu$ [169], but more recent analyses have found even smaller values of α. In Ref. [201] the authors obtain $\alpha = (\Gamma\, G\mu)^\chi$ with $\chi = 1.5$ during the radiation era and $\chi = 2.5$ during matter dominance. The authors of Ref. [202] find $\alpha \simeq 0.6\,\Gamma\,(G\mu)^\chi$ with $\chi = 1.2$ in the radiation era and $\chi = 1.5$ in

the matter era. Furthermore, in Ref. [203] it is suggested that the simulation results of Ref. [198] should be interpreted as predicting a network with 10-20% of the loop energy density in the form of large loops with $\alpha \simeq 0.1$ and the remainder in the form of very small loops with $\alpha \simeq \Gamma(G\mu)^{\chi}$ with $\chi > 1$. On account of the rapidly evolving state of the field, we will consider both large and small values of α below.

Fig. 3.16 shows t_{RH}, $t_{=}$, and t_f in GeV^{-1} units as functions of the VEV v for large loops with $\alpha = 0.1$. The model parameters were set to $m = 10^3$ GeV, $c = 1$, $\gamma = 0.1$, $\Gamma = 50$. In this plot we also indicate the present time $t_0 \simeq 6.6 \times 10^{41}$ GeV and the matter-radiation equality time $t_{eq} \simeq 3.5 \times 10^{36}$ GeV with dotted lines. The value of t_f is shown for two values of the frequency, $f = 10^{-7}\,Hz$ and $f = 10^{2}\,Hz$. These values span most of the range relevant for gravitational wave searches. For these large loops, $t_{=}$ is always much less than t_{eq}, and all loops formed after $t_{=}$ will decay predominantly into gravitational radiation. At the lower frequency $f = 10^{-7}\,Hz$, t_f lies below t_{eq} but above t_{RH}, and is never much less than $t_{=}$. This suggests that the gravitational wave signal at this frequency will not be attenuated much by the enhanced rate of particle emission by the loops. On the other hand, the value of t_f for $f = 10^{2}\,Hz$ lies well below both t_{RH} and $t_{=}$, indicating that the high-frequency gravitational wave signal will be reduced.

The values of t_{RH}, $t_{=}$, and t_f for very small loops, $\alpha = 0.6\,\Gamma\,(G\mu)^{1.5}$, are shown in Fig. 3.17 as a function of the VEV v. This value of α corresponds to the estimate of Ref. [202] for loops emitted in the matter era. Even smaller values of α are suggested in Ref. [201]. As before, the other model parameters were taken to be $m = 10^3$ GeV, $c = 1$, $\gamma = 0.1$, and $\Gamma = 50$, and the dotted lines denote the present time $t_0 \simeq 6.6 \times 10^{41}$ GeV and the matter-radiation equality time $t_{eq} \simeq 3.5 \times 10^{36}$ GeV. This figure indicates that the prospects for gravitational radiation from small flat-direction string loops are much less promising than for large loops. Indeed, $t_{=}$ is larger than the present time t_0 for $v \lesssim 2 \times 10^{12}$ GeV. Such small loops will decay

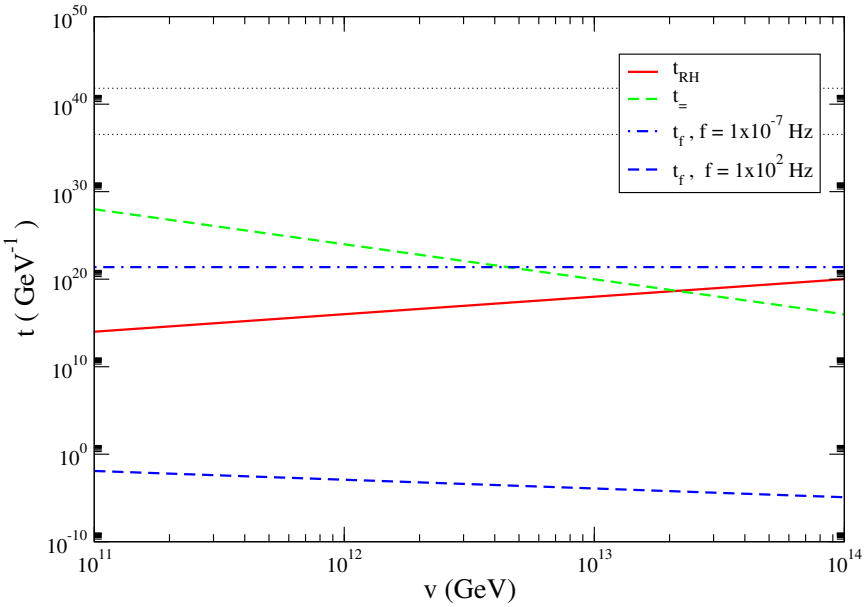

Figure 3.16. Dependence of the times of interest t_{RH}, $t_{=}$, and t_f on the VEV v for $\alpha = 0.1$. The black dotted lines indicate the present time $t_0 \simeq 6.6 \times 10^{41}$ GeV^{-1} and the matter-radiation equality time $t_{eq} \simeq 3.5 \times 10^{36}$ GeV^{-1}.

almost entirely to particles instead of gravitational radiation. Even when $t_{=}$ is less than t_0, the curves for t_f show that the gravitational wave signal is very suppressed relative to the signal from large loops. At low frequencies $f \simeq 10^{-7}\,Hz$ there is no signal at all since t_f exceeds the present time t_0; the loops are simply too small to radiate into this frequency range. Even for frequencies near $f = 10^2\,Hz$, there will be a gravitational wave signal only for $v \gtrsim 3 \times 10^{12}$ GeV. Despite the reduction in the gravitational wave signal, small loops may be observable through their copious emission of particles.

In summary, we find that the large width of flat-direction cosmic strings greatly enhances the rate at which they decay into their constituent particles through cusp annihilation. With this enhancement, our preliminary analysis indicates that string loops that are initially large ($\alpha \simeq 0.1$) decay predominantly into gravitational waves,

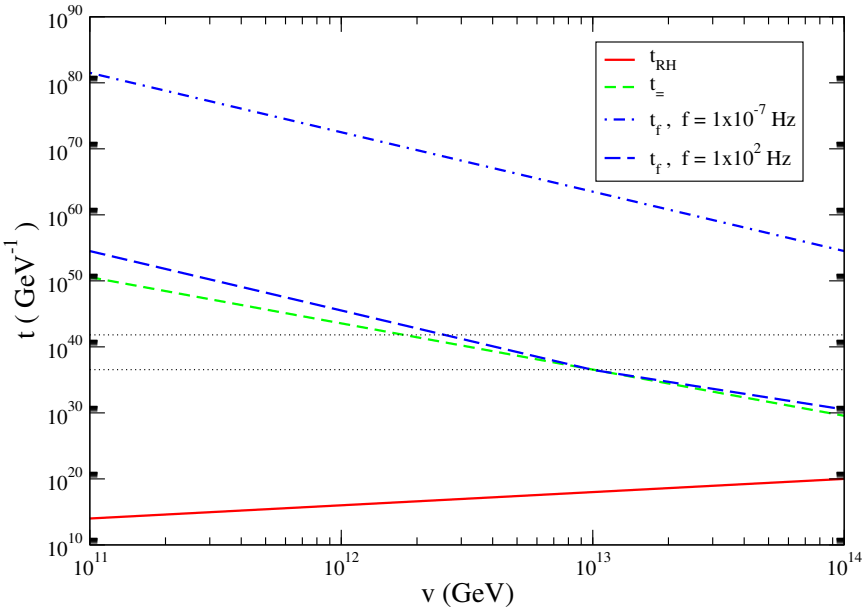

Figure 3.17. Dependence of the times of interest t_{RH}, $t_{=}$, and t_f on the VEV v for the representative small initial loop size parameter $\alpha = 0.6\,\Gamma\,(G\mu)^{1.5}$. The black dotted lines indicate the present time $t_0 \simeq 6.6 \times 10^{41}$ GeV^{-1} and the matter-radiation equality time $t_{eq} \simeq 3.5 \times 10^{36}$ GeV^{-1}.

while very small loops ($\alpha \ll \Gamma\, G\mu$) decay primarily into particles. The typical size of string loops when they are formed is an unresolved problem, and well-motivated arguments in favor of large loops, very small loops, or possibly both at once, can be found in the literature. In the face of this uncertainty, we will focus on two particular choices of the loop size parameter α to estimate the observational signatures from flat-direction cosmic strings. To compute the gravitational wave signals we will set $\alpha = 0.1$ for all loops, as suggested in Ref. [198]. Our results can be rescaled appropriately when only a fraction of the loops are large. To estimate the signals from particle emission due to cusp annihilation, we will instead assume that α is sufficiently small that all loops decay mostly into particles. This is plausible for flat-direction strings for which the rate of particle emission by cusp annihilation is enhanced. Again, it is straightforward to modify our results to accommodate larger values of α.

Finally, let us also mention that the picture of loop formation by flat-direction strings might be different from that of ordinary cosmic strings. For example, the enhanced rate of particle emission by cusp annihilation could potentially smooth out small fluctuations over scales larger than the (naïve) gravitational radiation scale $\Gamma G\mu\, t$. String loops can also remain bound to the parent string, as illustrated in Fig. 3.10. This could modify the distribution of initial string loop sizes. The rate of cusp formation on these bound loops may also be different from that on free loops.

3.5.2 Gravitational Wave Signatures

Cosmic strings can give rise to two types of gravitational wave signals. The combination of many string loop decays produces a smooth *stochastic* background of gravitational radiation [189]. On top of this background, individual cusps can produce intense bursts of gravity waves [119]. Gravitational wave detectors are sensitive to both types of signals. For the string tensions of interest, $G\mu \lesssim 10^{-10}$, the stochastic background is the more promising one [120, 121, 122] and we will focus on it. To estimate this gravitational wave background due to flat-direction cosmic strings we will assume that all string loops are large when they are formed, with $\alpha \simeq 0.1$ [198]. If only a fraction of the loops produced are large, as advocated in Ref. [203], our results can be rescaled by this fraction.

We compute the gravitational radiation density due to cosmic string decays following Ref. [194]. Consider radiation in the frequency range $(f, f+df)$ observed today that was emitted at time $\tilde{t}$. Keeping track of only the lowest mode,[12] this radiation was emitted by loops of size $(\tilde{\ell} - d\tilde{\ell}, \tilde{\ell})$, where

$$\tilde{\ell} = \frac{2}{f}\frac{a(\tilde{t})}{a(t_0)}, \qquad d\tilde{\ell} = \frac{2}{f^2}\frac{a(\tilde{t})}{a(t_0)}\, df. \tag{3.82}$$

[12] In Ref. [123] this was shown to be a good approximation for computing the stochastic background.

Loops of this size at time $\tilde{t}$ were formed at the earlier time t_i given by

$$t_i = \left(\frac{1}{\alpha + \Gamma G\mu}\right)\left[\tilde{\ell} + \Gamma G\mu\tilde{t}\right], \tag{3.83}$$

over the time range

$$dt_i = \left(\frac{1}{\alpha + \Gamma G\mu}\right)\frac{2}{f^2}\frac{a(\tilde{t})}{a(t_0)}\,df. \tag{3.84}$$

These relations follow from the loop evolution equation $\ell(t) = \alpha\, t_i - \Gamma G\mu(t - t_i)$, valid for $t \geq t_i$ and $\ell(t) \geq \ell_=$.

The rate at which loops are formed during the string scaling regime can be estimated using the results of numerical simulations or from simple analytic models like the one presented in Section 3.4. These predict a net energy flux into loops of

$$\frac{d\rho_{loop}}{dt} \simeq \frac{\rho_\infty}{t}, \tag{3.85}$$

where

$$\rho_\infty \simeq \zeta\mu\, t^{-2}, \tag{3.86}$$

with $\zeta \simeq 10$, and ρ_∞ being the scaling energy density of long strings. This result can be obtained by summing Eq. (3.62) over all string species that have equilibrated. It follows that the rate per unit volume that loops of initial size $\alpha\, t$ are formed is

$$\frac{dn}{dt} \simeq \frac{\zeta}{\alpha}\, t^{-4}. \tag{3.87}$$

Applying this result to loops formed in the time range $(t_i - dt_i, t_i)$, the number density of loops radiating into the frequency range of interest at time $\tilde{t}$ is

$$dn(\tilde{t}) \simeq \frac{\zeta}{\alpha}\, t_i^{-4} dt_i \left[\frac{a(t_i)}{a(\tilde{t})}\right]^3. \tag{3.88}$$

The redshift factor in this expression accounts for the dilution of the loops as they evolve from t_i to $\tilde{t}$. Given that each loop radiates gravity waves with a power $\Gamma G\mu^2$, we can combine everything and sum over $\tilde{t}$ to find the signal. The total gravitational

wave density at the present frequency f is

$$\begin{aligned}\Omega_{GW}(f) &:= \frac{f}{\rho_c}\frac{d\rho_{GW}}{df} \\ &= \frac{1}{\rho_c}\int_{\bar{t}_f}^{t_0} d\tilde{t}\,\Theta(\tilde{\ell}-\ell_=)\,\Gamma G\mu^2\, f\frac{dn(\tilde{t})}{df}\,\left[\frac{a(\tilde{t})}{a(t_0)}\right]^4 \\ &\simeq \frac{2}{f}\frac{\Gamma G\mu^2}{\rho_c}\frac{\zeta}{\alpha(\alpha+\Gamma G\mu)}\int_{\bar{t}_f}^{t_0} d\tilde{t}\,\Theta(\tilde{\ell}-\ell_=)\,\left[\frac{a(\tilde{t})}{a(t_0)}\right]^5\left[\frac{a(t_i)}{a(\tilde{t})}\right]^3 t_i^{-4}.\end{aligned} \tag{3.89}$$

Here, ρ_c is the critical density, and t_i and $\tilde{\ell}$ are functions of $\tilde{t}$ defined by Eqs. (3.82) and (3.83). The integration limits range between $\bar{t}_f := max(t_f, 10^5\ \mathrm{GeV}^{-1})$ and t_0, where t_f is given in Eq. (3.81).[13] Noting that $a \propto t^{2/3}$ during the matter era ($t < t_{RH}$ and $t > t_{eq}$) and $a \propto t^{1/2}$ during the radiation era ($t_{RH} < t < t_{eq}$), this equation can be integrated straightforwardly. Relative to the treatment of Ref. [194], we have included a cutoff of $\tilde{\ell} > \ell_= = \alpha\, t_=$ through a step function. This accounts for the loops only being able to radiate efficiently into gravity waves if their length is greater than $\ell_=$. It is this cutoff, along with the additional redshifting that occurs during reheating after thermal inflation, that suppresses the gravitational wave signal from flat-direction strings compared to ordinary strings.

In Fig. 3.18 we show the stochastic gravitational wave signal from initially large cosmic string loops as a function of frequency. We have used the parameter values $\alpha = 0.1$, $\Gamma = 50$, $m = 10^3$ GeV, and $\gamma = 0.1$ in making this plot. The solid lines show the gravitational wave density from flat-direction cosmic strings, including the cutoff $\tilde{\ell} > \ell_=$ and the additional redshifting during reheating after thermal inflation. The dashed lines indicate what the signal would be for ordinary cosmic strings, without the cutoff $\tilde{\ell} > \ell_=$ or reheating effects. At lower frequencies the relevant loops are

[13] Normally the lower limit would simply be t_f, but in the present case the flat-direction string network only reaches scaling at $t \simeq 10^5\ \mathrm{GeV}^{-1}$. Numerically, we find that this additional cutoff has no visible effect because the gravity waves emitted shortly after the end of thermal inflation are diluted away during the subsequent reheating. Gravity waves from the phase transition [124] will also be diluted by thermal inflation.

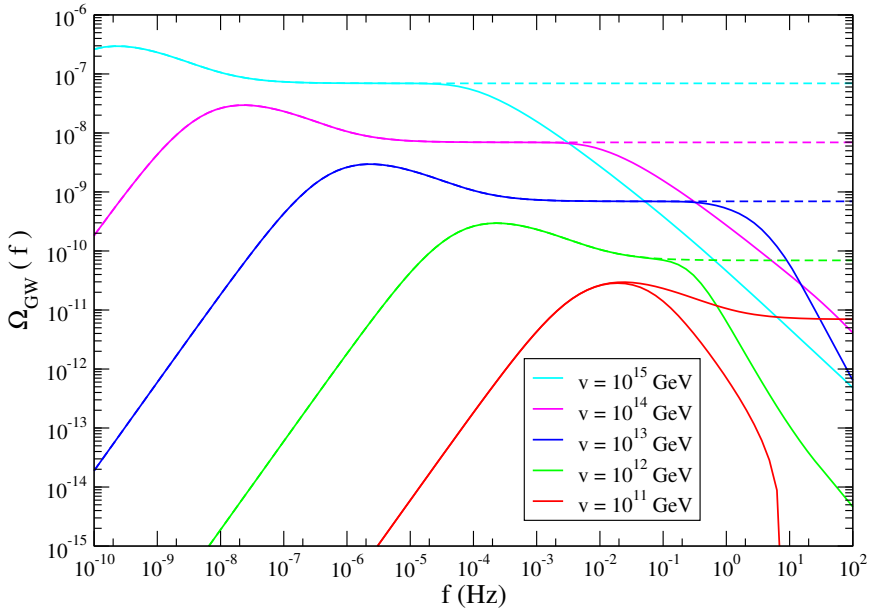

Figure 3.18. Gravitational wave density for flat-direction cosmic strings as a function of frequency for four different values of the VEV v. The solid lines include the cutoff $\tilde{\ell} > \ell_{=}$ due to cusp annihilation. The dashed lines show what the gravitational wave density would be without this cutoff.

formed later on, at times greater than t_{RH} and $t_{=}$, and there is no change to the signal. At higher frequencies, the cutoff on the loop size and the additional dilution during reheating both suppress the gravitational wave signals. As can be seen in Fig. 3.16, the cutoff $\ell > \ell_{=} = \alpha\, t_{=}$ is more important for lower values of v (and $G\mu$), while the reheating dilution is more significant at larger values of v since t_{RH} is larger. This is why the shape of the high frequency cutoff changes as we increase v.

The attenuation of high frequency gravitational wave signals is relevant to LIGO and Advanced LIGO, which can potentially probe down to $\Omega_{GW}(f) \simeq 10^{-9}$ at frequencies around $f = 10^{2}\, Hz$ [125]. Fig. 3.18 indicates that LIGO is not expected to be able to find evidence for flat-direction cosmic strings. On the other hand, the prospects for discovery at LISA and from measurements of pulsar timing are promising. The LISA probe is expected to cover portions of the range $10^{-4}\, Hz \lesssim f \lesssim 10^{-2}\, Hz$ down

to $\Omega_{GW}(f) \simeq 10^{-11}$ [126]. Since the gravitational wave signal from large flat-direction string loops is mostly unmodified in this frequency range, LISA will be able to probe a sizeable portion of the model parameter space. Limits from pulsar timing are currently $\Omega_{GW}(f) \lesssim 3 \times 10^{-8}$ in the frequency range 10^{-7}–$10^{-8}\,Hz$ [127], which is again low enough that the gravitational wave signal from flat-direction cosmic strings is unsuppressed. From this bound we obtain the constraint $v \lesssim 10^{14}$ GeV. It is expected that this limit will be improved to $\Omega_{GW}(f) \lesssim 10^{-10}$ by upcoming experiments [127]. Note that flat-direction cosmic strings offer the interesting possibility that LISA and pulsar timing experiments could detect a stochastic gravitational wave background with $\Omega_{GW}(f) \gtrsim 10^{-9}$, while (Advanced) LIGO sees nothing even though it is sensitive to signals at this level. This would be a suggestive hint for flat-direction cosmic strings.

Here it may also be helpful to compare the gravitational wave (GW) signatures from cosmic string network and from other astronomical sources[128, 129]. The GW sources that may be detected at current and incoming laser interferometer experiments (e.g. LIGO and LISA) fall into two major categories: those individual events that occur at certain space-time points in the universe, and those that contribute to the stochastic background. Sources for individual events include: mergers of binaries, massive star collapse (supernovae and hypernovae), rapidly rotating neutron stars, the inspiral and merger of supermassive blackholes etc. These sources typically give strong signals and can be distinguished according to their different frequency bands and different time evolution of their waveforms. But the discovery of an individual event partly depends on 'luck', although many of them are estimated to occur at an optimistic rate. It is also speculated that some of the 'violent' events are accompanied by gamma ray bursts, which makes them easier to be distinguished from other sources. The possible sources of stochastic GW background include: processes in the

early universe, e.g. vacuum fluctuations predicted by inflationary models, also some other postulated mechanisms string GW with horizon-size wavelength, e.g. 1st order phase transition in early universe, Goldstone modes that arise in SUSY and string theories. As we have mentioned before, GW from cosmic string network can produce both individual bursts from cusps or kinks and stochastic background from normal vibrations. In this sense, it is possible to distinguish GW signals from a cosmic string network and those from other sources by their differences in waveforms evolution and density–frequency distribution.

3.5.3 Particle Emission Signatures: Dark Matter

Having studied the gravitational wave signatures of string loops that are large when they are formed, let us now consider the possibility that the typical initial loop size is very small, $\alpha \ll \Gamma G\mu$, as suggested in Refs. [201, 202]. If α is sufficiently small, nearly all the energy of a loop is released as particle excitations of the fields making up the string. This is plausible for flat-direction cosmic strings due to their enhanced rate of particle emission by cusp annihilation relative to ordinary cosmic strings. In the (a, b) models of flat-direction strings presented in Section 3.2, the fields making up the string consist of two chiral supermultiplets and one massless vector (gauge) supermultiplet. When the chiral supermultiplets develop VEVs, it is more convenient to describe the theory in terms of a heavy massive vector supermultiplet, with mass on the order of gv, as well as a light supermultiplet with mass on the order of m [76]. This light multiplet is light on account of the flatness of the potential. Cusp annihilation will produce both the heavy and the light states making up the string. These particles will subsequently decay, and can be a potential source of dark matter and high energy cosmic rays. We consider both of these possible signatures in turn, assuming that all string loops are very small and decay entirely into particles rather than gravitational waves.

To compute the dark matter density from decaying string loops we again make use of Eq. (3.85) that specifies the rate at which the scaling string network transfers its energy into loops. Contributions to the dark matter density from loops produced before the network attains scaling are diluted away by the subsequent reheating process after the thermal inflation period.[14] If a fraction ϵ_1 of the energy emitted by the cusp annihilations of loops eventually becomes dark matter (such as a neutralino or gravitino LSP), the total dark matter density at the present time from the strings is

$$\rho_{DM}^{strings} \simeq \epsilon_1 \int_{t_{fo}}^{t_0} dt\, \zeta\, \frac{\mu}{t^3} \left[\frac{a(t)}{a_0}\right]^3 , \tag{3.90}$$

where t_0 is the present time and t_{fo} is the time at which the DM particles freeze out of equilibrium. The factor of $[a(t)/a_0]^3$ accounts for the additional dilution of the dark matter (or the constituent string fields) after they are produced. It is convenient to split the integration into three pieces: $t_{eq} < t$, $t_{RH} < t < t_{eq}$, and $t_{fo} < t < t_{RH}$. These integrations are straightforward and yield

$$\begin{aligned} \Omega_{DM}^{strings} &\simeq 6\pi\epsilon_1\zeta\, G\mu \left[\ln\left(\frac{t_0}{t_{eq}}\right) + \left(\frac{t_{eq}}{t_{RH}}\right)^{1/2} + \ln\left(\frac{t_{RH}}{t_{fo}}\right)\left(\frac{t_{eq}}{t_{RH}}\right)^{1/2}\right] \\ &\lesssim 30\,\epsilon_1 \left(\frac{\gamma}{0.1}\right)^{1/2} \left(\frac{\zeta}{10}\right) \left(\frac{v}{10^{14}\ \mathrm{GeV}}\right) \left(\frac{m}{10^3\ \mathrm{GeV}}\right)^{3/2} , \end{aligned} \tag{3.91}$$

where γ is the prefactor appearing in Eq. (3.56). Numerically, the largest contribution comes from the third term, from the integration range $t_{fo} < t < t_{RH}$. We have bounded the logarithm in this term from above in making this estimate. For reasonable values of the model parameters, the amount of dark matter produced by decaying loops is safely small, although smaller values of v are preferred. This differs from the much stronger constraints on regular cosmic strings that are able to decay into dark matter [173], which is due to the dilution from reheating after thermal inflation.

There is an additional contribution to the DM density from the out-of-equilibrium decays of the oscillating flat-direction fields during reheating. If a small fraction ϵ_2

[14] We have verified this using the result of Section 3.4.

of these decays ends up as dark matter, the present contribution to the DM energy density will be

$$\rho_{DM}^{\phi} \simeq \int_{t_{fo}}^{t_{RH}} dt\, \epsilon_2\, \Gamma_\phi\, \rho_\phi \left[\frac{a(t)}{a_0}\right]^3 . \tag{3.92}$$

Parametrizing $\rho_\phi(t) \simeq T_{RH}^4 [a(t_{RH})/a(t)]^3$ and using $t_{RH}\Gamma_\phi \simeq 1$, we find

$$\Omega_{DM}^{\phi} \simeq 10^7\, \epsilon_2 \left(\frac{T_{RH}}{\mathrm{GeV}}\right). \tag{3.93}$$

Thus, the branching fraction ϵ_2 into DM particles must be very small. Note that ϵ_1 and ϵ_2 can be very different from each other. The particles emitted from a cusp annihilation can include some of the heavier component fields making up the string. On the other hand, the decays of the flat-direction fields after thermal inflation involve only the light modes. The decays of these states into superpartners (such as a neutralino or heavier gravitino LSP) can therefore be highly suppressed or kinematically inaccessible, allowing for $\epsilon_2 \ll \epsilon_1$.

3.5.4 Particle Emission Signatures: Visible Matter

In addition to dark matter, the decays of very small string loops can produce hadrons, leptons, and photons. This particle injection will be spread out over time as the scaling string network continually rids itself of excess energy by forming loops. Visible particles created by loop decays can imprint themselves upon the early universe in a number of ways. The energetic products from loop decays at temperatures below 5 MeV can disrupt the predictions of big-bang nucleosynthesis (BBN). At later times, energetic photons from loop decays can modify the blackbody spectrum of the cosmic microwave background (CMB). Some of the decay products from string loops can also be highly energetic, producing ultra-high-energy cosmic rays and contributing to the extragalactic diffuse gamma-ray background. We consider the possible signatures from cosmic strings from each of these effects. As for our dark matter estimates, we assume that all loops are so small that they decay entirely into particles.

To estimate the effects of decaying string loops on BBN we make use of the results of Ref. [131]. In this work the authors used the successful predictions of BBN to place limits on the combination $m_X Y_X$ for a long-lived particle X of mass m_X, relic density (per unit entropy) Y_X, and lifetime τ_X, decaying at time $t \simeq \tau_X$. In contrast to a long-lived relic particle whose decays can be treated as being instantaneous, cosmic string loops are produced and decay continuously. These decays therefore have a cumulative effect on the light element abundances. To obtain a limit for decaying string loops we interpret the bounds from Ref. [131] as limits on the total energy injected within a comoving volume, $m_X Y_X = \Delta E/S$, where S is the total entropy within the volume a^3.

The total energy injected into the comoving volume a^3 by string loops that decay during the time interval (t_a, t_b) is

$$\begin{aligned} \frac{\Delta E}{S} &= \frac{1}{S}\int_{t_a}^{t_b} dt\, \mu\, \zeta\, t^{-3}\, a^3(t) \\ &\simeq (10^{-11}\ \text{GeV}) \left(\frac{1s}{t_a}\right)^{1/2} \left(\frac{\zeta}{10}\right) \left(\frac{G\mu}{2\times 10^{-11}}\right). \end{aligned} \tag{3.94}$$

In writing this expression, we have implicitly assumed that t_a and t_b both lie within the era of radiation dominance, as is relevant for BBN. The strongest limits on energy injection from BBN come from the relative fractions of deuterium and lithium-6 relative to hydrogen. Both of these are formed at times later than $t \gtrsim 100\, s$. Since the visible decay products from the loops thermalize quickly relative to the Hubble time, we set $t_a = 100\, s$ to find the bounds due to the deuterium and lithium-6 abundances [131]. Assuming a hadronic branching fraction of order unity, the total energy injection per unit entropy must be less than $\Delta E/S \lesssim 10^{-14}$ GeV.[15] This bound is satisfied provided $v \lesssim 10^{13}$ GeV.

Late-time energy injection is also constrained by the the nearly perfect blackbody spectrum of the CMB observed by COBE/FIRAS [132]. Photons produced by the

[15]The bound is fairly independent of the mass of the decaying particle.

decays of string loops that occur after the time $t_{dC} \simeq 10^{31}$ GeV^{-1} can distort this spectrum. Before t_{dC}, double Compton scattering ($e + \gamma \rightarrow e + \gamma + \gamma$) efficiently thermalizes any additional photons that are created. The precise form of the spectral distortions created after t_{dC} depends on the time at which the photons were injected. However, the net constraint from the non-observation of such distortions can be reduced to a constraint on the total photon energy created after t_{dC}, $\Delta\rho_\gamma/\rho_\gamma \lesssim 7 \times 10^{-5}$ [133, 134, 135]. The net photon injection from decaying string loops can be estimated using the rate of energy deposition by the network. If all the energy injected is in the form of photons (possibly after cascading), the total injection is

$$\begin{aligned} \frac{\Delta\rho_\gamma}{\rho_\gamma}(t_0) &\simeq \frac{1}{\rho_{\gamma 0}} \int_{t_{dC}}^{t_0} dt\, \frac{\partial\rho}{\partial t} \left[\frac{a(t)}{a(t_0)}\right]^4 \\ &\simeq 6\pi\,\zeta\, G\mu\, \left[\ln\left(\frac{t_{eq}}{t_{dC}}\right) + \frac{1}{\Omega_{\gamma 0}}\right] \\ &\simeq (8 \times 10^{-5}) \left(\frac{\zeta}{10}\right) \left(\frac{G\mu}{2 \times 10^{-11}}\right). \end{aligned} \tag{3.95}$$

Numerically, the dominant contribution to the injected photon energy comes from the most recent era, $t > t_{eq}$, leading to a non-zero value for the Compton y parameter [134, 136] which quantifies deviations away from the black body spectrum. It is expected that the constraints on photon injection will be improved in the future by the ARCADE experiment [137].

Decaying cosmic string loops can also generate cosmic rays. The corresponding energy spectrum depends on the energies of the particles emitted in the loop decays. Recall that the fields making up the flat-direction strings consist of a light chiral supermultiplet and a heavy massive vector supermultiplet. In each cusp annihilation, both the heavy and the light states can be produced. The decays of the heavy states, with masses on the order of $g\,v$, can generate ultra-high-energy cosmic rays (UHECR) [138]. Decays of the light states, with masses on the order of $m \ll v$, contribute to the extragalactic diffuse gamma-ray background (EDGRB) [139]. To determine the relevant bounds and prospects, we will assume that the energy released

in each cusp annihilation goes initially into a fraction F_l of the light states (with soft energy) and a fraction F_h to the heavy states. We expect $F_l \sim 1$, with F_h possibly smaller.

The contribution of decaying string loops to the EDGRB was studied in Ref. [139]. Data from the EGRET experiment [140] constrains the rate of energy emission into the light scalar states with masses on the order of 1000 GeV (that decay into lower-energy gamma rays) at the present time to $\partial\rho_{loop}/\partial t_0 \lesssim 4.5 \times 10^{-23}\,\mathrm{eV}\,cm^{-3}\,s^{-1} = 2.3\times10^{-97}\ \mathrm{GeV}^5$. Equating this bound with Eq. (3.85) evaluated at the present time, we obtain the bound [139]

$$F_l \left(\frac{\zeta}{10}\right)\left(\frac{G\mu}{2\times10^{-11}}\right) \lesssim 1. \tag{3.96}$$

This does not represent a significant constraint beyond those found above. The heavy component states making up the string can also contribute to the EDGRB through the photons they produce in cascade decays. The limit in this case is about the same as from the decays of the light states given in Eq.(3.96), but with F_l replaced by F_h. These constraints from the gamma-ray background on decaying cosmic string loops will be strengthened by the upcoming GLAST experiment [141]. However, the range of the model that can be probed may ultimately be limited by astrophysical background contributions to the gamma-ray flux.

Ultra-high-energy cosmic rays can be produced by cusp annihilation if some of the heavier states making up the string are created. When the heavy states decay, their products are highly energetic, making them a source of high-energy neutrinos and UHECRs. Estimates of the UHECR flux for strings that decay into particles were made in Ref. [142] and are directly applicable to flat-direction cosmic strings. These authors find that for energies greater than about 6×10^9 GeV, the only relevant cosmic ray flux consists of neutrinos. The fluxes of highly energetic protons and photons are very suppressed because they are attenuated by their interactions with the cosmic background. Extrapolating the predictions of Ref. [142], the neutrino signal from

decaying strings can be probed directly at Ice Cube [143] down to $G\mu \lesssim 10^{-12}/F_h$ in the energy range 10^5 GeV-10^8 GeV. The Auger project is sensitive to UHECR showers induced by energetic neutrinos in the energy range 10^9 GeV-10^{11} GeV [144]. The Auger measurements imply the constraint

$$G\mu \lesssim (3 \times 10^{-13})/F_h. \tag{3.97}$$

For $F_h = 1$, this corresponds to $v \lesssim 10^{13}$ GeV.

Our analysis indicates that the visible matter signatures from decays of flat-direction string loops are consistent with observations provided $G\mu$ is small enough. However, there is another visible matter signature that is challenging to reproduce in models of flat-direction strings, namely the baryon asymmetry of the universe. Flat-direction strings are formed following a period of thermal inflation. The typically low reheating temperature after thermal inflation, Eq. (3.57), combined with the large amount of dilution from the inflationary expansion and reheating imply that baryogenesis mechanisms that operate at or above the electroweak scale will no longer work. Instead, the baryon asymmetry must be produced at very late times. This can arise from the strings themselves [145, 146, 147], from the non-thermal production of particles during reheating that have baryon-number violating decays [89, 148, 149, 150, 151], or by the Affleck-Dine mechanism [152].

3.5.5 String Loops and Zero Modes

In our discussion of radiation from cosmic string loops, we implicitly assumed that there do not exist any *zero mode* excitations along the strings. Zero modes are fermionic or bosonic field fluctuations with vanishing energy that are localized on the string. The existence of zero modes on cosmic strings can alter the picture of loop radiation in important ways [153, 154, 155, 156].

These undamped, particle-like excitations can be excited when a string loop is formed. As the loop radiates and shrinks, the number density of the zero modes builds

up. Eventually the angular momentum of the zero modes balances the tendency of the loop to shrink, and a quasi-stable loop remnant, or *vorton*, is left over. If such vortons are sufficiently long-lived and numerous, they behave like quasi-stable matter and can further modify the predictions of BBN or create too much dark matter. The presence of vortons typically leads to extremely strong constraints on the underlying field theory [156].

For the flat-direction strings we are studying, fermionic zero modes [157, 153] are of particular relevance. It was shown in Ref. [52, 53] that such modes are a generic feature of supersymmetric cosmic string solutions. In the present case, we also have supersymmetry breaking operators present in the Lagrangian. We find that adding a supersymmetry breaking gaugino mass destroys all the fermionic zero modes. A recent study also suggests that more generally, even for supersymmety case fermionic zero modes do not form on closed string loops at all [158]. The existence of bosonic zero modes depends on the other fields in the theory and their couplings, and are less generic [153]. We do not consider them here.

Zero modes, either bosonic or fermionic, are also unlikely to stabilize flat-direction cosmic strings simply because these strings are relatively wide. For the phase transition leading to flat-direction cosmic strings, we expect that the radius at which the zero modes would stabilize a string loop, if they were to exist, is usually much smaller than the width of the string [50]. As discussed above for cusp annihilation, when the separation between a pair of antiparallel string segments approaches the string width these segments will annihilate into their constituent fields, and the loop will decay before stabilizing as a vorton.

3.5.6 Lensing by Cosmic Strings

While an indirect gamma ray or gravitational wave signal from cosmic strings would be exciting, ideally one would like a direct observation to confirm their existence.

This can be achieved by observing gravitational lensing by a string. The primary gravitational effect of the large mass density contained within a cosmic string is to modify the surrounding spacetime such that it is flat, but with a deficit angle of $\Delta\theta = 8\pi\, G\mu$ [159]. When light from a galaxy passes by a (non-relativistic) cosmic string, the deficit angle produces a distinctive double image with an angular separation of [169, 159]

$$\Delta\alpha = 8\pi\, G\mu\, \frac{D_{ls}}{D_{os}}\, \sin\phi, \tag{3.98}$$

where D_{ls} is the distance from the lensing string to the source galaxy, D_{os} is the distance from the observer to the source, and $\sin\phi$ is the angle between the string axis and the line-of-sight. From a single lensing event it is possible to determine $\Delta\alpha$ directly, as well as D_{os} by measuring the redshift of the source. Given that a single string lensing event is found, it is likely that the same string will also lens the images of other galaxies that are nearby on the sky [160]. By observing several galaxies lensed by the same string, the tension of that string can be determined [161].

The gravitational lensing signatures from flat-direction strings are even richer than those of ordinary strings because of the stability of higher winding modes. If many lensed images from different strings are observed, it may be possible to measure tensions of several strings and obtain clues about the mass spectrum of the higher winding modes. In this respect, flat-direction cosmic strings are similar to (p, q) cosmic superstrings. Both types of cosmic strings also have junctions connecting different winding modes. These can produce triple images, in addition to the double images produced by a lone string [162]. Since the spectrum of tensions of flat-direction strings is very different from that of (p, q) strings, the observation of many gravitational lensing events might allow one to distinguish between them. Unfortunately, the probability of observing a lensed image from a flat-direction string is very small due the indirect bounds on the tension, $G\mu \lesssim 10^{-11}$. This is smaller than the expected sensitivity of $G\mu \simeq 10^{-8}$ from upcoming optical surveys [163], and $G\mu \simeq 10^{-9}$ from the SKA [164],

radio survey [165]. The results of Ref. [161] also suggest that it will be difficult to determine the string tension accurately enough to distinguish between flat-direction string winding modes with similar values of the winding number N.

CHAPTER 4

Hidden Sector and Non-thermal Dark Matter Production–Constraint from Cosmology

4.1 Introduction

In chapter 3 we have seen much interesting phenomenology of cosmic strings from supersymmetric flat directions, which reflects features of certain symmetry breaking in a hidden sector of SUSY. Meanwhile, for more general hidden sector scenario with gauge symmetry broken via the Higgs mechanism (including non-SUSY and SUSY without flat-direction), cosmic strings are a very promising cosmological probes or tests. In another work [166] we study the non-thermal dark matter production from cosmic string network on general grounds and try to find constraints on the related hidden sector models.

To be self-consistent, let me briefly review some relevant facts on cosmic string network evolution, although we have discussed this in more detail in chapter 3. The evolution of cosmic string networks in the early universe has been studied extensively. It is found that the long strings in the network stretch with the Hubble expansion, as well as form closed string loops by the process of *reconnection* when they intersect themselves and each other. After an initial transient, these two processes balance each other such that the string network reaches a *scaling* regime, in which the total energy density of the network makes up a small, constant fraction of the dominant

matter or radiation energy density of the universe [176, 177, 178, 179, 180, 181]. This string energy fraction is largely independent of the initial conditions, and is about $G\mu$ relative to the critical density, where $G = 1/(8\pi M_{\rm Pl}^2)$ is Newton's constant and μ is the string tension. In terms of the scale of spontaneous symmetry breaking η from which the strings arise, the tension is on the order of

$$\mu \simeq \eta^2. \tag{4.1}$$

Cosmic string scaling can be modified if the strings have significant interactions with the thermal background. Such interactions include various scattering processes between the string and the particles in the plasma which are charged under the extended gauge group, and lead to an effective frictional force on the strings. Whether such interactions are present depends on the details of the model and the process we are considering.

A possible decay product of the string loops formed by a scaling cosmic network is dark matter (DM). Indirect evidence for cold dark matter has been obtained from a number of sources. Together, they indicate a dark matter density of [183]

$$\Omega_{DM} h^2 = 0.1048 \pm 0.0008 \tag{4.2}$$

This dark matter density can be explained by the existence of a new stable particle with a mass on the order of the electroweak scale. Such particles are common in extensions of the SM that stabilize the electroweak scale against quantum corrections such as supersymmetry [184], universal extra dimensions [185], and little Higgs models with T-parity [186].

String loops can produce DM (and other particles) in a number of ways. For local cosmic strings, corresponding to the spontaneous breakdown of a gauge symmetry, the direct emission of particles by the strings is thought to be suppressed [187].[1] Instead, loops lose most of their energy by oscillating and emitting gravitational

[1] However, see Refs. [180, 188] for arguments to the contrary.

radiation [189]. However, when the loop radius shrinks down to the order of the string it will self-annihilate into its constituent fields [173]. The subsequent decays of these states can produce dark matter. An even larger source of string annihilation and particle production by closed loops is the formation of *cusps* [190]. As we have introduced in chapter 3, these are points on the loop where the string segment folds back on itself and briefly approaches the speed of light [191, 192]. In the vicinity of a cusp, a small portion of the string will self-annihilate creating particles and dark matter [190, 193]. In many simple solutions for the motion of a string loop, a cusp is found to occur about once per loop oscillation period [191, 192, 194, 196, 197].

The amount of dark matter created by a cosmic string network mainly depends on two factors. First is the symmetry breaking scale η, which is a common determinant for the power of various loop decay channel as we will see. The other essential factor is the size of the string loops that are formed by the network, which is a determinant for the initial density of the loops. Unfortunately, while the evolution of the long (horizon length) strings is well understood, the details of loop formation are less clear. These details are closely related to the spectrum of small fluctuations on long strings. Significant advances have been made recently in this direction, both in numerical simulations [198, 199, 200], as well as in analytic models Ref. [201, 202, 203, 204, 205, 206]. In the present work we will mostly adopt the results of Refs. [202, 203, 204, 205] to characterize the initial loop size spectrum.

In the picture of loop formation that emerges from Refs. [202, 203, 204, 205], fluctuations on long strings are created near the horizon scale $d_H \sim t$, which is also the scale that charaterizes the long string network in the scaling regime. After they are formed these fluctuations grow less quickly than the horizon, and thereby shrink relative to the characteristic scale of the long string network. The fluctuation spectrum that emerges is a power law in the fluctuation size that increases going to smaller scales. This power law is eventually cut off well below the horizon by

gravitiational radiation damping, which erases very small fluctuations. The cut-off occurs when the fluctuation size falls below the gravitational radiation scale [202]

$$l_{GW} = \Gamma\,(G\mu)^{1+2\,\chi} \tag{4.3}$$

where $\Gamma \simeq 50$ is a constant and $\chi = 0.10$ during radiation and 0.25 during the matter era. The small fluctuation spectrum on long strings is therefore peaked near l_{GW}. This peak implies that l_{GW} sets the typical initial loop size ℓ_i as well [202, 203, 204, 205],

$$\ell_i \simeq l_{GW}. \tag{4.4}$$

Both the number and energy densities of the loops formed are dominated by loops of this initial size. However, recent simulations (and the analytic model of Ref. [206]) also point toward a significant loop population near the horizon scale, with $\ell_i \simeq (0.1)\,t_i$. We will therefore consider larger loops as well in our analysis.

The primary goal of this work is to compute the dark matter density generated by a network of cosmic strings in the scaling regime. We also calculate the dark matter generated when *frictional* interactions with the background plasma modify the evolution of the network[2]. A necessary condition for the viability of a cosmic string network is that the dark matter density it generates not exceed the WMAP bound. Our results therefore provide a constraint on theories of new physics that lead to the formation of cosmic strings, such as models containing new $U(1)$ gauge groups [171, 172]. This chapter is organized as follows. In Section 4.2 we derive a general formula for the production of dark matter by cosmic string loops. In Section 4.3, we apply this formula to compute the amount of dark matter produced

[2]We studied a special case of non-thermal dark matter production from loop decays in chapter 3. But there we only focused on the situation when the loop formation size is very small and the loops decay entirely into particles. This can be a valid situation for flat direction strings, since for them the cusp annihilation has a large chance to dominate over gravitational radiation due to the large string width. In this chapter we study the DM production on much more general grounds.

by string loops formed in the scaling regime. In Section 4.4 we extend our results to compute the dark matter density from cosmic strings loops when friction plays an important role in the evolution of the string network.

Before proceeding, let us point out that the production of dark matter by the decays of cosmic string loops was considered previously in Ref. [173]. We update and extend this work in a number of ways. Most importantly, we make use of the recent results on the size distribution of string loops when they are formed from Refs. [202, 203, 204, 205]. We also consider the evolution of cosmic string networks both with and without friction. When friction is relevant, we extend Ref. [173] by using the analytic model of Ref. [179] to describe the long string network. Furthermore, we concentrate on cusping as the primary source of particle production by cosmic strings.

4.2 A Formula for Dark Matter from Cosmic Strings

Let us denote the initial *invariant* length of a string loop formed at cosmic time t_i by ℓ_i. The invariant length ℓ of a loop is defined in relation to its energy in the cosmological frame by

$$E_{loop} = \mu\, \ell. \tag{4.5}$$

If the loop is boosted with speed ν, the invariant length ℓ will exceed the proper length of the loop in its rest frame by a factor of $\gamma = 1/\sqrt{1-\nu^2}$.

The key quantity characterizing loop formation is

$$r(\ell_i, t_i)\, d\ell_i\, dt_i, \tag{4.6}$$

the number density of string loops formed in the time interval $(t_i, t_i + dt_i)$ with initial length in the range $(\ell_i, \ell_i + d\ell_i)$. The form of the function $r(\ell_i, t_i)$ is constrained by the evolution of the long string network. In particular, the total rate at which energy is transferred from the long string network to loops is typically a known quantity [179].

We can use this fact to impose the constraint

$$\frac{d\rho_{loop}}{dt_i} = \int d\ell_i \; \mu \, \ell_i \, r(\ell_i, t_i), \tag{4.7}$$

where $d\rho_{loop}/dt$ is the rate of energy transfer into loops from the long string network.

Consider the evolution of a loop of initial size ℓ_i formed at time t_i. The length of this loop is described by the function

$$\ell(t; \ell_i, t_i) \tag{4.8}$$

which is the solution to the equation

$$\mu \frac{d\ell}{dt} = -P_{tot}, \qquad \text{with} \qquad \ell(t_i; \ell_i, t_i) = \ell_i, \tag{4.9}$$

where P_{tot} is the total rate of energy loss from the loop. We will assume that P_{tot} is positive so that ℓ is monotonically decreasing in time. Under this assumption, the loop will eventually decay away completely at the time $t_{co}(\ell_i, t_i)$, defined implicitly by

$$0 = \ell(t_{co}; \ell_i, t_i). \tag{4.10}$$

While the loop is decaying, it will emit a fraction of its energy in the form of (cold) dark matter. We will write this fraction as $P_{DM} \leq P_{tot}$.

To find the total rate of dark matter production by the collection of string loops, consider loops with initial size in the range $(\ell_i, \ell_i + d\ell_i)$ formed in the time interval $(t_i, t_i + dt_i)$. There are $r(\ell_i, t_i) d\ell_i dt_i$ such loops per unit volume initially. As time goes on, this collection of loops is diluted by the cosmic expansion by a factor of a^{-3}. This is the *only* modification of their density until they decay away completely at time $t_{co}(\ell_i, t_i)$. At time $\tilde{t}$, this collection of loops will produce dark matter at the rate P_{DM}. This dark matter will thermalize if it is produced before the freeze-out time $\tilde{t} < t_{fo}$, and redshift as a^{-3} after this time. Thus, we have

$$\Delta\rho_{DM} = \int d\ell_i \int_{t_\eta}^{t_0} dt_i \int_{t_{fo}}^{\tilde{t}_{co}(\ell_i, t_i)} d\tilde{t} \;\; r(\ell_i, t_i) \left[\frac{a(t_i)}{a(\tilde{t})}\right]^3 \; P_{DM} \; \left[\frac{a(\tilde{t})}{a(t_0)}\right]^3 \; \Theta(t_{co} - t_{fo}). \tag{4.11}$$

The integral over t_i runs between the string network formation time t_η and the present time $t_0 \simeq 4 \times 10^{41}$ GeV^{-1}. Typically, t_η is on the order of

$$t_\eta \simeq \frac{M_{\rm Pl}}{\eta^2}, \tag{4.12}$$

where η is the scale of spontaneous symmetry breaking. The integration over the decay time $\tilde{t}$ runs from the freeze-out time t_{fo} to either t_{co} or t_0, whichever is smaller. Thus, we have defined $\bar{t}_{co}(\ell_i, t_i)$ by

$$\bar{t}_{co}(\ell_i, t_i) = \begin{cases} t_{co}(\ell_i, t_i) & : \quad t_{co} < t_0 \\ t_0 & : \quad t_{co} \geq t_0 \end{cases} . \tag{4.13}$$

Any restriction on the integration limits of ℓ_i are encoded in the support of the function $r(\ell_i, t_i)$.

It is often the case that P_{DM} and P_{tot} depend on $\tilde{t}$ only through $\tilde{\ell} = \ell(\tilde{t}; \ell_i, t_i)$. If so, it is convenient to change the integration variable from $\tilde{t}$ to $\tilde{\ell}$. The corresponding Jacobian is simply $(\partial\tilde{\ell}/\partial\tilde{t})^{-1} = -\mu/P_{tot}$, where P_{tot} is the total power released by a loop of length $\tilde{\ell}$. It follows that

$$\Delta\rho_{DM} = \int d\ell_i \int_{t_\eta}^{t_0} dt_i \int_{\ell_x(\ell_i,t_i)}^{\bar{\ell}_{fo}(\ell_i,t_i)} d\tilde{\ell}\, r(\ell_i, t_i) \left[\frac{a(t_i)}{a(t_0)}\right]^3 \mu \frac{P_{DM}}{P_{tot}} \tag{4.14}$$

The limits on the $\tilde{\ell}$ integration depend on the functions

$$\bar{\ell}_{fo}(\ell_i, t_i) = \begin{cases} \ell(t_{fo}; \ell_i, t_i) & : \quad t_i < t_{fo} \\ \ell_i & : \quad t_i > t_{fo} \end{cases} , \tag{4.15}$$

as well as

$$\ell_x(\ell_i, t_i) = \begin{cases} 0 & : \quad t_{co}(\ell_i, t_i) < t_0 \\ \ell(t_0; \ell_i, t_i) & : \quad t_{co}(\ell_i, t_i) > t_0 \end{cases} . \tag{4.16}$$

Eqs. (4.11) and (4.14) are our main results. We will apply them to a couple of interesting special cases below.

4.3 Dark Matter Production from a Scaling Network

As a first application of our main result, Eq. (4.11), we compute the dark matter density produced by a network of cosmic strings in the scaling regime due to the cusping of closed string loops. To simplify the analysis, we focus on monochromatic loop formation distributions with

$$\ell_i = \alpha\, t_i. \tag{4.17}$$

This relation implies $r(\ell_i, t_i) \propto \delta(\ell_i - \alpha t_i)$. More general distributions can be obtained by introducing a weight function and summing the final result over different values of α.

In the string scaling regime, the rate at which the long string network transfers energy into loops is [179]

$$\frac{d\rho_{loop}}{dt_i} = \zeta\, \mu\, t_i^{-3}, \tag{4.18}$$

with $\zeta \simeq 10$ a constant characterizing the mean properties of the long string network. Imposing the constraint of Eq. (4.7) on the loop formation rate $r(\ell_i, t_i)$, we obtain

$$r(\ell_i, t_i) = \frac{\zeta}{\alpha}\, t_i^{-4}\, \delta(\ell_i - \alpha\, t_i). \tag{4.19}$$

All that remains to do is to specify the evolution of the loop length and the power emitted as dark matter, and apply Eq. (4.11).

Cosmic string loops lose energy to gravitational radiation as well as cusping, and shrink as a result. The rate of energy emission into gravity waves is [169]

$$P_{grav} = \Gamma\, G\mu^2, \tag{4.20}$$

where μ is the string tension, $G = 1/(8\pi\, M_{\rm Pl}^2)$, and $\Gamma \simeq 50$ is a dimensionless constant.

Loops also lose energy when they form cusps, which are points on the loops that briefly fold back upon themselves and approach the speed of light. Near the apex

of a cusp, a portion of the string overlaps and self-annihilates. Summing over many cusps, the net rate at which a loop loses energy to cusping is given by [193]

$$P_{cusp} = \mu\, p_c \sqrt{\frac{w}{\ell}}, \tag{4.21}$$

where p_c is the probability for a cusp to form per period of loop oscillation. Several studies suggest $p_c \simeq 1$ [192, 194, 195, 196]. Comparing the cusp power of Eq. (4.21) to the gravitational wave power of Eq. (4.20), we see that cusping is the dominant energy-loss mechanism by loops when they are shorter than $\ell < \ell_=$ with

$$\ell_= = w \left(\frac{p_c}{\Gamma G \mu}\right)^2. \tag{4.22}$$

The particles produced by cusping can decay into dark matter. Provided $p_c \gtrsim \Gamma G\mu$, we expect cusping to be the dominant source of dark matter from cosmic strings.

If loops can lose energy to gravitational radiation and cusping, the loop length evolves according to

$$\mu \frac{d\ell}{dt} = P_{tot} = -\Gamma G \mu^2 - \mu\, p_c \sqrt{\frac{w}{\ell}}. \tag{4.23}$$

The solution of this equation subject to the initial condition $\ell(t_i) = \ell_i$ is given implicitly by

$$t - t_i = \frac{\ell_=}{\Gamma G \mu}\left[\left(\frac{\ell_i - \ell}{\ell_=}\right) - 2\left(\sqrt{\frac{\ell_i}{\ell_=}} - \sqrt{\frac{\ell_i}{\ell_=}}\right) + 2\,\ln\left(\frac{1+\sqrt{\ell_i/\ell_=}}{1+\sqrt{\ell/\ell_=}}\right)\right]. \tag{4.24}$$

Suppose that a fraction ϵ_{cusp} of the energy emitted by a string loop cusp (eventually) takes the form of cold dark matter. It follows that

$$P_{DM} = \epsilon_{cusp}\, P_{cusp}. \tag{4.25}$$

Putting this into Eq. (4.14) and making use of Eq. (4.19), we find the dark matter density due to cusping to be

$$\begin{aligned} \Delta\rho_{DM} &= \int_0^\infty d\ell_i \int_{t_\eta}^{t_0} dt_i \int_{\ell_x(\ell_i,t_i)}^{\ell_{fo}(\ell_i,t_i)} d\tilde{\ell}\; r(\ell_i,t_i)\left(\frac{a_i}{a_0}\right)^3 \mu\, \frac{\epsilon_{cusp} P_{cusp}(\tilde{\ell})}{P_{tot}(\tilde{\ell})} \qquad (4.26)\\ &= \int_{t_\eta}^{t_0} dt_i\, \frac{\zeta}{\alpha}\, t_i^{-4}\left(\frac{a_i}{a_0}\right)^3 \epsilon_{cusp}\,\mu\,\ell_= \left[\sqrt{\frac{\ell}{\ell_=}} - \ln\left(1+\sqrt{\ell/\ell_=}\right)\right]_{\ell_x(\alpha\, t_i, t_i)}^{\bar{\ell}_{fo}(\alpha\, t_i, t_i)} \Theta(\bar{\ell}_{fo})\,\Theta(\ell_x). \end{aligned}$$

The Θ functions in this expression account for the fact that only those loops that decay after t_{fo} and before t_0 can contribute to the dark matter density. Numerically, we find that the integrand of Eq. (4.26) is peaked around the earliest value of t_i for which loops formed at that time decay after t_{fo}. Thus, the dominant contribution to the dark matter density will come from loops decaying shortly after t_{fo}.

To be concrete, we evaluate Eq. (4.26) assuming a weakly-interacting massive dark matter particle with a freeze-out time of $t_{fo} = 2 \times 10^{16}$ GeV^{-1}. This corresponds approximately to a freeze-out temperature of 5 GeV, which is in the range expected for a stable, weakly-interacting particle with a mass on the order of 100 GeV. We also set the loop network parameter to $\zeta = 10$, the cusping probability to $p_c = 1$, and the branching fraction into dark matter equal to unity, $\epsilon_{cusp} = 1$. In realistic models we expect that ϵ_{cusp} could be much smaller than unity. Our results can therefore be interpreted as providing an upper bound on ϵ_{cusp} within the underlying gauge theory model.

In Fig. 4.1 we show the dark matter relic density due to cusping as a function of the initial loop size parameter α, normalized to $\Gamma G\mu$, with the other parameter values as described above. We normalize α to $\Gamma G\mu$ because, in the absence of cusping, a loop is long-lived relative to the Hubble time at formation ($\sim t_i$) provided $\alpha/\Gamma G\mu > 1$, and short-lived otherwise. From this plot, we see that increasing the initial loop size α well above $\Gamma G\mu$ increases the final dark matter density. The reason for this is that the integration over t_i in Eq. (4.26) is dominated by the earliest times for which loops produced at t_i decay after t_{fo}. Since larger loops are longer-lived, loops contributing to the dark matter density can be formed at earlier times, when the integrand of Eq. (4.26) is larger. As $\alpha/\Gamma G\mu$ decreases, the dark matter density curves flatten out for lower values of the VEV η. In these flat regions, cusping dominates the evolution of the loops contributing to the dark matter, and these loops are short-lived even though $\alpha/\Gamma G\mu > 1$. When the VEV is larger $\eta \gtrsim 10^{13}$ GeV, gravitational radiation

becomes more important than cusping. Loops then become short-lived only when $\alpha/\Gamma\, G\mu < 1$. When α becomes very small, cusping again takes over and the curves flatten out. In Fig. 4.2 we show the dependence of the dark matter density due to string cusping as a function of the symmetry breaking VEV η. The other string model parameters are as described above. This plot shows a general increase in the dark matter density up to large values of η, and then a fall-off. Short-lived loops, with $\alpha \leq \Gamma\, G\mu$, and smaller values of η decay mostly through cusping at time t_{fo}. Using Eq. (4.14), it is possible to show that Ω_{DM} increases as η^2 in this case. As η is increased further, gravitational radiation becomes more important than cusping, and loops lose most of their energy to gravity waves instead of dark matter. Thus, the dark matter density falls for these very large values of η, with $\Omega_{DM} \propto (\alpha\, \eta)^{-1/2}$ in this regime. The precise value of η at which the cross-over occurs depends on the value of α, with smaller initial loops being more prone to cusping. For very large initial loops, $\alpha = 0.1$, a similar cross-over occurs. For our estimates of the dark matter density created by scaling cosmic strings to be trustworthy, the string network must have attained scaling by the time the loops relevant to dark matter were formed. Furthermore, loops formed in the phase transition at time t_η, and while the string network was evolving towards scaling, must have decayed away before t_{fo}. The approach of a string network to scaling depends on the details of the phase transition, and a study of it is beyond the scope of the present work. However, we can derive a consistency condition based on the requirement that loops formed in the initial phase transition at time t_η have decayed away before t_{fo}. This leads to

$$\eta \gtrsim p_c^{-2/5} \left(\frac{\alpha}{0.1}\right)^{3/5} 2 \times 10^3 \text{ GeV}. \tag{4.27}$$

Thus, our analysis can potentially be consistent with the phenomenogically interesting case of strings obtained from the breakdown of a new $U(1)$ gauge symmetry only slightly above the electroweak scale provided p_c is not too small and α is not too large.

Together, our results show that the density of dark matter generated by string loops from cusping with $p_c = 1$ in the scaling regime is safely small for $\eta \lesssim 10^{11}$ GeV. For values of the symmetry-breaking VEV larger than this, the string-induced dark matter density depends on the initial loop size. Loops of initial size $\alpha = \Gamma\,(G\mu)^{1.2}$, motivated by the results of Refs. [202, 203, 204, 205] appear to generate a safely small dark matter density. Larger loops, with $\alpha \sim 0.1$, can lead to a much larger dark matter density. If such large loops are typical, the branching fraction into dark matter ϵ_{cusp} must be significantly less than unity if the cosmic strings are to avoid overproducing dark matter. Let us also point out that for models with a new $U(1)$ gauge symmetry broken only slightly above the electroweak scale, the dark matter produced by the corresponding cosmic string network in the scaling regime is acceptably sparse.

Before moving on, let us mention that we have treated the loops as having no net motion relative to the thermal background, even though it is found in Refs. [202, 203, 204, 205] that small loops ($\alpha < \Gamma\, G\mu$) are highly boosted. The most important effect of this boost is to increase the cusping power P_{cusp} by a factor of $\gamma^{1/2}$ (for short-lived loops), where γ is the boost factor. The decay products will also be boosted. Numerically, we do not expect that the boost factor will change our results for the dark matter density by more than about an order of magnitude.

4.4 Dark Matter Production with Friction

The evolution of a cosmic string network can be modified if the strings have significant interactions with the thermal background. As we will discuss below, the relevance of these interactions to the string network depends on the details of the symmetry breaking from which the cosmic strings arose. Such interactions, when present, tend to slow the motion of the strings by creating an effective frictional force on them [207, 208, 179]. This in turn changes the density and rate of growth of the

network. The frictional forces on strings decrease as the universe cools, and eventually become unimportant relevant to the Hubble damping from the expansion of spacetime. Frictional effects also change the way cosmic string loops form and decay. In this section we apply the result of Eq. (4.11) to compute the density of dark matter created by a cosmic string network evolving under the influence of frictional forces.

For local (gauge) cosmic strings, the dominant interaction between the strings and the thermal background comes from Aharonov-Bohm scattering [209]. This results from the phase change experienced by the charged particle as it is transported around the string. The effective frictional force induced by this scattering can be characterized by a *friction length* ℓ_f given by [207, 179]

$$\ell_f = \frac{\mu}{\beta T^3}, \tag{4.28}$$

where the dimensionless quantity β is [207]

$$\beta = \frac{2\,\zeta(3)}{\pi^2} \sum_a b_a \, \sin^2(\pi\nu_a), \tag{4.29}$$

with the sum running over relativistic degrees of freedom, ν_a is the phase change of a particle transported around the string, and $b_a = 1\,(3/4)$ for bosons (fermions). If the underlying U(1) gauge symmetry (subgroup) is broken by the condensation of a single field of charge Q, ν_a is equal to Q_a/Q, where Q_a is the symmetry charge of the light particle species a. Therefore, we expect β to be of order unity when a non-integer value of Q_α/Q is realized by the model, i.e. there is a residual symmetry, and to vanish otherwise. In the case where Aharonov-Bohm scattering is irrelevant, friction can be induced by Everett scattering[210], which is in general sub-leading when Aharonov-Bohm effect is present. It originates from the normal coupling between the component fields of the strings and the charged particles in the plasma. However, friction can be irrelevant if the processes we consider occurs at late enough time $t > t_*$ (t_* is defined in the next paragraph), or when the particles charged under the extended

gauge group all freeze out. Thus, it is sensible to consider cosmic strings both with and without friction.

Frictional effects on the long string network become unimportant when the friction length grows larger than the Hubble length. This occurs at the time t_* defined by the relation

$$H(t_*) = 1/\ell_f(t_*). \tag{4.30}$$

Friction is only relevant for the long string network when $t < t_*$. For $\beta = \mathcal{O}(1)$ and radiation domination, t_* has the parametric size[3]

$$t_* \simeq \frac{M_{\rm Pl}^3}{\eta^4}, \tag{4.31}$$

where η denotes the symmetry breaking VEV. This is parametrically larger than the typical (radiation-era) formation time $t_\eta \sim M_{\rm Pl}/\eta^2$. For the most part, we will focus on strings with $\eta > 10^5$ GeV for which $t_* < t_{eq}$, the matter-radiation equality time.

The evolution of a cosmic string network in the presence of friction was studied in Ref. [179]. In their analytic model, the long string network is characterized by an effective correlation length L and a mean velocity ν. The energy density of the network is given in terms of these variables as

$$\rho_\infty = \frac{\mu}{L^2}. \tag{4.32}$$

If the initial string density is larger than the scaling density, as would be expected if the symmetry breaking phase transition is second-order or weakly first-order, the string network evolves very quickly to the *Kibble regime* [168, 179]. In this regime, with the universe assumed to be radiation dominated, the string network variables L

[3]Due to the many uncertainties involved in this description of cosmic strings within the friction-dominated regime, we only list and use here the leading parametric dependences of the string network parameters.

and ν have the parametric dependences [179]

$$L(t) \simeq \left(\frac{t}{t_*}\right)^{1/4} t \tag{4.33}$$

$$\nu(t) \simeq \left(\frac{t}{t_*}\right)^{1/4}. \tag{4.34}$$

There is a similar Kibble regime while the universe is matter dominated with exponents for L and ν of $1/2$ instead of $1/4$. The Kibble regime only lasts while $t < t_*$. From Eqs. (4.28) and (4.31) we see that the friction length grows as

$$\ell_f \simeq \left(\frac{t}{t_*}\right)^{1/2} t. \tag{4.35}$$

As t approaches t_*, the friction length catches up to the long string length L as well as the horizon, and the string network transitions into the usual scaling regime with $L \propto t$ and $\nu \sim 1$.

During the friction-dominated Kibble regime, the rate at which energy is transferred from the long string network to loops is on the order of

$$\frac{d\rho_{loop}}{dt_i} \simeq \mu \left(\frac{t_*}{t_i}\right)^{1/2} t_i^{-3}, \qquad t_i < t_*. \tag{4.36}$$

This is parametrically larger than during the scaling regime, as can be seen by comparing with Eq. (4.18). Once a loop is formed, its subsequent evolution in the Kibble regime is also considerably different than during scaling. In particular, the typical initial loop size as well as the subsequent loop evolution are both strongly modified. Based on Eq. (4.11), it is clear that the amount of dark matter in the presence of friction will be significantly altered.

4.4.1 Loop Production and Evolution with Friction

The evolution of linear perturbations on long strings and closed string loops in the presence of friction was studied in Refs. [207, 208]. In Ref. [208] it was found that linear fluctuations on a long string of wavelength larger than ℓ_f are overdamped and stretched. For wavelengths smaller than ℓ_f, the damping time is on the order of ℓ_f,

which is much longer than the typical period of oscillation but much shorter than the Hubble time. Hence these small fluctuations oscillate and lose energy to friction very quickly relative to the Hubble time. Given these results and the picture of loop formation of Ref. [205], we expect that the typical initial loop size during friction is on the order of ℓ_f.[4] Fluctuations smaller than ℓ_f are damped out quickly, while those larger than ℓ_f grow more slowly than the long string correlation length L, and therefore shrink relative to L. Thus, we expect that fluctuations build up near ℓ_f, which in turn sets the typical size of a loop when it is formed. Even so, given the many uncertainties in this estimate, we will also consider loops of size close to the long string scale L. The correct answer will lie between these two extremes.

To model the evolution of string loops during friction, we will take the results of Ref. [208] for the evolution of a circular loop to be representative of the evolution of general loops. (Indeed, friction tends to make the loops more circular.) Ref. [208] finds that loops smaller than ℓ_f oscillate freely and lose their energy to the thermal background according to

$$\mu \frac{d\ell}{dt}\bigg|_{friction} \simeq -\mu \frac{\ell}{\ell_f}. \tag{4.37}$$

Therefore such loops lose energy over the time scale ℓ_f, much less than the Hubble time in the friction regime. We do not expect these interactions between the strings and the thermal background to be a significant source of dark matter.

The motion of loops larger than ℓ_f is overdamped. They evolve according to

$$R\dot{R} \simeq -\frac{\ell_f}{2a} \tag{4.38}$$

where R is the comoving coordinate radius of the loop (and aR corresponds to the physical loop radius). The solution of Eqn. (4.38) implies that loops of initial size smaller than the long string scale L shrink down to size ℓ_f in less than about a Hubble

[4] We emphasize however that the picture of loop formation obtained in Ref. [205] was developed under the assumption of long string scaling, and did not take friction into account.

time. Once they do, the overdamping approximation of Eq. (4.38) breaks down, and the loops begin to oscillate and decay away.

In summary, loops are formed in the friction regime with a typical initial length between ℓ_f and L. For initial loops of length $\ell_f(t_i)$, the loop formation rate per unit volume per unit length is

$$r(\ell_i, t_i) \simeq \left(\frac{t_*}{t_i}\right) t_i^{-4}\, \delta(\ell_i - \ell_f(t_i)), \quad t_i < t_*. \tag{4.39}$$

The rate is effectively reduced by a factor of $(t_i/t_*)^{1/4}$ if the initial loop size is $L(t_i)$ instead of ℓ_f. These loops shrink down to length ℓ_f in less than about a Hubble time. Once a loop becomes smaller than ℓ_f it starts to execute underdamped oscillations, transferring its energy to the thermal background and decaying away over the time scale ℓ_f. The loop length ℓ then evolves according to

$$\frac{d\ell}{dt} = -\frac{\ell}{\ell_f} - \Gamma\, G\mu - p_c\sqrt{\frac{w}{\ell}}. \tag{4.40}$$

Here, the first term comes from friction, the second from gravitational radiation, and the third from cusping.

Before going on to compute the dark matter density generated by the decaying loops, let us make note of the fact that at the end of the friction-dominated Kibble regime, the long string network is smoothed out nearly all the way up to the Hubble scale. In the loop formation picture of Ref. [202, 203, 204, 205], small fluctuations on long strings giving rise to loops originate from fluctuations of Hubble size that have slowly shrunk. Thus it will take some time for small scale structure to build up on the long strings, and the typical initial loop size will be initially larger than the gravitational damping length l_{GW}. We follow Ref. [179] and model this transitional period by writing the initial typical loop size parameter as

$$\alpha_{eff}(t) = \frac{1 + \alpha(t/t_*)^\xi}{1 + (t/t_*)^\xi}, \qquad t > t_*, \tag{4.41}$$

with the exponent $\xi \simeq 1$. A naïve application of the results of Refs. [202, 203, 204, 205] suggests that $\xi = 0.9$ in the radiation era. We will study a range of values of ξ.

4.4.2 Dark Matter with Friction

The discussion above provides all the ingredients needed to evaluate the dark matter density in the presence of friction using Eq. (4.11). We do so here under the assumption that loop cusping is the dominant source of dark matter from the strings. Our results are presented in Fig. 4.3, where we show the dark matter density due to cosmic strings as a function of the symmetry breaking VEV η. In making this plot, we have also set $\zeta = 10$, $p_c = 1$, $\epsilon_{cusp} = 1$, and we have again taken the freeze-out time to be $t_{fo} = 2 \times 10^{16}$ GeV^{-1}. We have also fixed an overall prefactor in Eq. (4.39) (equal to $\zeta/2$) to ensure that the loop formation rate is continous as t_i crosses t_*. The different curves in Fig. 4.3 correspond to different values of the (scaling regime) loop size parameter α and the exponent ξ appearing in Eq. (4.41).

The dark matter density curves in Fig. 4.3 show three distinct regions, with the transitions between them occurring around $\eta = 10^8$ GeV and 10^{12} GeV. For values of η well above 10^{12} GeV, the curves coincide with those obtained in the absence of friction. Such large values of η imply a value of t_* that is much smaller than the freeze-out time t_{fo}, so that all loops generated while friction is relevant decay away before t_{fo}. On the other hand, when η lies below 10^{12} GeV, the most important contribution to the dark matter comes from loops formed while friction dominates the network evolution, $t_i < t_*$.

In the region 10^8 GeV $\lesssim \eta \lesssim 10^{12}$ GeV most of the DM is produced by loops that are formed in the friction era, with $t_i < t_*$. This is why the dark matter density is independent of the scaling value of α for this range of η. The largest contribution to the DM in this region comes from loops that are also long-lived, with $t_i < t_{fo}$. This enhances the amount of dark matter formed because, with the loop distribution function of Eq. (4.39), the integrand of the t_i integral in Eq. (4.11) is a rapidly decreasing function of t_i. Increasing η in this region leads to larger initial loop sizes that further extend the loop lifetime. However, the minimal value of t_i for which

loops decay after t_{fo} decreases more slowly with increasing η than t_*. The sharp transition near $\eta = 10^{12}$ GeV occurs when these two quantities become equal. When this happens, increasing η further decreases the initial loop size (see Eq. (4.41)) for the dominant DM loops, and these loops go quickly from being long-lived to being short-lived, with the dominant loops being formed near $t_i = t_{fo} < t_*$. The transition becomes more gradual when the exponent ξ in Eq. (4.41) becomes less than $\xi = 1.0$, which can be seen by comparing with the curve for $\xi = 0.7$.

When η falls below $\eta \lesssim 10^8$ GeV, the initial loop size (equal to ℓ_f) becomes small enough that the loops are short-lived, decaying away within a Hubble time. Thus, the majority of the dark matter produced for these smaller values of η comes from loops formed near the freeze-out time, $t_i \simeq t_{fo}$, with initial size close to $\ell_f(t_{fo})$. As η decreases below 10^8 GeV, we find that a larger fraction of the energy of each loop is lost to cusping, thereby increasing the dark matter density.

As a summary of this chapter, we have investigated the non-thermal dark matter produced by the decays of cosmic string loops, for a general loop formation distribution. We focus on the production channel where the component fields of the strings are released during cusp annihilation and then decay to DM candidates. We have calculated the amount of non-thermal dark matter generated when the string network is in the *scaling* regime, and when its evolution is dominated by friction forces. In both cases, we found that the density of DM can be dangerous if the associated symmetry breaking scale η is higher than 10^{10}GeV, while safely small when η is lower than that value.

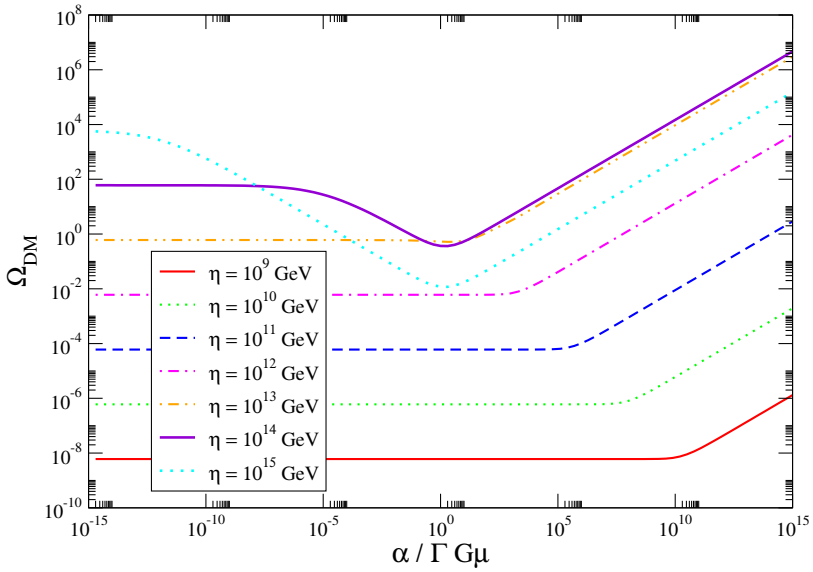

Figure 4.1. Dark matter density due to loop cusping for $\epsilon_{cusp} = 1$, $p_c = 1$, $\zeta = 10$, and $t_{fo} = 2 \times 10^{16}$ GeV as a function of the initial loop size parameter α. The various lines correspond to different values of the symmetry breaking VEV η.

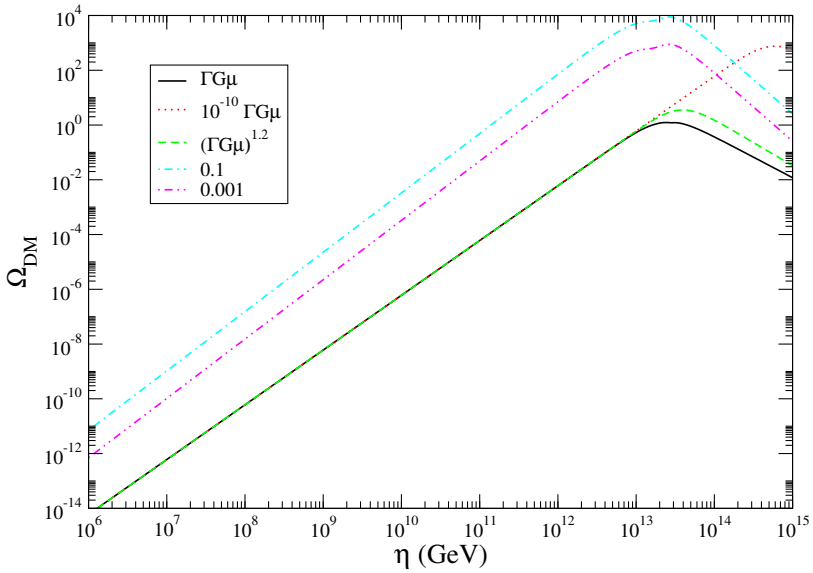

Figure 4.2. Dark matter density due to loop cusping for $\epsilon_{cusp} = 1$, $\zeta = 10$, $p_c = 1$, and $t_{fo} = 2 \times 10^{16}$ GeV as a function of the symmetry breaking VEV η. The various lines correspond to different values of the initial loop size parameter α.

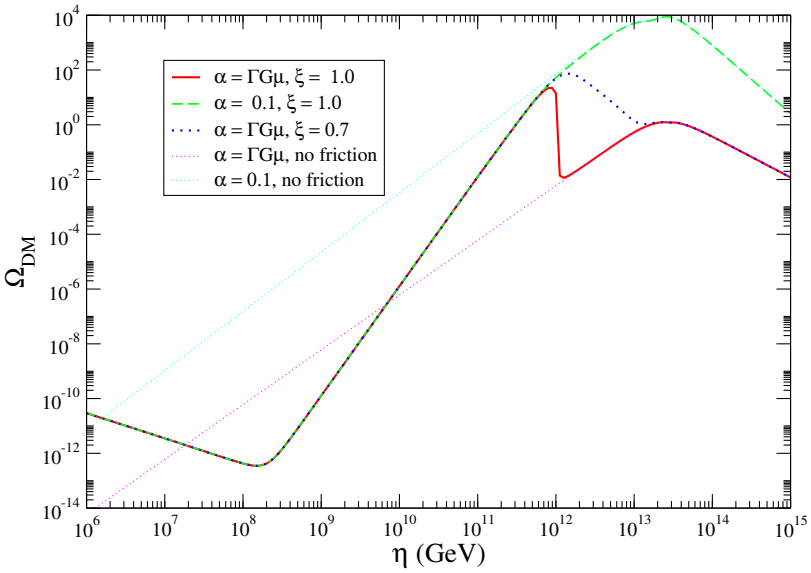

Figure 4.3. Dark matter density due to loop cusping for $\epsilon_{cusp} = 1$, $p_c = 1$, and $t_{fo} = 2{\times}10^{16}$ GeV as a function of the symmetry breaking VEV η in the presence of friction. The various lines correspond to different values of the initial loop size parameter α.

CHAPTER 5

Conclusions

A *Hidden sector*, which is composed of SM singlet fields and the interactions between them, is an extension beyond the *visible* world composed of the known particles and the four familiar fundamental forces acting on them. Although without direct practical motivation for solving any particular, known problem, a hidden sector seems an inevitable by-product in those theories seeking solutions to significant problems such as the unification of fundamental forces and the gauge hierarchy problem. As we have seen, such a sector is well-motivated in the contexts of GUT theories, string-inspired models, SUSY breaking models, etc. More interestingly, although called 'hidden', the SM singlets can in fact couple to the SM fields in significant ways, such as tree-level mixing with the SM gauge bosons or Higgs boson. We can thus expect that these singlets may have an important influence on 'visible' sector physics. The study of the phenomenological implications of a hidden sector is therefore a worthwhile field to pursue. One generically-motivated hidden sector scenario is that associated with a beyond-the-SM gauge symmetry which is broken via the Higgs mechanism. In chapters 2-4, I have reviewed three pieces of my work related to this scenario, which discuss its LHC phenomenology and cosmological implications. In this conclusion chapter, I would like to begin by summarizing the work presented in the previous chapters.

1. **Signatures of Hidden Higgs at the LHC** The Large Hadron Collider holds much promise for discovering new particles and interactions. Many ideas of

physics beyond the SM that explain electroweak symmetry breaking involve states that are coupled directly to the Standard Model gauge bosons. For example, supersymmetry, technicolor and extra dimensions all have exotic states that are direct participants in the electroweak story. However, there are states that do not couple to the SM gauge bosons that may contribute to understanding the full picture of EWSB (e.g., singlet states that get vevs to produce the μ term in supersymmetry) or help solve other problems not directly connected to electroweak physics (e.g., singlets breaking exotic gauge groups in string-inspired theories).

In this work, we have investigated a renormalizable interaction between the SM Higgs boson and a Higgs boson of a hidden sector. This gives us one of the most incisive methods to probe the existence of states that have no SM gauge charges. The phenomenological challenge to this scenario is that all couplings of the mixed Higgs bosons are less than the would-be SM couplings for a SM Higgs boson of the same mass. However, small compensating advantages were exploited here: a reduced coupling means a reduced width, which turns a trans-TeV Higgs boson into a definable narrow-width state to search for, and the existence of two Higgs bosons enables us to search for decays of the heavier Higgs boson to the lighter one. In both cases, we were able to study examples from the parameter space of discovery. We therefore like to emphasize the importance of searching for a Higgs boson in standard channels well into the trans-TeV mass region. We also like to reemphasize, from the point of view of these hidden sector ideas, that there is a potential opportunity to discover both a heavy Higgs boson and a light Higgs boson through $H \to hh$ decays. This is an especially attractive channel to exploit in the circumstance that a light h boson is particularly hard to find due to reduced production cross-section which

is generically predicted in these theories.

2. **Cosmic Strings from SUSY Flat Directions**

Cosmic strings can be formed in a generic way during cosmological phase transition associated with the breaking of certain hidden sector gauge symmetry, e.g. when a $U(1)'$ is completely broken. We study the theory and phenomenology of cosmic strings in a particular but well-motivated setup: when the strings are formed when the symmetry is broken along SUSY flat-direction. We find that such cosmic strings behave in ways that are qualitatively different from both ordinary (abelian Higgs) cosmic strings as well as (p, q) cosmic superstrings. These differences in behavior may be distinguishable through probes of the early universe.

- Abelian gauge symmetry breaking along a flat direction can give rise to strongly Type-I cosmic strings with tension $\mu \simeq 0.1\pi v^2$, gauge profile width of v^{-1} and scalar profile width $w \sim m^{-1}$, where $m \ll v$ characterizes the flatness of the potential. These flat-direction strings are likely to be formed after thermal inflation through flux-trapping.
- The tension of the strings increases very slowly with their winding number N. Thus, higher-winding mode strings $N = 2, 3, \ldots$ are energetically stable. This enables strings to be attracted to one another and zipper, creating stable formations with winding number $N_1 + N_2$ or $|N_1 - N_2|$, where N_1 and N_2 are the original string winding numbers.
- Zippering affects the evolution of the resulting string network. Applying a simple network evolution model to flat-direction strings suggests that a large number of string modes develop roughly equal densities in the early universe. The total energy density is about the same as for a single string,

but it is distributed among many species.

- Flat-direction strings radiate gravitationally. However, in contrast to ordinary cosmic strings, they also may be able to radiate copiously into matter. The strings are expected to fully radiate away, as there is no vorton obstruction for the supersymmetric flat-direction strings under consideration.
- In contrast to GUT strings, flat-direction strings are generically compatible with current direct observational constraints, $G\mu \lesssim 3 \times 10^{-7}$ [95, 96, 97, 98, 99]. If the typical initial loop length is close to the horizon scale, LISA and upcoming millipulsar timing probes may be able to detect the gravitational wave signal from these strings. However, the gravity wave signal at higher frequencies is suppressed for flat-direction strings, making their detection at LIGO extremely challenging.
- Particle emission from cusp annihilation is likely to be the dominant loop decay mechanism if the loop length is always much smaller than the horizon. This intriguing prospect for flat-direction cosmic strings entertains the possibility that ultra-high-energy cosmic rays or nonthermal dark matter originate from their particle emission. If all loops decay entirely into particles, the constraints from BBN, the CMB blackbody, and UHECRs imply the bound $v \lesssim 10^{13}$ GeV, corresponding to $G\mu \lesssim 10^{-13}$.
- The multi-tension network of flat-direction strings formed in the early universe is in contrast to the standard single-tension string networks, but similar to (p, q) cosmic superstring networks, and thus may mimic the latter by giving rise to multiple lensing events. However, the spectrum of tensions of flat-direction strings is constrained by indirect bounds, and may be too low to be observed in the near future.

3. **Non-thermal Dark Matter from Cosmic String Decays**

For those hidden sector models that can produce cosmic strings, consideration on the dark matter relic density from string loop decays can put constraints on the parameters or structure of the models, e.g. the symmetry breaking scale.

In the work presented in chapter 4, we have studied the dark matter density created by the decays of loops of (local) cosmic strings. Dark matter is produced by the string loops when they form cusps. At a cusp, a small portion of the string loop annihilates into its constituent fields, which can then cascade down to lighter states such as dark matter particles. Our results provide constraints on extensions of the gauge symmetry group of the standard model that give rise to cosmic strings in the early universe.

The string loops that give decay to dark matter are themselves created continually by the network of long, horizon-length strings. We have studied the amount of dark matter generated when this network is in the *scaling* regime, and when when its evolution is dominated by frictional forces. Both cases are physically relevant as the presence or absence of significant frictional interactions depends on the details of the symmetry breaking from which the strings arose.

For a string network in the scaling regime (in the absence of friction) the induced dark matter density can be dangerously large when the symmetry breaking VEV η exceeds 10^{10} GeV. The amount of dark matter is also enhanced when the initial loop size approaches a significant fraction of the cosmological horizon, although much smaller initial loop sizes can also generate dangerously large amounts of dark matter. Therefore if loops are formed with near-horizon

size, to be consistent with the observed dark matter relic density, the branching fraction into dark matter from cusp annihilation must be considerably less than unity in some parameter regions.

String networks that are strongly influenced by friction can also generate a dangerously large dark matter density. This occurs for values of the symmetry breaking scale greater than about 10^{11} GeV. For very large values of the symmetry breaking scale, above about 10^{13} GeV, the frictional effects decouple well before the dark matter is created.

More Comments on Hidden Sector

At the end of this thesis, I would like to make some more comments, which are outside the main scope of the thesis, but are important for us to get a more complete understanding of *hidden sector*. The work I have done focuses on one well-motivated hidden sector scenario wherein an extended gauge symmetry is broken perturbatively via the Higgs mechanism. Meanwhile, there is another class of hidden sector models which is almost equally well-motivated——those where supersymmetry or extended gauge symmetry is broken by strong dynamics, or even more interestingly those in a confining phase. As mentioned in the introduction, the only known way in four dimensional theories of *generating*, not just *stabilizing* a hierarchy of mass scale is dimensional transmutation enabled by strong dynamics. In particular, a hidden sector with strong dynamics is almost ubiquitous in SUSY breaking models. Generally in these models, there seems no obvious counterparts of tree-level renormalizable mixing between hidden sector and SM gauge boson or Higgs. Therefore in these models the interaction between the visible sector and hidden sector is in general mediated by higher dimensional operators due to some messenger sector. However, recent works have revealed that even in these scenarios, the hidden sector may still have non-

negligible visible effects—for example, it could play an important role in determining soft SUSY breaking parameters in visible sectors [212, 213, 214, 215]. Recent, interesting studies also exist concerning the collider phenomenology of such hidden sectors known as 'hidden valley' models [216, 217, 218, 219]. In a nutshell, whether it involves a perturbative Higgs mechanism or strong dynamics, hidden sectors have proved to be a rewarding subject to study both for understanding the visible SM world and for exploring possible new matter and forces beyond our current knowledge.

APPENDIX

Appendix

Unitarity Inequalities

The 15 relevant processes that give non-vanishing constant amplitudes when $s \to \infty$ (with $m_W, m_V \ll m_H, m_h$) are

1. $W_L^+W_L^- \to W_L^+W_L^-$ (s-, t-channels)

2. $Z_LZ_L \to Z_LZ_L$ (s-, t-, u-channels)

3. $Z_LZ_L \to W_L^+W_L^-$ (only the s-channel Higgs exchange is relevant)

4. $HH \to HH$ (only contact graphs are relevant), in mass eigenstates, including:

(4.1) $hh \to hh$

(4.2) $hh \to hH$

(4.2) $hh \to HH$

(4.4) $HH \to hH$

(4.5) $HH \to HH$

5. $HH \to W_L^+W_L^-/Z_LZ_L$ (t-,u- channel gauge boson exchange and s-channel Higgs exchange are all relevant), including:

(5.1) $hh \to W_L^+W_L^-/Z_LZ_L$

(5.2) $hH \to W_L^+W_L^-/Z_LZ_L$

(5.3) $HH \to W_L^+W_L^-/Z_LZ_L$

6. $V_LV_L \to V_LV_L$ (s-, t-, u-channels)

7. $HH \to V_LV_L$ (t-,u- channel gauge boson exchange and s-channel Higgs exchange are all relevant), including:

(7.1) $hh \to V_LV_L$

(7.2) $hH \to V_LV_L$

(7.3) $HH \to V_LV_L$

The corresponding conditions derived from those 15 processes are listed below in order:

$$\frac{G_F(\cos^2\omega m_h^2 + \sin^2\omega m_H^2)}{4\sqrt{2}\pi} \leq \frac{1}{2} \tag{1}$$

$$\frac{3G_F(\cos^2\omega m_h^2 + \sin^2\omega m_H^2)}{8\sqrt{2}\pi} \leq \frac{1}{2} \tag{2}$$

$$\frac{G_F(\cos^2\omega m_h^2 + \sin^2\omega m_H^2)}{8\sqrt{2}\pi} \leq \frac{1}{2} \tag{3}$$

$$\left|\frac{3}{8\pi}(\lambda\cos^4\omega + \rho\sin^4\omega + \eta\sin^2\omega\cos^2\omega)\right| \leq \frac{1}{2} \tag{4}$$

$$\left|\frac{3}{8\pi}[-\lambda\cos^3\omega\sin\omega + \rho\sin^3\omega\cos\omega - \frac{1}{2}\eta(-\sin\omega\cos^3\omega + \cos\omega\sin^3\omega)]\right| \leq \frac{1}{2} \tag{5}$$

$$\left|\frac{1}{4\pi}[-\frac{3}{2}\lambda\sin^2\omega\cos^2\omega - \frac{3}{2}\rho\sin^2\omega\cos^2\omega - \frac{1}{4}\eta(\sin^4\omega + \cos^4\omega - 4\sin^2\omega\cos^2\omega)]\right| \leq \frac{1}{2} \tag{6}$$

$$\left|\frac{3}{8\pi}[-\lambda\sin^3\omega\cos\omega + \rho\cos^3\omega\sin\omega - \frac{1}{2}\eta(-\cos\omega\sin^3\omega + \sin\omega\cos^3\omega)]\right| \leq \frac{1}{2} \tag{7}$$

$$\left|\frac{3}{8\pi}(\lambda\sin^4\omega + \rho\cos^4\omega + \eta\cos^2\omega\sin^2\omega)\right| \leq \frac{1}{2} \tag{8}$$

$$\left|\frac{1}{16\pi}\{-4\sqrt{2}G_Fc_\omega^2m_h^2 - \frac{6c_\omega}{v}(-\lambda vc_\omega^3 + \rho\xi s_\omega^3 - \frac{1}{2}\eta vc_\omega s_\omega^2 + \frac{1}{2}\eta\xi s_\omega c_\omega^2) - \frac{2s_\omega}{v}[-3\lambda vc_\omega^2 s_\omega - 3\rho\xi s_\omega^2 c_\omega - \frac{1}{2}\eta v(-2s_\omega c_\omega^2 + s_\omega^3) - \frac{1}{2}\eta\xi(-2c_\omega s_\omega^2 + c_\omega^3)]\}\right| \leq \frac{1}{2} \tag{9}$$

$$\left|\frac{1}{16\pi}\{-2\sqrt{2}G_F s_\omega c_\omega(m_h^2+m_H^2)-\frac{2c_\omega}{v}[-3\lambda v c_\omega^2 s_\omega-3\rho\xi s_\omega^2 c_\omega \right. \tag{10}$$
$$-\frac{1}{2}\eta v(-2s_\omega c_\omega^2+s_\omega^3)-\frac{1}{2}\eta\xi(-2c_\omega s_\omega^2+c_\omega^3)]-\frac{2s_\omega}{v}[-3\lambda v s_\omega^2 c_\omega+3\rho\xi c_\omega^2 s_\omega$$
$$\left.-\frac{1}{2}\eta v(-2c_\omega s_\omega^2+c_\omega^3)-\frac{1}{2}\eta\xi(2s_\omega c_\omega^2-s_\omega^3)]\}\right|\leq\frac{1}{2}$$
$$\left|\frac{1}{16\pi}\{-4\sqrt{2}G_F s_\omega^2 m_H^2-\frac{6s_\omega}{v}(-\lambda v s_\omega^3-\rho\xi c_\omega^3-\frac{1}{2}\eta v s_\omega c_\omega^2-\frac{1}{2}\eta\xi c_\omega s_\omega^2)\right. \tag{11}$$
$$\left.-\frac{2c_\omega}{v}[-3\lambda v s_\omega^2 c_\omega+3\rho\xi c_\omega^2 s_\omega-\frac{1}{2}\eta v(-2c_\omega s_\omega^2+c_\omega^3)-\frac{1}{2}\eta\xi(2s_\omega c_\omega^2-s_\omega^3)]\}\right|\leq\frac{1}{2}$$
$$\frac{3G_F^{'}(\sin^2\omega m_h^2+\cos^2\omega m_H^2)}{8\sqrt{2}\pi}\leq\frac{1}{2} \tag{12}$$
$$\left|\frac{1}{16\pi}\{-4\sqrt{2}G_F^{'}s_\omega^2 m_h^2+\frac{6s_\omega}{\xi}(-\lambda v c_\omega^3+\rho\xi s_\omega^3-\frac{1}{2}\eta v c_\omega s_\omega^2+\frac{1}{2}\eta\xi s_\omega c_\omega^2)\right. \tag{13}$$
$$\left.-\frac{2c_\omega}{\xi}[-3\lambda v c_\omega^2 s_\omega-3\rho\xi s_\omega^2 c_\omega-\frac{1}{2}\eta v(-2s_\omega c_\omega^2+s_\omega^3)-\frac{1}{2}\eta\xi(-2c_\omega s_\omega^2+c_\omega^3)]\}\right|\leq\frac{1}{2}$$
$$\left|\frac{1}{16\pi}\{+2\sqrt{2}G_F^{'}s_\omega c_\omega(m_h^2+m_H^2)+\frac{2s_\omega}{\xi}[-3\lambda v c_\omega^2 s_\omega-3\rho\xi s_\omega^2 c_\omega\right. \tag{14}$$
$$-\frac{1}{2}\eta v(-2s_\omega c_\omega^2+s_\omega^3)-\frac{1}{2}\eta\xi(-2c_\omega s_\omega^2+c_\omega^3)]-\frac{2c_\omega}{\xi}[-3\lambda v s_\omega^2 c_\omega+3\rho\xi c_\omega^2 s_\omega$$
$$\left.-\frac{1}{2}\eta v(-2c_\omega s_\omega^2+c_\omega^3)-\frac{1}{2}\eta\xi(2s_\omega c_\omega^2-s_\omega^3)]\}\right|\leq\frac{1}{2}$$
$$\left|\frac{1}{16\pi}\{-4\sqrt{2}G_F^{'}c_\omega^2 m_H^2-\frac{6c_\omega}{\xi}(-\lambda v s_\omega^3-\rho\xi c_\omega^3-\frac{1}{2}\eta v s_\omega c_\omega^2-\frac{1}{2}\eta\xi c_\omega s_\omega^2)\right. \tag{15}$$
$$\left.+\frac{2s_\omega}{\xi}[-3\lambda v s_\omega^2 c_\omega+3\rho\xi c_\omega^2 s_\omega-\frac{1}{2}\eta v(-2c_\omega s_\omega^2+c_\omega^3)-\frac{1}{2}\eta\xi(2s_\omega c_\omega^2-s_\omega^3)]\}\right|\leq\frac{1}{2}$$

BIBLIOGRAPHY

BIBLIOGRAPHY

[1] J. Wess and J. Bagger, *Princeton, USA: Univ. Pr. (1992) 259 p*

[2] S. P. Martin, arXiv:hep-ph/9709356.

[3] P. Langacker, arXiv:0801.1345 [hep-ph].

[4] R. Blumenhagen, M. Cvetic, P. Langacker and G. Shiu, Ann. Rev. Nucl. Part. Sci. **55**, 71 (2005) [arXiv:hep-th/0502005].

[5] T. G. Rizzo, arXiv:hep-ph/0610104.

[6] M. Bowen, Y. Cui and J. D. Wells, JHEP **0703**, 036 (2007) [arXiv:hep-ph/0701035].

[7] B. Holdom, Phys. Lett. B **259**, 329 (1991). K. S. Babu, C. F. Kolda and J. March-Russell, Phys. Rev. D **57**, 6788 (1998) [arXiv:hep-ph/9710441]. T. G. Rizzo, Phys. Rev. D **59**, 015020 (1999) [arXiv:hep-ph/9806397]. J. Erler and P. Langacker, Phys. Lett. B **456**, 68 (1999) [arXiv:hep-ph/9903476]. T. Appelquist, B. A. Dobrescu and A. R. Hopper, Phys. Rev. D **68**, 035012 (2003) [arXiv:hep-ph/0212073]. J. Kumar and J. D. Wells, arXiv:hep-ph/0606183.

[8] R. Schabinger and J. D. Wells, Phys. Rev. D **72**, 093007 (2005) [arXiv:hep-ph/0509209].

[9] B. Patt and F. Wilczek, arXiv:hep-ph/0605188.

[10] M. J. Strassler and K. M. Zurek, hep-ph/0604261, hep-ph/0605193. M. J. Strassler, arXiv:hep-ph/0607160.

[11] R. Barbieri, T. Gregoire and L. J. Hall, arXiv:hep-ph/0509242. Z. Chacko, Y. Nomura, M. Papucci and G. Perez, JHEP **0601**, 126 (2006) [arXiv:hep-ph/0510273]. S. Chang, L. J. Hall and N. Weiner, arXiv:hep-ph/0604076.

[12] For related discussion with zero vevs, see T. Binoth and J. J. van der Bij, Z. Phys. C **75**, 17 (1997) [arXiv:hep-ph/9608245].

[13] A. Djouadi, J. Kalinowski and M. Spira, Comput. Phys. Commun. **108**, 56 (1998) [arXiv:hep-ph/9704448].

[14] B. W. Lee, C. Quigg and H. B. Thacker, Phys. Rev. D **16**, 1519 (1977).

[15] J. F. Gunion, H. E. Haber, G. L. Kane and S. Dawson, *The Higgs Hunter's Guide,* Addison-Wesley: Redwood City, CA, 1990. SCIPP-89/13

[16] L. Reina, arXiv:hep-ph/0512377.

[17] ALEPH, DELPHI, L3, OPAL, SLD Collaborations, Phys. Rept. **427**, 257 (2006) [arXiv:hep-ex/0509008]. LEP Electroweak Working Group, "A combination of preliminary electroweak measurements and constraints on the standard model," arXiv:hep-ex/0612034.

[18] M. E. Peskin and J. D. Wells, Phys. Rev. D **64**, 093003 (2001) [arXiv:hep-ph/0101342].

[19] T. Stelzer and W. F. Long, Comput. Phys. Commun. **81**, 357 (1994) [arXiv:hep-ph/9401258].

[20] F. Maltoni and T. Stelzer, JHEP **0302**, 027 (2003) [arXiv:hep-ph/0208156].

[21] J. Pumplin, D. R. Stump, J. Huston, H. L. Lai, P. Nadolsky and W. K. Tung, JHEP **0207**, 012 (2002) [arXiv:hep-ph/0201195].

[22] ATLAS Technical Design Report, Vol. II, CERN/LHCC/99-14 (1999).

[23] See Section 19.2.10 of [22]. See also, K. Iordanidis and D. Zeppenfeld, Phys. Rev. D **57**, 3072 (1998) [arXiv:hep-ph/9709506].

[24] T. Han, G. Valencia and S. Willenbrock, Phys. Rev. Lett. **69**, 3274 (1992) [arXiv:hep-ph/9206246].

[25] See Section 9.3.1.3 of [22].

[26] For other $H \to hh$ search studies, see, e.g., A. Djouadi, W. Kilian, M. Muhlleitner and P. M. Zerwas, Eur. Phys. J. C **10**, 45 (1999) [arXiv:hep-ph/9904287]. U. Ellwanger, J. F. Gunion, C. Hugonie and S. Moretti, arXiv:hep-ph/0305109. J. F. Gunion and M. Szleper, arXiv:hep-ph/0409208.

[27] S. Catani, D. de Florian, M. Grazzini and P. Nason, JHEP **0307**, 028 (2003) [arXiv:hep-ph/0306211].

[28] J. M. Campbell and R. K. Ellis, Phys. Rev. D **60**, 113006 (1999), Phys. Rev. D **62**, 114012 (2000), Phys. Rev. D **65**, 113007 (2002).

[29] E. Richter-Was, D. Froidevaux, F. Gianotti, L. Poggioli, D. Cavalli and S. Resconi, Int. J. Mod. Phys. A **13**, 1371 (1998).

[30] U. Baur, T. Plehn and D. L. Rainwater, Phys. Rev. D **67**, 033003 (2003) [arXiv:hep-ph/0211224].

[31] S. Dawson, S. Dittmaier and M. Spira, Phys. Rev. D **58**, 115012 (1998) [arXiv:hep-ph/9805244].

[32] H. B. Nielsen and P. Olesen, Nucl. Phys. B **61**, 45 (1973).

[33] M. B. Hindmarsh and T. W. B. Kibble, Rept. Prog. Phys. **58**, 477 (1995) [hep-ph/9411342].

[34] A. Vilenkin and E. P. S. Shellard, *Cosmic Strings and Other Topological Defects*, Cambridge University Press, Cambridge UK, 1994.

[35] T. W. B. Kibble, J. Phys. A **9**, 1387 (1976).

[36] D. P. Bennett and F. R. Bouchet, Phys. Rev. Lett. **60**, 257 (1988); D. P. Bennett and F. R. Bouchet, Phys. Rev. D **41**, 2408 (1990).

[37] B. Allen and E. P. S. Shellard, Phys. Rev. Lett. **64**, 119 (1990).

[38] C. J. A. Martins and E. P. S. Shellard, Phys. Rev. D **53**, 575 (1996) [hep-ph/9507335]; C. J. A. Martins and E. P. S. Shellard, Phys. Rev. D **54**, 2535 (1996) [hep-ph/9602271]; C. J. A. Martins and E. P. S. Shellard, Phys. Rev. D **65**, 043514 (2002) [hep-ph/0003298].

[39] G. R. Vincent, M. Hindmarsh and M. Sakellariadou, Phys. Rev. D **56**, 637 (1997) [astro-ph/9612135]; G. Vincent, N. D. Antunes and M. Hindmarsh, Phys. Rev. Lett. **80**, 2277 (1998) [hep-ph/9708427].

[40] V. Vanchurin, K. D. Olum and A. Vilenkin, Phys. Rev. D **74**, 063527 (2006) [gr-qc/0511159].

[41] For reviews, see for example H. E. Haber and G. L. Kane, Phys. Rept. **117**, 75 (1985); S. P. Martin, [hep-ph/9709356]; D. J. H. Chung et al., Phys. Rept. **407**, 1 (2005) [hep-ph/0312378]; M. A. Luty, [hep-th/0509029].

[42] R. Blumenhagen, M. Cvetic, P. Langacker and G. Shiu, Ann. Rev. Nucl. Part. Sci. **55**, 71 (2005) [hep-th/0502005]; P. Langacker, hep-ph/9805486; P. Langacker and J. Wang, Phys. Rev. D **58**, 115010 (1998) [hep-ph/9804428]; J. R. Espinosa, Nucl. Phys. Proc. Suppl. **62**, 187 (1998) [hep-ph/9707541]; M. Cvetic and P. Langacker, Phys. Rev. D **54**, 3570 (1996) [hep-ph/9511378]; M. Cvetic and P. Langacker, Mod. Phys. Lett. A **11**, 1247 (1996) [hep-ph/9602424].

[43] P. Langacker, N. Polonsky and J. Wang, Phys. Rev. D **60**, 115005 (1999) [hep-ph/9905252]; D. Suematsu, Phys. Rev. D **59**, 055017 (1999) [hep-ph/9808409].

[44] C. T. Hill, H. M. Hodges and M. S. Turner, Phys. Rev. D **37**, 263 (1988).

[45] K. Freese, T. Gherghetta and H. Umeda, Phys. Rev. D **54**, 6083 (1996) [hep-ph/9512211].

[46] T. Barreiro, E. J. Copeland, D. H. Lyth and T. Prokopec, Phys. Rev. D **54**, 1379 (1996) [hep-ph/9602263].

[47] A. A. Penin, V. A. Rubakov, P. G. Tinyakov and S. V. Troitsky, Phys. Lett. B **389**, 13 (1996) [hep-ph/9609257].

[48] W. B. Perkins and A. C. Davis, Phys. Lett. B **428**, 254 (1998) [hep-ph/9803303].

[49] A. Yung, Nucl. Phys. B **562**, 191 (1999) [hep-th/9906243]; K. Evlampiev and A. Yung, Nucl. Phys. B **662**, 120 (2003) [hep-th/0303047]; M. Shifman and A. Yung, [hep-th/0703267].

[50] S. C. Davis, P. Binetruy and A. C. Davis, Phys. Lett. B **611**, 39 (2005) [hep-th/0501200].

[51] M. Donaire and A. Rajantie, Phys. Rev. D **73**, 063517 (2006) [hep-ph/0508272].

[52] S. C. Davis, A. C. Davis and M. Trodden, Phys. Lett. B **405**, 257 (1997) [hep-ph/9702360].

[53] S. C. Davis, A. C. Davis and M. Trodden, Phys. Rev. D **57**, 5184 (1998) [hep-ph/9711313].

[54] M. Endo, M. Kawasaki and T. Moroi, Phys. Lett. B **569**, 73 (2003) [hep-ph/0304126].

[55] R. Jeannerot, J. Rocher and M. Sakellariadou, Phys. Rev. D **68**, 103514 (2003) [hep-ph/0308134]. J. Rocher and M. Sakellariadou, JCAP **0503**, 004 (2005) [hep-ph/0406120]. J. Rocher and M. Sakellariadou, Phys. Rev. Lett. **94**, 011303 (2005) [hep-ph/0412143].

[56] P. Laguna and R. A. Matzner, Phys. Rev. Lett. **62**, 1948 (1989).

[57] L. M. A. Bettencourt and T. W. B. Kibble, Phys. Lett. B **332**, 297 (1994) [hep-ph/9405221].

[58] L. M. A. Bettencourt, P. Laguna and R. A. Matzner, Phys. Rev. Lett. **78**, 2066 (1997) [hep-ph/9612350].

[59] P. Salmi, A. Achucarro, E. J. Copeland, T. W. B. Kibble, R. de Putter and D. A. Steer, Phys. Rev. D **77**, 041701 (2008) [arXiv:0712.1204 [hep-th]].

[60] E. J. Copeland and N. Turok, "Cosmic String Interactions,", FERMILAB-PUB-86-127-A (1986).

[61] See for example, E. P. S. Shellard, Nucl. Phys. B **283**, 624 (1987).

[62] R. A. Matzner, Comput.Phys. **2**, 51 (1988).

[63] A. Achucarro and R. de Putter, Phys. Rev. D **74**, 121701 (2006) [hep-th/0605084].

[64] S. H. Tye, I. Wasserman and M. Wyman, Phys. Rev. D **71**, 103508 (2005) [Erratum-ibid. D **71**, 129906 (2005)] [astro-ph/0503506].

[65] E. J. Copeland and P. M. Saffin, JHEP **0511**, 023 (2005) [hep-th/0505110].

[66] L. Leblond and M. Wyman, Phys. Rev. D **75**, 123522 (2007) [astro-ph/0701427].

[67] A. Avgoustidis and E. P. S. Shellard, [0705.3395 [astro-ph]].

[68] For a review of cosmic strings from superstring theory, see:
J. Polchinski, [hep-th/0412244].

[69] N. T. Jones, H. Stoica and S. H. H. Tye, JHEP **0207**, 051 (2002) [hep-th/0203163]; S. Sarangi and S. H. H. Tye, Phys. Lett. B **536**, 185 (2002) [hep-th/0204074]. N. T. Jones, H. Stoica and S. H. H. Tye, Phys. Lett. B **563**, 6 (2003) [hep-th/0303269].

[70] G. Dvali and A. Vilenkin, JCAP **0403**, 010 (2004) [hep-th/0312007].

[71] E. J. Copeland, R. C. Myers and J. Polchinski, JHEP **0406**, 013 (2004) [hep-th/0312067].

[72] J. Polchinski, AIP Conf. Proc. **743**, 331 (2005) [Int. J. Mod. Phys. A **20**, 3413 (2005)] [hep-th/0410082].

[73] M. G. Jackson, N. T. Jones and J. Polchinski, JHEP **0510**, 013 (2005) [hep-th/0405229].

[74] E. J. Copeland, R. C. Myers and J. Polchinski, Comptes Rendus Physique **5**, 1021 (2004).

[75] A. Hanany and K. Hashimoto, JHEP **0506**, 021 (2005) [hep-th/0501031].

[76] D. E. Morrissey and J. D. Wells, JHEP **0701**, 102 (2007) [hep-ph/0606234].

[77] S. P. Martin, Phys. Rev. D **61**, 035004 (2000) [hep-ph/9907550].

[78] C. H. Taubes, Commun. Math. Phys. **72**, 277 (1980).

[79] L. M. A. Bettencourt and R. J. Rivers, Phys. Rev. D **51**, 1842 (1995) [hep-ph/9405222].

[80] J. M. Speight, Phys. Rev. D **55**, 3830 (1997) [hep-th/9603155].

[81] L. Jacobs and C. Rebbi, Phys. Rev. B **19**, 4486 (1979).

[82] K. J. M. Moriarty, E. Myers and C. Rebbi, Phys. Lett. B **207**, 411 (1988).

[83] E. Myers, C. Rebbi and R. Strilka, Phys. Rev. D **45**, 1355 (1992).

[84] A. Rajantie, M. Sakellariadou and H. Stoica, [0706.3662 [hep-th]].

[85] E. J. Copeland, T. W. B. Kibble and D. A. Steer, Phys. Rev. Lett. **97**, 021602 (2006) [hep-th/0601153]; E. J. Copeland, T. W. B. Kibble and D. A. Steer, [hep-th/0611243].

[86] G. Lazarides, C. Panagiotakopoulos and Q. Shafi, Phys. Rev. Lett. **56**, 557 (1986); G. Lazarides and Q. Shafi, Nucl. Phys. B **392**, 61 (1993).

[87] K. Yamamoto, Phys. Lett. B **168**, 341 (1986).

[88] D. H. Lyth and E. D. Stewart, Phys. Rev. D **53**, 1784 (1996) [hep-ph/9510204].

[89] K. Yamamoto, Phys. Lett. B **194**, 390 (1987).

[90] S. Hannestad, Phys. Rev. D **70**, 043506 (2004) [astro-ph/0403291].

[91] K. Ichikawa, M. Kawasaki and F. Takahashi, Phys. Rev. D **72**, 043522 (2005) [astro-ph/0505395].

[92] A. Rajantie, Int. J. Mod. Phys. A **17**, 1 (2002) [hep-ph/0108159].

[93] J. J. Blanco-Pillado, K. D. Olum and A. Vilenkin, [0706.1577 [hep-th]].

[94] H. Firouzjahi, L. Leblond and S. H. Henry Tye, JHEP **0605**, 047 (2006) [arXiv:hep-th/0603161].

[95] M. Wyman, L. Pogosian and I. Wasserman, Phys. Rev. D **72**, 023513 (2005) [Erratum-ibid. D **73**, 089905 (2006)] [astro-ph/0503364].

[96] A. A. Fraisse, JCAP **0703**, 008 (2007) [astro-ph/0603589].

[97] L. Pogosian, I. Wasserman and M. Wyman, [astro-ph/0604141].

[98] U. Seljak, A. Slosar and P. McDonald, JCAP **0610**, 014 (2006) [astro-ph/0604335].

[99] N. Bevis, M. Hindmarsh, M. Kunz and J. Urrestilla, Phys. Rev. D **75**, 065015 (2007) [astro-ph/0605018]; N. Bevis, M. Hindmarsh, M. Kunz and J. Urrestilla, [astro-ph/0702223].

[100] R. A. Battye, B. Garbrecht and A. Moss, JCAP **0609**, 007 (2006) [astro-ph/0607339]; R. A. Battye, B. Garbrecht, A. Moss and H. Stoica, [0710.1541 [astro-ph]].

[101] A. Vilenkin, Phys. Lett. B **107**, 47 (1981).

[102] N. Turok, Nucl. Phys. B **242**, 520 (1984).

[103] C. J. Burden, Phys. Lett. B **164**, 277 (1985).

[104] T. Vachaspati and A. Vilenkin, Phys. Rev. D **31**, 3052 (1985).

[105] D. Garfinkle and T. Vachaspati, Phys. Rev. D **36**, 2229 (1987).

[106] X. Siemens and K. D. Olum, Nucl. Phys. B **611**, 125 (2001) [Erratum-ibid. B **645**, 367 (2002)] [gr-qc/0104085]. X. Siemens, K. D. Olum and A. Vilenkin, Phys. Rev. D **66**, 043501 (2002) [gr-qc/0203006].

[107] J. Polchinski and J. V. Rocha, Phys. Rev. D **74**, 083504 (2006) [hep-ph/0606205]; J. Polchinski and J. V. Rocha, Phys. Rev. D **75**, 123503 (2007) [gr-qc/0702055].

[108] J. Polchinski, [0707.0888 [astro-ph]].

[109] V. Vanchurin, K. Olum and A. Vilenkin, Phys. Rev. D **72**, 063514 (2005) [gr-qc/0501040]; V. Vanchurin, K. D. Olum and A. Vilenkin, Phys. Rev. D **74**, 063527 (2006) [gr-qc/0511159]; K. D. Olum and V. Vanchurin, Phys. Rev. D **75**, 063521 (2007) [astro-ph/0610419].

[110] M. Srednicki and S. Theisen, Phys. Lett. B **189**, 397 (1987).

[111] T. Damour and A. Vilenkin, Phys. Rev. Lett. **78**, 2288 (1997) [gr-qc/9610005].

[112] M. Peloso and L. Sorbo, Nucl. Phys. B **649**, 88 (2003) [hep-ph/0205063].

[113] R. H. Brandenberger, Nucl. Phys. B **293**, 812 (1987).

[114] E. Babichev and M. Kachelriess, Phys. Lett. B **614**, 1 (2005) [hep-th/0502135].

[115] J. M. Quashnock and D. N. Spergel, Phys. Rev. D **42**, 2505 (1990).

[116] J. J. Blanco-Pillado and K. D. Olum, Phys. Rev. D **59**, 063508 (1999) [gr-qc/9810005], K. D. Olum and J. J. Blanco-Pillado, Phys. Rev. D **60**, 023503 (1999) [gr-qc/9812040].

[117] C. Ringeval, M. Sakellariadou and F. Bouchet, JCAP **0702**, 023 (2007) [astro-ph/0511646].

[118] C. J. A. Martins and E. P. S. Shellard, Phys. Rev. D **73**, 043515 (2006) [astro-ph/0511792].

[119] T. Damour and A. Vilenkin, Phys. Rev. D **64**, 064008 (2001) [gr-qc/0104026], T. Damour and A. Vilenkin, Phys. Rev. D **71**, 063510 (2005) [hep-th/0410222].

[120] X. Siemens, J. Creighton, I. Maor, S. Ray Majumder, K. Cannon and J. Read, Phys. Rev. D **73**, 105001 (2006) [gr-qc/0603115].

[121] C. J. Hogan, Phys. Rev. D **74**, 043526 (2006) [astro-ph/0605567].

[122] X. Siemens, V. Mandic and J. Creighton, [astro-ph/0610920].

[123] M. R. DePies and C. J. Hogan, Phys. Rev. D **75**, 125006 (2007) [astro-ph/0702335].

[124] C. Grojean and G. Servant, Phys. Rev. D **75**, 043507 (2007) [hep-ph/0607107].

[125] B. Abbott *et al.* [LIGO Scientific Collaboration], Astrophys. J. **659**, 918 (2007) [astro-ph/0608606].

[126] http://lisa.nasa.gov

[127] F. A. Jenet *et al.*, Astrophys. J. **653**, 1571 (2006) [astro-ph/0609013].

[128] C. Cutler and K. S. Thorne, arXiv:gr-qc/0204090.

[129] B. F. Schutz, Class. Quant. Grav. **16**, A131 (1999) [arXiv:gr-qc/9911034].

[130] R. Jeannerot, X. Zhang and R. H. Brandenberger, JHEP **9912**, 003 (1999) [hep-ph/9901357].

[131] M. Kawasaki, K. Kohri and T. Moroi, Phys. Rev. D **71**, 083502 (2005) [astro-ph/0408426].

[132] D. J. Fixsen, E. S. Cheng, J. M. Gales, J. C. Mather, R. A. Shafer and E. L. Wright, Astrophys. J. **473**, 576 (1996) [astro-ph/9605054].

[133] R. H. Brandenberger, B. Carter and A. C. Davis, Phys. Lett. B **534**, 1 (2002) [hep-ph/0202168].

[134] W. Hu and J. Silk, Phys. Rev. D **48**, 485 (1993).

[135] K. Hagiwara *et al.* [Particle Data Group], Phys. Rev. D **66**, 010001 (2002).

[136] T. Kanzaki, M. Kawasaki, K. Kohri and T. Moroi, [0705.1200 [hep-ph]].

[137] A. Kogut *et al.*, New Astron. Rev. **50**, 925 (2006) [astro-ph/0609373].

[138] P. Bhattacharjee, Phys. Rev. D **40**, 3968 (1989),
J. H. MacGibbon and R. H. Brandenberger, Nucl. Phys. B **331**, 153 (1990).

[139] P. Bhattacharjee, Q. Shafi and F. W. Stecker, Phys. Rev. Lett. **80**, 3698 (1998) [hep-ph/9710533].

[140] P. Sreekumar *et al.* [EGRET Collaboration], Astrophys. J. **494**, 523 (1998) [astro-ph/9709257].

[141] E. D. Bloom [GLAST team Collaboration], Space Sci. Rev. **75**, 109 (1996).

[142] U. F. Wichoski, J. H. MacGibbon and R. H. Brandenberger, Phys. Rev. D **65**, 063005 (2002) [hep-ph/9805419].

[143] K. Filimonov [IceCube Collaboration], AIP Conf. Proc. **870**, 215 (2006), J. Becker [IceCube Collaboration], J. Phys. Conf. Ser. **60**, 219 (2007).

[144] P. Facal San Luis [Pierre Auger Collaboration], [0706.4322 [astro-ph]].

[145] M. Kawasaki and K. i. Maeda, Phys. Lett. B **208**, 84 (1988) [Phys. Lett. B **209**, 271 (1988)].

[146] M. Mohazzab, Phys. Lett. B **350**, 13 (1995) [arXiv:hep-ph/9409274].

[147] I. Dasgupta, Phys. Rev. D **55**, 3318 (1997) [arXiv:hep-ph/9604356].

[148] G. Lazarides, C. Panagiotakopoulos and Q. Shafi, Phys. Lett. B **183**, 289 (1987); G. Lazarides, C. Panagiotakopoulos and Q. Shafi, Nucl. Phys. B **307**, 937 (1988).

[149] S. Dimopoulos and L. J. Hall, Phys. Lett. B **196**, 135 (1987).

[150] J. Cline and S. Raby, Phys. Rev. D **43**, 1781 (1991).

[151] K. S. Babu, R. N. Mohapatra and S. Nasri, Phys. Rev. Lett. **97**, 131301 (2006) [hep-ph/0606144]; K. S. Babu, R. N. Mohapatra and S. Nasri, Phys. Rev. Lett. **98**, 161301 (2007) [hep-ph/0612357].

[152] E. D. Stewart, M. Kawasaki and T. Yanagida, Phys. Rev. D **54**, 6032 (1996) [hep-ph/9603324]; G. N. Felder, H. Kim, W. I. Park and E. D. Stewart, JCAP **0706**, 005 (2007) [hep-ph/0703275].

[153] E. Witten, Nucl. Phys. B **249**, 557 (1985).

[154] B. Carter, Phys. Lett. B **238**, 166 (1990) [hep-th/0703023].

[155] R. H. Brandenberger, B. Carter, A. C. Davis and M. Trodden, Phys. Rev. D **54**, 6059 (1996) [hep-ph/9605382].

[156] A. C. Davis, [hep-ph/0305008].

[157] R. Jackiw and P. Rossi, Nucl. Phys. B **190**, 681 (1981).

[158] M. Postma and B. Hartmann, [0706.0416 [hep-th]].

[159] A. Vilenkin, ApJ, **282**, L51 (1984)

[160] D. Huterer and T. Vachaspati, Phys. Rev. D **68**, 041301 (2003) [astro-ph/0305006].

[161] M. Oguri and K. Takahashi, Phys. Rev. D **72**, 085013 (2005) [astro-ph/0509187].

[162] B. Shlaer and M. Wyman, Phys. Rev. D **72**, 123504 (2005) [hep-th/0509177].

[163] M. A. Gasparini, P. Marshall, T. Treu, E. Morganson and F. Dubath, [0710.5544 [astro-ph]].

[164] P. Diamond and S. Rawlings, Frontiers **23**, 13 (2006).

[165] K. J. Mack, D. H. Wesley and L. J. King, [astro-ph/0702648].

[166] Y. Cui and D. E. Morrissey, MCTP-08-09, NSF-KITP-08-17

To appear...

[167] H. B. Nielsen and P. Olesen, Nucl. Phys. B **61**, 45 (1973).

[168] M. B. Hindmarsh and T. W. B. Kibble, Rept. Prog. Phys. **58**, 477 (1995) [hep-ph/9411342].

[169] A. Vilenkin and E. P. S. Shellard, *Cosmic Strings and Other Topological Defects*, Cambridge University Press, Cambridge UK, 1994.

[170] T. W. B. Kibble, J. Phys. A **9**, 1387 (1976).

[171] R. Blumenhagen, M. Cvetic, P. Langacker and G. Shiu, Ann. Rev. Nucl. Part. Sci. **55**, 71 (2005) [hep-th/0502005]; P. Langacker, hep-ph/9805486; P. Langacker and J. Wang, Phys. Rev. D **58**, 115010 (1998) [hep-ph/9804428]; J. R. Espinosa, Nucl. Phys. Proc. Suppl. **62**, 187 (1998) [hep-ph/9707541]; M. Cvetic and P. Langacker, Phys. Rev. D **54**, 3570 (1996) [hep-ph/9511378]; M. Cvetic and P. Langacker, Mod. Phys. Lett. A **11**, 1247 (1996) [hep-ph/9602424].

[172] P. Langacker, N. Polonsky and J. Wang, Phys. Rev. D **60**, 115005 (1999) [hep-ph/9905252]; D. Suematsu, Phys. Rev. D **59**, 055017 (1999) [hep-ph/9808409].

[173] R. Jeannerot, X. Zhang and R. H. Brandenberger, JHEP **9912**, 003 (1999) [hep-ph/9901357].

[174] T. Matsuda, JCAP **0604**, 005 (2006) [arXiv:hep-ph/0509064].

[175] A. Vilenkin, Phys. Rept. **121**, 263 (1985).

[176] T. W. B. Kibble, Nucl. Phys. B **252**, 227 (1985) [Erratum-ibid. B **261**, 750 (1985)].

[177] D. P. Bennett and F. R. Bouchet, Phys. Rev. Lett. **60**, 257 (1988); D. P. Bennett and F. R. Bouchet, Phys. Rev. D **41**, 2408 (1990).

[178] B. Allen and E. P. S. Shellard, Phys. Rev. Lett. **64**, 119 (1990).

[179] C. J. A. Martins and E. P. S. Shellard, Phys. Rev. D **53**, 575 (1996) [hep-ph/9507335]; C. J. A. Martins and E. P. S. Shellard, Phys. Rev. D **54**, 2535 (1996) [hep-ph/9602271]; C. J. A. Martins and E. P. S. Shellard, Phys. Rev. D **65**, 043514 (2002) [hep-ph/0003298].

[180] G. R. Vincent, M. Hindmarsh and M. Sakellariadou, Phys. Rev. D **56**, 637 (1997) [astro-ph/9612135]; G. Vincent, N. D. Antunes and M. Hindmarsh, Phys. Rev. Lett. **80**, 2277 (1998) [hep-ph/9708427].

[181] V. Vanchurin, K. D. Olum and A. Vilenkin, Phys. Rev. D **74**, 063527 (2006) [gr-qc/0511159].

[182] For reviews of dark matter, see:
G. Jungman, M. Kamionkowski and K. Griest, Phys. Rept. **267**, 195 (1996) [arXiv:hep-ph/9506380]; L. Bergstrom, Rept. Prog. Phys. **63**, 793 (2000) [arXiv:hep-ph/0002126]; K. A. Olive, arXiv:astro-ph/0301505. G. Bertone, D. Hooper and J. Silk, Phys. Rept. **405**, 279 (2005) [arXiv:hep-ph/0404175].

[183] D. N. Spergel *et al.* [WMAP Collaboration], Astrophys. J. Suppl. **170**, 377 (2007) [arXiv:astro-ph/0603449].

[184] For reviews, see for example H. E. Haber and G. L. Kane, Phys. Rept. **117**, 75 (1985); S. P. Martin, [hep-ph/9709356]; D. J. H. Chung et al., Phys. Rept. **407**, 1 (2005) [hep-ph/0312378]; M. A. Luty, [hep-th/0509029].

[185] T. Appelquist, H. C. Cheng and B. A. Dobrescu, Phys. Rev. D **64**, 035002 (2001) [arXiv:hep-ph/0012100]; G. Servant and T. M. P. Tait, Nucl. Phys. B **650**, 391 (2003) [arXiv:hep-ph/0206071]; H. C. Cheng, J. L. Feng and K. T. Matchev, Phys. Rev. Lett. **89**, 211301 (2002) [arXiv:hep-ph/0207125]. F. Burnell and G. D. Kribs, Phys. Rev. D **73**, 015001 (2006) [arXiv:hep-ph/0509118]. K. Kong and K. T. Matchev, JHEP **0601**, 038 (2006) [arXiv:hep-ph/0509119].

[186] H. C. P. Cheng and I. Low, JHEP **0408**, 061 (2004) [arXiv:hep-ph/0405243]; J. Hubisz and P. Meade, Phys. Rev. D **71**, 035016 (2005) [arXiv:hep-ph/0411264]. A. Birkedal, A. Noble, M. Perelstein and A. Spray, Phys. Rev. D **74**, 035002 (2006) [arXiv:hep-ph/0603077].

[187] M. Srednicki and S. Theisen, Phys. Lett. B **189**, 397 (1987).

[188] S. Borsanyi and M. Hindmarsh, arXiv:0712.0300 [hep-ph].

[189] A. Vilenkin, Phys. Lett. B **107**, 47 (1981).

[190] R. H. Brandenberger, Nucl. Phys. B **293**, 812 (1987).

[191] T. W. B. Kibble and N. Turok, Phys. Lett. B **116**, 141 (1982).

[192] N. Turok, Nucl. Phys. B **242**, 520 (1984).

[193] J. J. Blanco-Pillado and K. D. Olum, Phys. Rev. D **59**, 063508 (1999) [gr-qc/9810005], K. D. Olum and J. J. Blanco-Pillado, Phys. Rev. D **60**, 023503 (1999) [gr-qc/9812040].

[194] T. Vachaspati and A. Vilenkin, Phys. Rev. D **31**, 3052 (1985).

[195] C. J. Burden, Phys. Lett. B **164**, 277 (1985).

[196] D. Garfinkle and T. Vachaspati, Phys. Rev. D **36**, 2229 (1987).

[197] J. M. Quashnock and D. N. Spergel, Phys. Rev. D **42**, 2505 (1990).

[198] V. Vanchurin, K. Olum and A. Vilenkin, Phys. Rev. D **72**, 063514 (2005) [gr-qc/0501040]; V. Vanchurin, K. D. Olum and A. Vilenkin, Phys. Rev. D **74**, 063527 (2006) [gr-qc/0511159]; K. D. Olum and V. Vanchurin, Phys. Rev. D **75**, 063521 (2007) [astro-ph/0610419].

[199] C. Ringeval, M. Sakellariadou and F. Bouchet, JCAP **0702**, 023 (2007) [astro-ph/0511646].

[200] C. J. A. Martins and E. P. S. Shellard, Phys. Rev. D **73**, 043515 (2006) [astro-ph/0511792].

[201] X. Siemens and K. D. Olum, Nucl. Phys. B **611**, 125 (2001) [Erratum-ibid. B **645**, 367 (2002)] [gr-qc/0104085]. X. Siemens, K. D. Olum and A. Vilenkin, Phys. Rev. D **66**, 043501 (2002) [gr-qc/0203006].

[202] J. Polchinski and J. V. Rocha, Phys. Rev. D **74**, 083504 (2006) [hep-ph/0606205]; J. Polchinski and J. V. Rocha, Phys. Rev. D **75**, 123503 (2007) [gr-qc/0702055].

[203] J. Polchinski, [0707.0888 [astro-ph]].

[204] J. V. Rocha, arXiv:0709.3284 [gr-qc].

[205] F. Dubath, J. Polchinski and J. V. Rocha, arXiv:0711.0994 [astro-ph].

[206] V. Vanchurin, arXiv:0712.2236 [gr-qc].

[207] A. Vilenkin, Phys. Rev. D **43**, 1060 (1991).

[208] J. Garriga and M. Sakellariadou, Phys. Rev. D **48**, 2502 (1993) [arXiv:hep-th/9303024].

[209] M. G. Alford and F. Wilczek, Phys. Rev. Lett. **62**, 1071 (1989).

[210] A. E. Everett, Phys. Rev. D **24**, 858 (1981).

[211] Y. Cui, S. P. Martin, D. E. Morrissey and J. D. Wells, [0709.0950 [hep-ph]].

[212] M. Dine, P. J. Fox, E. Gorbatov, Y. Shadmi, Y. Shirman and S. D. Thomas, Phys. Rev. D **70**, 045023 (2004) [arXiv:hep-ph/0405159].

[213] A. G. Cohen, T. S. Roy and M. Schmaltz, JHEP **0702**, 027 (2007) [arXiv:hep-ph/0612100].

[214] H. Murayama, Y. Nomura and D. Poland, Phys. Rev. D **77**, 015005 (2008) [arXiv:0709.0775 [hep-ph]].

[215] P. Langacker, G. Paz, L. T. Wang and I. Yavin, Phys. Rev. Lett. **100**, 041802 (2008) [arXiv:0710.1632 [hep-ph]].

[216] M. J. Strassler and K. M. Zurek, Phys. Lett. B **651**, 374 (2007) [arXiv:hep-ph/0604261].

[217] M. J. Strassler, arXiv:hep-ph/0607160.

[218] T. Han, Z. Si, K. M. Zurek and M. J. Strassler, arXiv:0712.2041 [hep-ph].

[219] M. J. Strassler, arXiv:0801.0629 [hep-ph].